Cessna Morphlight

Morphing Civil Single Engine Propeller Aircraft

Technische Universiteit Delft

Milan van Dijk	4209141
Yannick van Dijk	4170105
Patrick Hemmen	4195612
Jasper Hemmes	4226216
Sylvain van der Meer	4214773
Esther de Mol	4216393
Gijs de Rooij	4152344
Rick Rosenkrantz	4224612
Aaron de Windt	4134249
Gajtan De Zutter	4220609

TUDelft

Background: chensiyuan

Cessna Morphlight

Morphing Civil Single Engine Propeller Aircraft

by

Milan van Dijk	4209141
Yannick van Dijk	4170105
Patrick Hemmen	4195612
Jasper Hemmes	4226216
Sylvain van der Meer	4214773
Esther de Mol	4216393
Gijs de Rooij	4152344
Rick Rosenkrantz	4224612
Aaron de Windt	4134249
Gajtan De Zutter	4220609

coached by

Antonio Grande
Roberto Merino Martinez
Ye Zhang

June 30, 2015

TU Delft Delft University of Technology

Preface

This project is performed as a Design Synthesis Exercise for the course AE3200 at Delft University of Technology.

We would like to express our gratitude to our principal tutor Antonio Grande, as well as our coaches Roberto Merino Martinez and Ye Zhang, for their support throughout this project.

Summary

This report describes the final design of the Cessna Morphlight. This new aircraft is similar to the Cessna 172S Skyhawk in its general shape, using a single propeller engine and carrying four people. The new aircraft features a fuel capacity of 200 L which is the same as the long range version of the old aircraft. The operational empty weight is reduced to 712 kg while the maximum take-off weight is allowed to increase by 100kg to 1,272kg. The range, endurance and cruise characteristics are improved while keeping the production cost under €375,000.

The range of the aircraft is increased from 1,181 km to 2,780 km and the endurance from less than seven hours to more than 21 hours. The cruise speed is increased from 230 km/h to 250 km/h and the takeoff and landing distances are decreased to 336 m and 284 m.

The sustainability analysis identified the materials which are well recyclable. One of the better materials is the widely used aluminium, but also thermoplastic composites score well. By using thermoplastic composites a recyclability of at least 80% is guaranteed.

Sweep, span, chord, twist, dihedral, camber and thickness are identified as morphing options of which span, chord, twist and camber are found to be most promising. A configuration trade-off is performed to arrive at the current configuration used for the Cessna Morphlight.

Through morphing, the Morphlight provides more flight performance capability and airport flexibility than the reference aircraft. Relevant performance characteristics are optimised to meet all requirements. Favourable basic planform dimensions including morphing amounts are determined. The feasible morphing amounts are limited by the zero Poisson structure and the Fowler flaps. The performance analysis shows that morphing is required to meet all requirements, proving its potential.

To reduce drag, increase lift and improve the overall efficiency of the aircraft, the aerodynamic properties of the airfoil, wing and complete aircraft are investigated using several tools, each with different features meant to be used for different tasks. A series of airfoils are analysed to in the end choose an ideal design. The effects of different wing planform shapes are analysed and the results passed to the final trade-of. A preliminary analysis of the effects of a raked wing section was performed. Furthermore aerodynamic coefficients, lift and pressure distributions are, throughout the project, calculated and passed to the different departments when requested. At last, CFD calculations are performed to check the accuracy of the results being calculated using the other tools.

To ensure stability and controllabilty an analysis is performed on the required size of the horizontal and vertical tail. To be able to do this first a weight and balance assessment is done to determine the centre of gravity range for which the aircraft should be stable and controllable. Furthermore the control surfaces are designed to be able to control the aircraft with similar characteristics as the Skyhawk. Both static and dynamic stability are ensured.

To allow for morphing, the wing box is split into three parts, and as ideal internal shape a wing box is assumed. To find the lightest design, an optimisation program is written. This program returns the lightest design of the wing box and the strut possible. With this program, a minimum mass of 62.29 kg is found, whereas without a strut the mass would be 87.82 kg. Due to restrictions of the program, the tip was heavily over designed, and further optimisation is done with ABAQUS. This further optimisation leads to a final mass of 38.87 kg.

A description of the aircraft subsystems is given. The engine is replaced by a more fuel efficient, but larger, hybrid diesel engine in order to meet the take-off fuel requirement. To improve the propulsive efficiency the fixed pitch propeller is replaced with a variable pitch three blade propeller. The electrical subsystem now features a fly-by-wire aileron actuation. The fixed gear is replaced by a retractable version made of steel in order to reduce drag. The Fowler flaps extend by 35% of the chord and deflect by 45 degrees. In order to meet the landing requirement, the increase in lift coefficient due to the flaps

is found to be 0.98. A speedbrake is added in order to meet the ground roll requirement.

To accommodate the new engine the fuselage nose is extended and to produce less drag the fuselage is given smoother curves. The wing planform is designed with an eye on low-cost mass production and good fuel storage capabilities. To allow the wing boxes to slide a UHMW-PE coating is used. The ribs are also able to slide using this same coating. Span extension is done with a rack and pinion mechanism, for which a total of four small electric motors are used. For the horizontal and vertical stabiliser a multi-spar design approach is taken, and for the elevators and rudder a multi-rib design.

The reference aircraft is almost entirely made out of aluminium. In order to reduce structural weight while maintaining structural integrity a different type of material was chosen after a material comparison. Both thermoset and thermoplastic CFRP were selected. The morphing parts use a zero-Poisson skin, made from unidirectional carbon fibres in a polyurethane matrix, strengthened by a thermoplastic honeycomb structure. The skin is glued to honeycomb structure. The flap tracks are made of aluminium 7075-T6 for its high strength to weight properties.

It is concluded that morphing the Skyhawk is a feasible option. Through morphing the Morphlight outperforms the Skyhawk by a substantial margin. Some recommendations for future design are provided. For example, morphing would be even more efficient when flying faster. The total cost of the Morphlight is €365,000.

Contents

Preface iii

Summary vi

List of Symbols and Abbreviations xii

1 Introduction 1

I Project Outline 3

2 Requirement Analysis 5
- 2.1 Top Level Requirements 5
- 2.2 System Requirements 6
- 2.3 Mission Profile 7

3 Functional Flow Diagram and Functional Breakdown Structure 9

4 Market Analysis 11
- 4.1 Primary Use. 11
- 4.2 Competitors 11
- 4.3 Current Fleet 13
- 4.4 Fuel Prices 13
- 4.5 Legislation 14
- 4.6 Future Market. 14

5 Sustainable Development 17

II Design 19

6 Design Options 21

7 Configuration Trade-off 23
- 7.1 Preliminary Trade-off 23
- 7.2 Detailed Trade-off 23
- 7.3 Concept Trade-off 26

8 Performance Analysis 29
- 8.1 Performance Optimisation 29
- 8.2 Verification 34
- 8.3 Validation 35
- 8.4 Performance Optimisation Results 36
- 8.5 Sensitivity Analysis 38
- 8.6 Payload-Range Diagram 39
- 8.7 Climb Performance 39
- 8.8 Flight Envelope 41
- 8.9 Estimated Noise and Emission Characteristics 41

9 Aerodynamics 43
- 9.1 Aerodynamic Tools 43
- 9.2 Airfoil Selection 44

9.3 Wing Planform Analysis . . . 47
9.4 Wing Rake . . . 48
9.5 Validation using Computational Fluid Dynamics . . . 49

10 Stability and Control 51
10.1 Longitudinal Stability and Control . . . 51
10.2 Lateral Stability and Control . . . 55
10.3 Directional Stability and Control . . . 56
10.4 Elevator Control Force . . . 58
10.5 Dynamic Stability . . . 60
10.6 Results of Stability and Control . . . 64

11 Structural Analysis 67
11.1 Approach to Structural Analysis . . . 67
11.2 Optimisation and Constraints . . . 72
11.3 Verification . . . 75
11.4 Validation . . . 76
11.5 Preliminary Structural Optimisation Results . . . 77
11.6 Load Transfer . . . 78
11.7 Further Optimisation . . . 79
11.8 Final Structural Optimisation Results . . . 81
11.9 Flutter Analysis . . . 81

12 Aircraft Subsystems 83
12.1 Powerplant and Thrust Delivery Method . . . 83
12.2 Electrical System . . . 85
12.3 Environmental Control System . . . 85
12.4 Fuel System . . . 86
12.5 Hydraulic System . . . 86
12.6 Landing Gear . . . 87
12.7 Flap Sizing . . . 90
12.8 Speedbrake Sizing . . . 91

13 Detailed Aircraft Layout 93
13.1 Fuselage . . . 93
13.2 Landing Gear . . . 93
13.3 Wing Shape . . . 93
13.4 Wing Skin . . . 94
13.5 Internal Wing Structure . . . 95
13.6 Strut . . . 96
13.7 Fuel Tanks . . . 96
13.8 Flaps . . . 96
13.9 Ailerons . . . 97
13.10 Empennage . . . 97

14 Material Selection 99
14.1 Fuselage . . . 100
14.2 Landing Gear . . . 101

14.3 Wing Skin . . . 101
14.4 Internal Wing Structure . . . 102
14.5 Flaps and Ailerons . . . 102
14.6 Empennage . . . 102
14.7 Sustainability . . . 102

15 Risk and RAMS **103**
15.1 Risk . . . 103
15.2 Reliability, Availability, Maintainability and Safety . . . 105

III Post Design **109**

16 Manufacturing, Assembly and Integration Plan **111**
16.1 Fuselage . . . 111
16.2 Wing Skin . . . 112
16.3 Internal Wing Structure . . . 113
16.4 Flaps and Ailerons . . . 114
16.5 Empennage . . . 114

17 Operations and Logistics **115**
17.1 Operational Support . . . 115
17.2 Post-DSE Planning . . . 116

18 Weight, Cost and Return on Investment **119**
18.1 Weight Budget . . . 119
18.2 Cost Budget. . . . 121
18.3 Cost Breakdown Structure . . . 122
18.4 Return on Investment . . . 123

IV Compliance and Conclusion **125**

19 Requirement Compliance Matrix **127**

20 Conclusion **129**
20.1 Recommendations . . . 130

Bibliography **131**

A Introduction to Zero Poisson's Ratio Skin **135**

List of Symbols and Abbreviations

Symbol	Variable	Unit
a	Acceleration	m/s²
a	Panel length	m
A	Aspect ratio	-
b	Wing span	m
B_p	Number of propeller blades	-
BPF	Blade pass frequency	Hz
c	Chord length	m
c_P	Specific fuel consumption	kg/J
C	Coefficient	-
D	Drag force	N
D	Total bending stiffness matrix	Pa
D_p	Propeller diameter	m
e	Oswald factor	-
E	Endurance	s
E	Young's modulus	Pa
f	Frequency	Hz
F	Force	N
F	Fuel flow	kg/s
$F.I.$	Tsaj-Hill index	-
g	Gravitational acceleration	m/s²
h	Height	m
H	Hinge moment	N · m
I	Moment of inertia	kg · m²
k	Stiffness	N/m
K	Non-dimensional mass moment of inertia	-
K_δ	Planform correction factor	-
l	Length	m
L	Lift	N
L	Rolling moment about X-axis	N · m
M	Bending moment	N · m
M	Mach number	-
M	Pitching moment about Y-axis	N · m
n	Load factor	-
N	Normal force	N
N	Yawing moment about Z-axis	N · m
p	Pressure	Pa
p	Roll rate	rad/s
P	Power	W
q	Pitch rate	rad/s
q	Shear flow	N/m
Q	Ply bending stiffness matrix	N/ m^2
r	Yaw rate	rad/s
R	Radius	m
R	Range	m
Re	Reynolds number	-
s	Distance	m
s_e	Control column pitch deflection	m

Symbol	Variable	Unit
S	Shear force	N
S	Wing area	m²
St	Strouhal number	-
t	Thickness	m
t	Time	s
T	Thrust	N
T	Torque	N· m
u^+	Non-dimensional parallel velocity	-
U	Flow velocity	m/s
U	Internal energy	J
U_τ	Frictional velocity	m/s
V	Airspeed	m/s
W	Weight	N
X	x-component of aerodynamic force	N
y^+	Non-dimensional wall distance	-
Y	y-component of aerodynamic force	N
Y	Yield stress	Pa
Z	z-component of aerodynamic force	N
α	Angle of attack	rad
α_δ	Airfoil lift effectiveness	-
β	Sideslip angle	rad
δ	Deflection	rad
γ	Flight path angle	rad
η	Propulsive efficiency	-
θ	Lay-up direction	rad
$\ddot{\theta}$	Angular acceleration	rad/s²
λ	Taper ratio	-
μ	Dynamic viscosity	kg/(m ·s)
μ	Non-dimensional mass	-
ρ	Air density	kg/m³
τ	Shear stress	Pa
τ_e	Elevator effectiveness factor	-
ω	Rotational speed	rad/s

Abbreviation	Description
CFD	Computational fluid dynamics
CFRP	Carbon fibre reinforced polymers
cg	Centre of gravity
EMC	Elastic Matrix Composite
FEM	Finite element method
MAC	Mean aerodynamic chord
MTOW	Maximum take-off weight
OEW	Operational empty weight
PEKK	Poly-Ether-Ketone-Ketone
PPS	Poly-Phenylene-Sulfide
ROI	Return of Investment
UHMW-PE	Ultra-high-molecular-weight polyethylene

1 Introduction

Inspired by birds that can change their wing shape according to their flight profile, morphing concepts are introduced in the aircraft industry aiming to improve flight performance across the entire flight envelope. Current aircraft are designed for multiple conditions, but they can only be optimal in one specific condition. In all other situations, they provide sub-optimal performance. In order to fly at the optimum condition in multiple cases, the aircraft shape should vary. Morphing aircraft can drastically change their shape during flight. Wing morphing concepts can be classified into three major categories: planform alternation, out-of-plane transformation, and airfoil adjustment. Morphing concepts are typically applied to experimental, unmanned, and military aircraft.

The mission is to design and develop a morphing, single engine propeller aircraft with improved performance characteristics, while maintaining the same level of safety and reliability. Therefore, the objective of this project is to improve a Cessna 172 Skyhawk using existing morphing concepts found in literature, within a catalogue price of €375,000 per aircraft, by 10 students in 11 weeks' time.

A renewed and improved aircraft requires a new name. The group has chosen the name Cessna Morphlight, which emphasises the morphing aspect while also stating the lightweight character of the superior aircraft. The Cessna Morphlight is capable of flying further and longer compared to the Skyhawk while carrying a higher useful load. In other words, the Cessna Morphlight provides 'more flight'.

The aim of this report is to provide the reader with the design process of the new Cessna Morphlight.

This report is structured in four parts. It starts with the outline of the project in Part I. This part includes the requirements, flow diagrams, market analysis, available budgets and the sustainable development strategy. Part II describes the design process followed to arrive at the final layout of the aircraft. Part III shows the production plan for the Cessna Morphlight along with the intended operational use, cost and return on investment for the company. Part IV states the compliance of the new Cessna Morphlight with the set of requirements. This part also contains the conclusions to this report.

Project Outline

The project outline provides the framework for this design project. It is used to define the requirements, functions, and viability for the aircraft. The project outline starts with a requirement analysis in Chapter 2. A functional flow diagram and a functional breakdown structure are provided in Chapter 3. The market analysis is performed and described in Chapter 4. Finally, Chapter 5 explains the sustainable development strategy.

2 Requirement Analysis

A thorough understanding of the requirements is essential for a suitable design fulfilling the needs of the stakeholders. Section 2.1 starts with an overview of the requirements as given by the stakeholders. Section 2.2 provides all system requirements. From the requirements, the mission profile of the aircraft was established in Section 2.3.

2.1. Top Level Requirements

Table 2.1 lists the requirements as set by the stakeholders for the Cessna 172 Skyhawk with morphing aspects called the Cessna Morphlight.

Table 2.1: Stakeholder requirements for the Cessna Morphlight

Category	Requirement		
Performance	Maximum range	$\geq$ 2,000	[km]
	Maximum endurance	$\geq$ 10	[h]
	Cruise speed	$\geq$ 250	[km/h]
	Cruise altitude	2,600	[m]
	Endurance altitude	$\geq$ 2,000	[m]
	Take-off ground roll	$\leq$ 200	[m]
	Take-off distance	$\leq$ 400	[m]
	Landing ground roll	$\leq$ 120	[m]
	Landing distance	$\leq$ 300	[m]
Safety and reliability	Compliance with regulations		
	Same safety as reference aircraft		
	Same reliability as reference aircraft		
	No additional maintenance for morphing aircraft over reference aircraft		
Sustainability	Take-off fuel consumption	$\leq$ 2.5	[L]
	Recyclability/reprocessability of morphing parts	80%	
Engineering budgets	Same engine power and fuselage dimensions as reference aircraft		
	Empty weight	$\leq$ 750	[kg]
	Take-off weight	$\geq$ 1,250	[kg]
	Fuel capacity	$\leq$ 200	[L]
	Morphing concepts only for wing, tail and landing gear		
Cost	Catalogue price	$<$ 375,000	[€]

2.2. System Requirements

The functional requirements and constraints for Morphlight are described in Tables 2.2 and 2.3 respectively. The constraints imposed by CS-23 certification specifications are found in Certification Specifications 23 [1].

From the market analysis (Chapter 4), an additional requirement was determined. The cruise speed of the aircraft should be higher than 277 km/h to be competitive with respect to the other aircraft in the market. This requirement is more stringent than the one provided as a top level requirement. However, it is not crucial to meet this requirement, but it is highly desirable to bring a competitive product to the market.

Table 2.2: Requirements for the Cessna Morphlight

Mission requirement	
REQ-MISS-1	This project shall improve a Cessna 172S Skyhawk using existing morphing concepts found in literature, within a budget of €375,000 per aircraft, by 10 students in 11 weeks' time
Functional requirements	
	Performance requirements
REQ-FUNC-PERF-1	The aircraft shall have a landing ground roll distance of at most 120 m at standard sea level conditions in the international standard atmosphere
REQ-FUNC-PERF-2	The aircraft shall have a take-off ground roll distance of at most 200 m at standard sea level conditions in the international standard atmosphere
REQ-FUNC-PERF-3	The aircraft shall have a maximum range of at least 2,000 km
REQ-FUNC-PERF-4	The aircraft shall provide an endurance time of at least 10 hours at loiter conditions
REQ-FUNC-PERF-5	The aircraft shall have a cruise speed of at least 250 km/h (Amended by REQ-FUNC-MRKT-1 to 277 km/h)
REQ-FUNC-PERF-6	The aircraft shall have a cruise altitude of 2,600 m
REQ-FUNC-PERF-7	The aircraft shall have a loiter altitude of at least 2,000 m
REQ-FUNC-PERF-8	The aircraft shall have a total landing distance of at most 300 m at standard sea level conditions in the international standard atmosphere
REQ-FUNC-PERF-9	The aircraft shall have a total take-off distance of at most 400 m at standard sea level conditions in the international standard atmosphere
REQ-FUNC-PERF-10	The aircraft shall have a range no less than the reference aircraft at cruise conditions
REQ-FUNC-PERF-11	The cruise speed shall be defined by the speed at 75% engine power
REQ-FUNC-PERF-12	The maximum range specified by REQ-FUNC-PERF-3 shall be obtained when transporting the payload described in REQ-CON-OPER-1
	Market requirements
REQ-FUNC-MRKT-1	The aircraft shall have a cruise speed of at least 277 km/h
	Safety requirements
REQ-FUNC-SFTY-1	The aircraft shall have the same safety as the reference aircraft
	Reliability requirements
REQ-FUNC-REL-1	The aircraft shall have the same reliability as the reference aircraft
REQ-FUNC-REL-2	The morphing systems on the aircraft shall not increase the maintenance frequency

Table 2.3: Constraints for the morphing aircraft

Constraints	
	Sustainability requirements
REQ-CON-SUST-1	The aircraft shall consume at most 2.5 L of fuel during engine start up, taxi, and take-off
REQ-CON-SUST-2	80% of the aircraft's morphing parts shall be recyclable
REQ-CON-SUST-3	The aircraft shall have a maximum fuel capacity of at most 200 L
	Weight requirements
REQ-CON-WGT-1	The aircraft shall have an empty weight of at most 750 kg
REQ-CON-WGT-2	The aircraft shall have a maximum take-off weight of at least 1,250 kg
	Operational requirements
REQ-CON-OPER-1	The aircraft shall be able to transport four persons (77 kg each [1]), including pilot(s), including luggage (54 kg), totalling 362 kg
REQ-CON-OPER-2	The aircraft shall provide accommodation for two pilots
	Propulsion requirements
REQ-CON-PROP-1	The aircraft shall have one internal combustion engine
REQ-CON-PROP-2	The maximum propulsive power provided by the aircraft shall be at most equal to that of the reference aircraft
REQ-CON-PROP-3	The aircraft shall be driven by a propeller
	Regulatory requirements
REQ-CON-REG-1	The aircraft shall comply with the EASA CS-23 certification specifications for normal, utility, aerobatic, and commuter category aeroplanes [1]
REQ-CON-REG-2	The aircraft shall carry reserve fuel, consisting of contingency fuel that is not less than 5% of the planned trip fuel and final reserve fuel to fly for an additional period of 45 minutes after performing the primary mission [2]
REQ-CON-REG-3	The aircraft shall have a minimum flight altitude of the sum of the maximum terrain or obstacle elevation, whichever is higher; plus 305 m [3]
	Geometrical requirements
REQ-CON-GEO-1	Morphing concepts shall only be applied to the wing, the tail, the landing gear and the engine of the aircraft
REQ-CON-GEO-2	The aircraft shall have the same fuselage dimensions as the reference aircraft
REQ-CON-GEO-3	The aircraft shall have a high wing mounted on top of the fuselage
	Economical requirements
REQ-CON-ECO-1	The cost of a single standard configuration aircraft shall be at most €375,000
	Resource requirements
REQ-CON-RSC-1	The project shall be completed within 11 weeks
REQ-CON-RSC-2	The project shall be completed by 10 students

2.3. Mission Profile

Based on the requirements, a mission profile for the aircraft can be drawn. Due to requirements REQ-FUNC-PERF-3 and REQ-FUNC-PERF-4, there are two possible mission profiles, depending on the choice of the operator. The mission profile for the range requirement is shown in Figure 2.1, while the endurance requirement's mission profile is shown in Figure 2.2.

For both missions, the aircraft has to stay in the air for another 45 minutes after the main mission, before landing [2]. This is usually to account for waiting times at the airport, before a landing strip becomes available. The aircraft must have sufficient fuel reserves on board for 45 minutes. Additionally, contingency fuel of 5% of the total trip fuel must be on board.

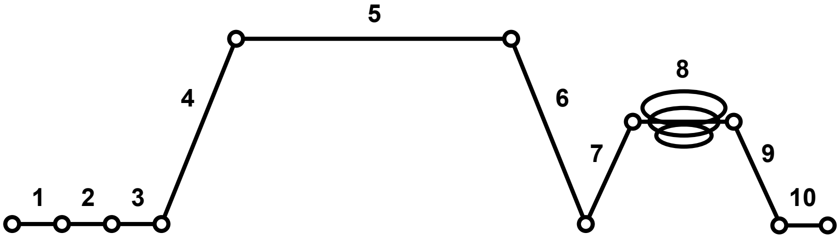

Figure 2.1: Mission profile for cruise and maximum range

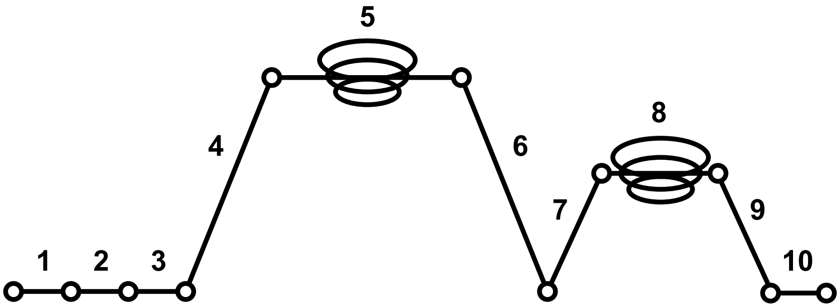

Figure 2.2: Mission profile for endurance

The stages of the mission profile are described in Table 2.4.

Table 2.4: Description of mission profile legs

Leg	Description	Details and Constraints
1	Engine start and warm up	
2	Taxi	
3	Take-off	Take-off ground roll ≤ 200 m; Total take-off distance ≤ 400 m; Cumulative fuel consumption leg 1-3 ≤ 2.5 L
4	Climb	Climb to mission altitude
5a	Cruise	Cruise speed ≥ 250 km/h; Cruise altitude 2,600 m
5b	Cruise	Maximum range cruise; Leg distance ≥ 2,000 km; Altitude > 305 m
5c	Loiter	Leg duration ≥ 10 h; Loiter altitude ≥ 2,000 m
6	Descent	Descend to airport
7	Climb	Climb to holding area
8	Loiter	Wait for landing slot; Leg duration: 45 min
9	Descent	Descend to airport
10	Landing	Landing ground roll ≤ 120 m; Total landing distance ≤ 300 m
	Complete mission	Fuel consumption ≤ 200 L (minus reserve and contingency fuel)

3

Functional Flow Diagram and Functional Breakdown Structure

The Functional Flow Diagram in Figure 3.1 shows the order of functions which the aircraft needs to perform. The top level shows all steps in the mission of the aircraft, namely pre-flight operations, take-off, flying, landing, and maintenance.

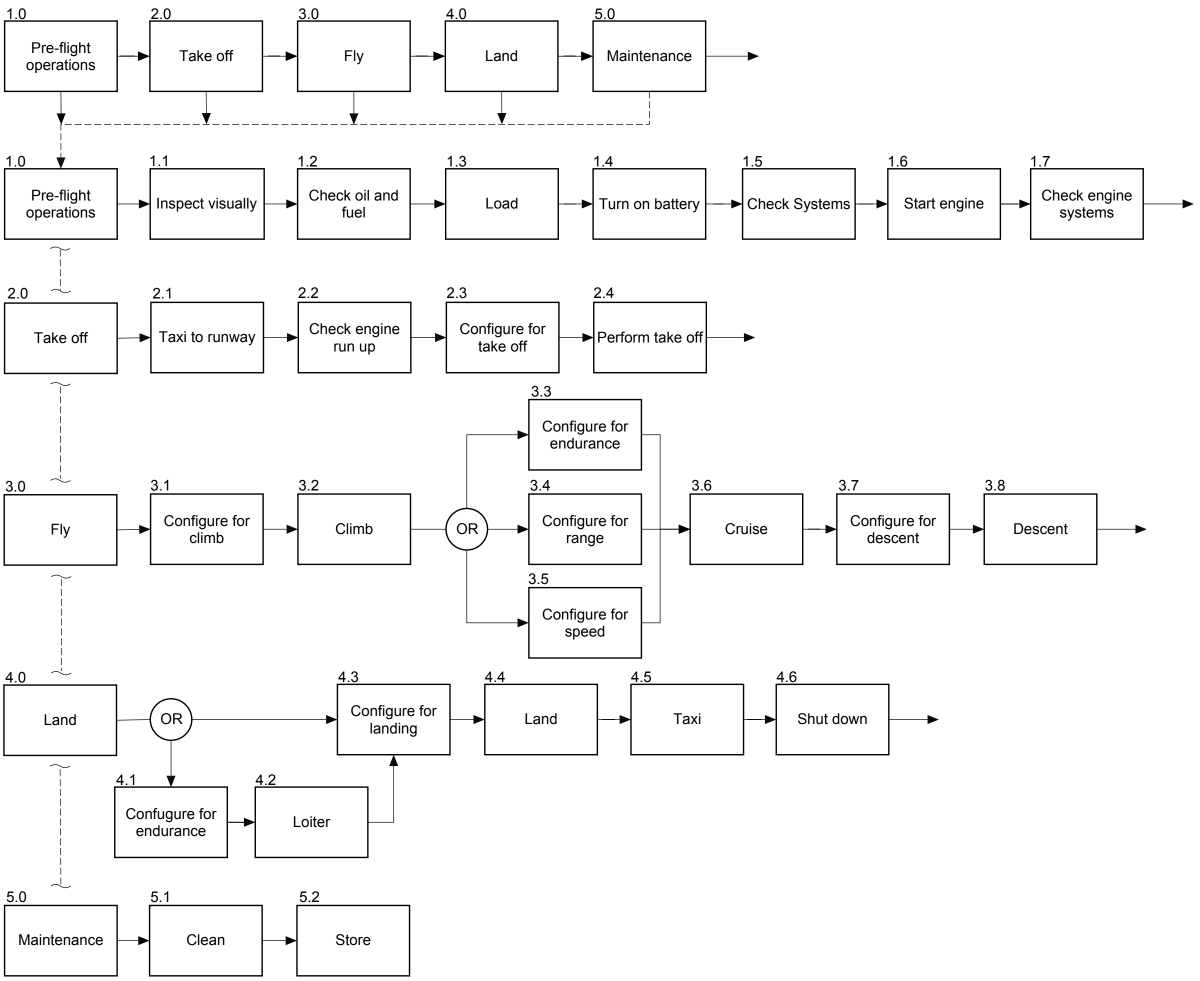

Figure 3.1: Functional Flow Diagram

The Functional Breakdown Structure shown in Figure 3.2 represents the functions which the aircraft must perform.

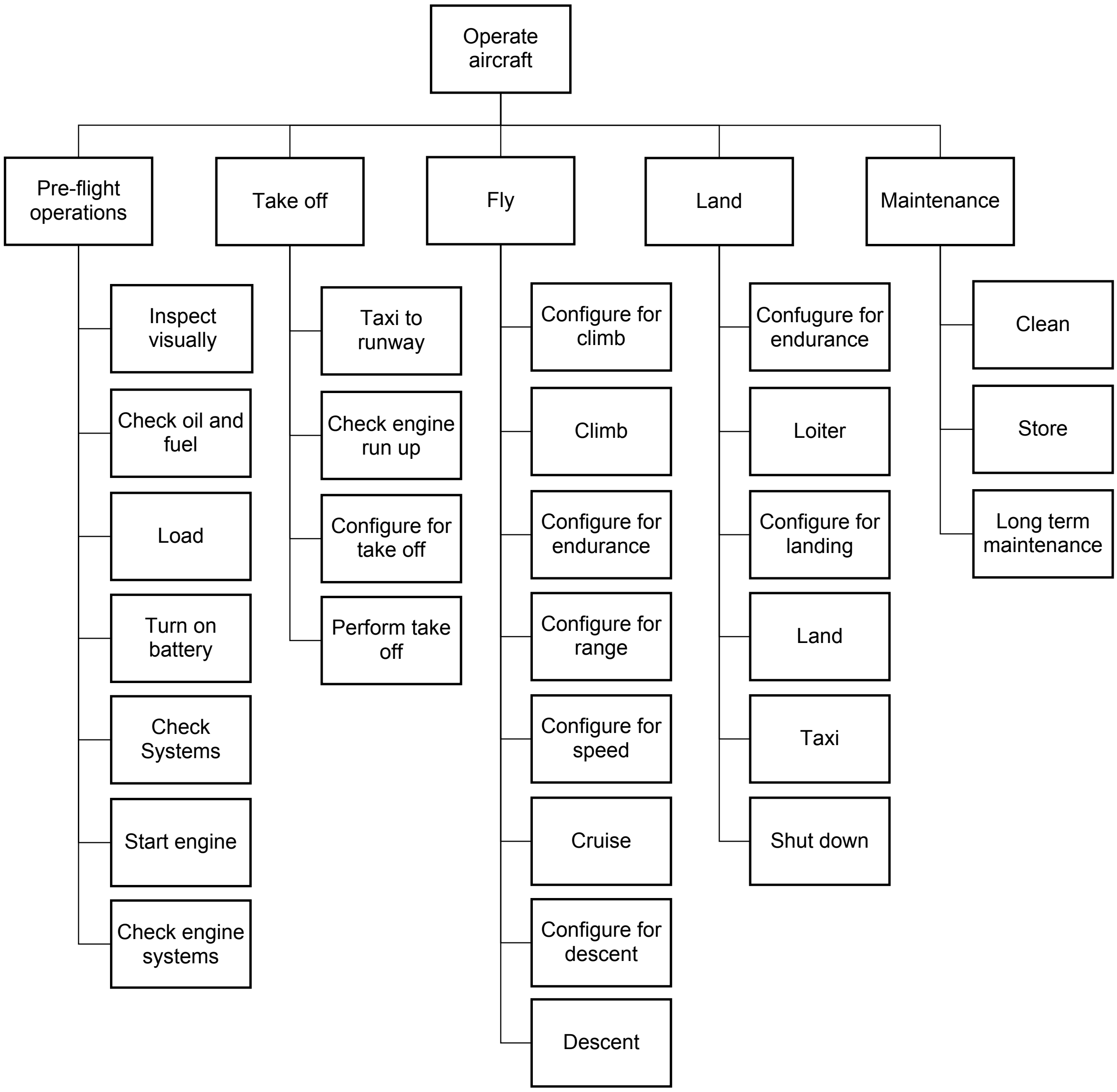

Figure 3.2: Functional Breakdown Structure

4 Market Analysis

The purpose of designing and producing a new aircraft is mainly driven by profit, although an eye must be kept on environmental effects. In order to make sure that a new product will do well, it is important to have knowledge about the target market. This chapter is dedicated to the market analysis. It handles the primary use of the Cessna Morphlight and evaluates the current competitors on the market. The age of the current general aviation (GA) plays a role in maintenance costs and is assessed as well. Furthermore, it discusses the possible advantages to be gained based on estimated fuel price development and possible near future changes in aviation legislation. Lastly, speculations of future markets are presented in this chapter as well. Since the general aviation market is dominated by United States manufacturers and customers, the emphasis is on the US market.

4.1. Primary Use

Aircraft only sell if the aircraft fulfils a certain need of a customer. For that particular reason, it is important to know the primary activities or problems which form the motivation of buying a four-seat single-engine piston aircraft.

According to the General Aviation Manufacturers Association (GAMA), 48% of the total hours flown by single engine piston aircraft in 2014 was personal flying, 27% was instructional and 11% was business [4, p. 24]. The large share of instructional flights emphasises the need to have a dual control layout, increasing the versatility of the aircraft. This is linked to REQ-CON-OPER-2. On the business side, the Cessna 172 is an excellent aircraft for aerial photography and sightseeing due to its high wing configuration. In order to safeguard this market, a geometrical constraint has been placed on the wing configuration (see REQ-CON-GEO-3).

4.2. Competitors

To ensure a sales realisation which renders a favourable return on investment, it is crucial to deliver a product for which a high demand exists. This can be accomplished by designing a product with superior characteristics with respect to its competitors. For that particular reason a close look is taken at the current aircraft which will share a common market with the Cessna Morphlight. Parameters such as maximum range and maximum endurance are considered to be of great importance for a customer. An analysis of the purchase and operational costs of the aircraft is performed as well. A selection of 11 aircraft form the basis of the competitor analysis. The aircraft are selected based on their single engine and four seat configuration. A list of the reference aircraft can be found in Table 4.1.

Table 4.1: The selected aircraft for the market analysis and their respective price

Aircraft	Catalogue price [$]
Cessna 172S Skyhawk	289,500
Cessna 182Q Skylane I	390,300
Cessna T182T	443,500
Cirrus SR20	441,050
Cirrus SR22 G3	449,000
Diamond DA40 Star	337,900
Mooney Ovation2 GX	434,275
Piper Archer III PA-28-181	299,500
Piper Arrow PA-28R-201	344,950
Piper Warrior III PA-28-161	290,000
Robin 160A Long Range	292,620

Buying an aircraft will allow the customer to travel a certain distance or stay in the air for a limited amount of kilometres or minutes, respectively. An expensive aircraft is expected to have a greater range or longer endurance. To compare the various aircraft, the prices a customer has to pay which enables him to travel one kilometre or stay in the air for one minute are plotted per aircraft. Additionally, the cruise speed is taken into consideration as well.

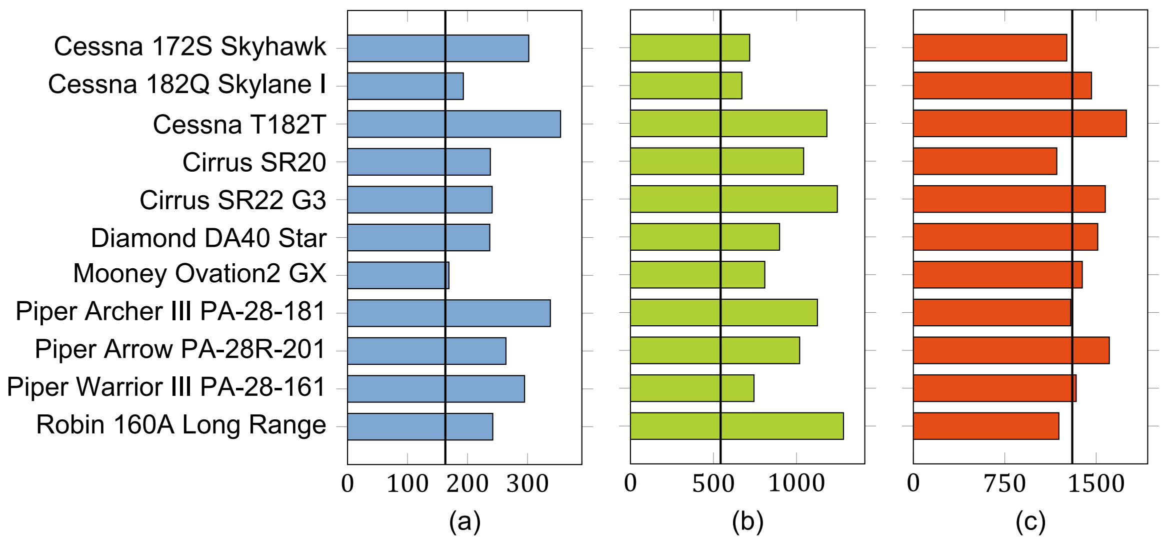

Figure 4.1: Costs (in $) for various reference aircraft. The vertical line indicates the cost of the Cessna Morphlight at its requirements and maximum catalogue price. (a) Cost per km in max range (b) Cost per minute in max endurance (c) Cost per km/h at cruise conditions

A distinction must be made between the aircraft depending on the price. Aircraft which cost more than $300,000 are handled differently in the market analysis. In order to be economically pleasing, the Cessna Morphlight must be able to show improved performance over the aircraft which cost less than $300,000. Failing to do so will make the customer decide to buy their aircraft elsewhere. Strong selling points can be thought of if the Cessna Morphlight outperforms current competing aircraft while costing less.

In order to produce an aircraft which has best value for maximum range, maximum endurance and cruise speed (see Figure 4.1), the Cessna Morphlight must be able to fly at least 1,931 km, be able to stay in the air for at least eight hours and six minutes, and have an efficient cruise speed of at least 277 km/h. Only the cruise speed criterion is not met by the requirements as stated in Section 2.2. In order to make the aircraft competitive, the cruise speed requirement is increased to 277 km/h.

The Cessna Morphlight must be able to take off in less than 200 metres, as stated in REQ-FUNC-PERF-

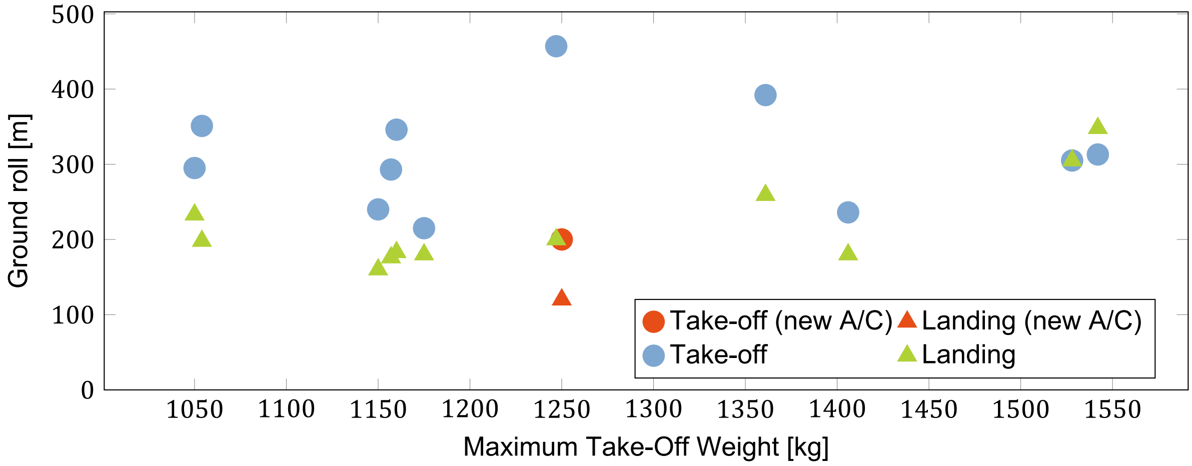

Figure 4.2: Landing and take-off distances versus maximum take-off weight of reference aircraft. No clearly visible correlation exists between the maximum take-off weight and the take-off ground roll, this is true for the landing ground roll as well

2. By looking at Figure 4.2 it becomes clear that this is a liable characteristic. The landing ground roll of 120 m will be more difficult to realise as the lower values for reference aircraft lie around 180 metres. This does mean, however, that the morphing aircraft will have the possibility to be deployed at limited length runways, improving the versatility of the aircraft.

The useful load of the Cessna Morphlight must be at least 500 kilograms as the empty weight shall not exceed 750 kilograms and the maximum take-off weight must be at least 1,250 kilograms. From the 11 selected aircraft, only three have a useful load higher than 500 kilograms, all costing more than 390,000 dollars. If the useful load of the Cessna Morphlight can be realised, it will excel in utility missions.

The significantly lower prices for second hand aircraft form a threat for the new Cessna Morphlight. The lower segment prices for a second hand Cessna 172 vary from 30,000 to 60,000 dollars. A potential customer must be convinced that the Cessna Morphlight is worth the difference in purchase cost because of the improved efficiency and flight characteristics. The importance of efficiency is stressed by the next section.

4.3. Current Fleet

The average age of single-engine piston aircraft in the US in 2014 was 40.7 years [4, p. 32]. This corresponds to the large increase in (US) production observed in the 1960s and 1970s in Figure 4.5. These aircraft are used beyond the flight hours and years they were originally designed for. A large share of the GA fleet was designed in accordance with the now outdated Civil Aviation Regulations (CAR) 3. The CAR3 certification lacks fatigue and continued airworthiness requirements [5]. As a consequence, little can be said about the ultimate lifetime of single-piston aircraft from that era.

Due to fatigue and corrosion, maintenance costs will increase over time. Also, mechanical failures are gradually introduced over the lifetime of the aircraft and will increase downtime, leading to a possible loss of income if the aircraft is used for commercial purposes. This favours the purchase of a reliable new aircraft. The number of flight hours per aircraft per year decreased from about 130 in the year 2000, to 90 in 2014 [4, p. 27]. The irregular use of an aircraft has a deteriorating impact on the condition of the aircraft [5, p. 6] and will even further increase maintenance.

4.4. Fuel Prices

After the oil crisis during the 1970s, fuel prices stabilised around $1 per gallon. At the start of the 21st century, fuel prices started rising to record highs (Figure 4.3). After the 2008 financial crisis, prices initially dropped sharply, only to increase again in the following years, to oscillate around $4 per gallon between 2011 and 2014[1]. In ten years, the fuel prices quadrupled.

An increase in fuel prices correlates to a decrease in flight activity and sales of general aviation aircraft. Behind the state of the economy, fuel prices are the most important driver for aircraft sales [6]. Figure 4.3 clearly shows big drops in flight activity after the recession of the early 1990s (with an associated increase in fuel prices), and parallel to the fuel price increase from 2000 onward. Around 1997 there is a temporary increase in flight activity, in phase with a short drop in fuel price.

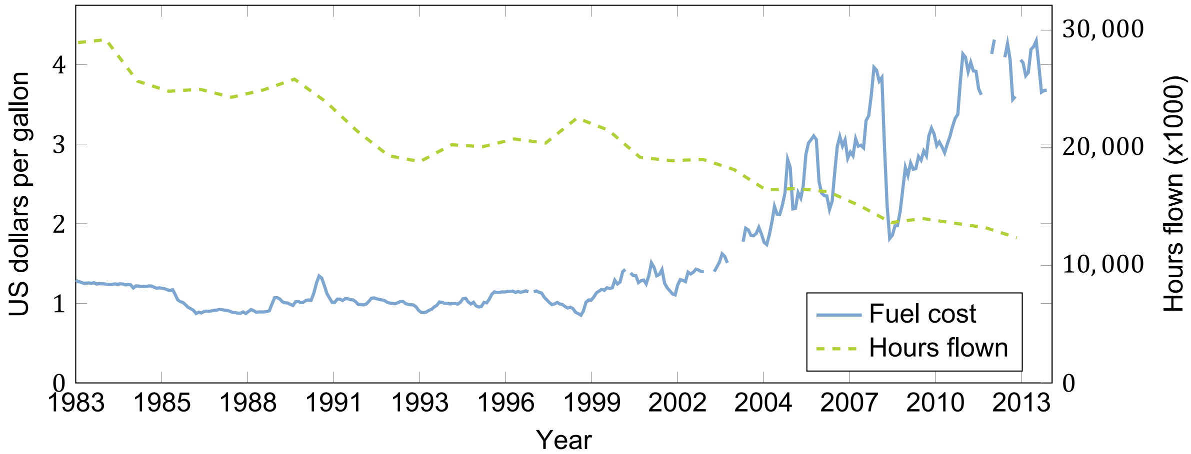

Figure 4.3: U.S. aviation gasoline retail sales by refiners (1983–2014) and total hours flown by US general aviation aircraft[1] [4]. For some months, fuel price data is unavailable.

From a rough analysis of the fuel consumption of the reference aircraft, it can be concluded that the fuel cost amounts to about 20% of the total expenses, excluding any taxes and maintenance costs. This calculation assumes the purchase of a new aircraft and operating it for 20 years.

4.5. Legislation

As of June 2013, the Federal Aviation Administration (FAA) issued a request for a candidate fuel which can replace the Low-lead 100 fuel currently used in light aircraft general aviation. It has started many industrial collaborative efforts in order to do so. The goal is to find a replacement fuel which least effects the general aviation fleet. The Airline Reporting Corporation (ARC) has performed user acceptance tests which showed that *"no market driven reason exists to move to a replacement fuel due to the limited size of the avgas market, diminishing demand, speciality nature of avgas, safety, liability, and the investment expense involved in a comprehensive approval and deployment process"* [7].

A hybrid aircraft will undergo limited consequences in both performance and economic properties due to fuel changes. The FAA is committed to the development of a new unleaded fuel by 2018. This shows that the design of an efficient and low emission aircraft may result in advantages due to a change in legislation over the next couple of years, as the production of unleaded fuel is highly likely to be more costly.

4.6. Future Market

The number of general aviation aircraft produced over the past decades is illustrated in Figures 4.4 and 4.5, worldwide and in the US respectively. Aircraft sales boomed in the 1960s and 70s but have since been more constant. Around 1970, there was an oil crisis. The big drop in produced units around 1980, is largely due to rapidly rising product liability costs [8, p. 975]. Over the course of 24 years, the costs per aircraft saw a 2,000-fold increase. Starting in 1995, sales have risen to peak in 2007, just before the start of the financial crisis. Consequently there was a sharp decrease in the aircraft production. Worldwide sales fell down, especially in the most prominent market, the USA, which additionally saw

[1] `http://www.eia.gov/dnav/pet/hist/LeafHandler.ashx?n=PET&s=EMA_EPPV_PTG_NUS_DPG&f=M` [cited 23 April 2015]

its market share diminish by almost 15% in just two years [4, p. 14].

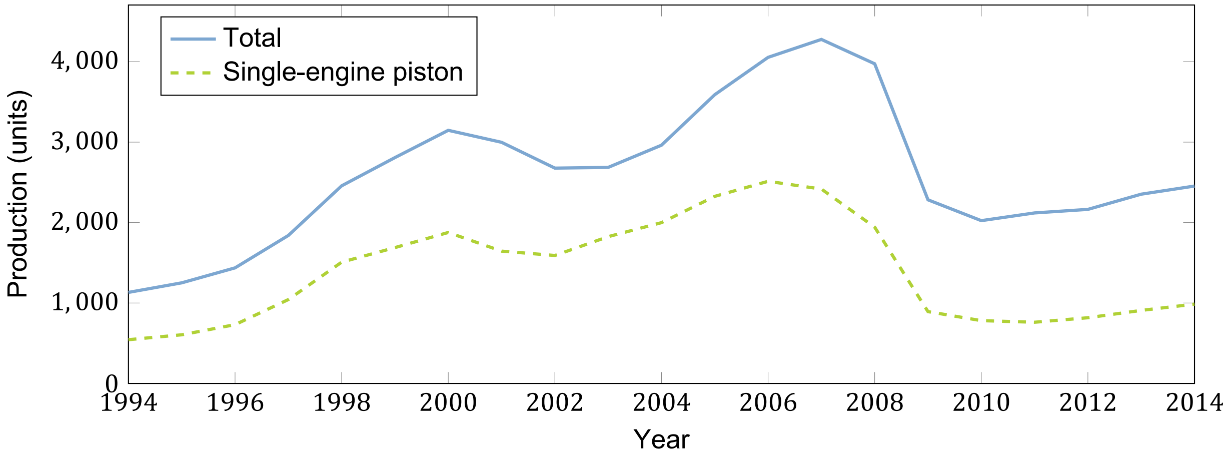

Figure 4.4: General aviation airplane shipments manufactured worldwide (1994–2014) [4, p. 13]

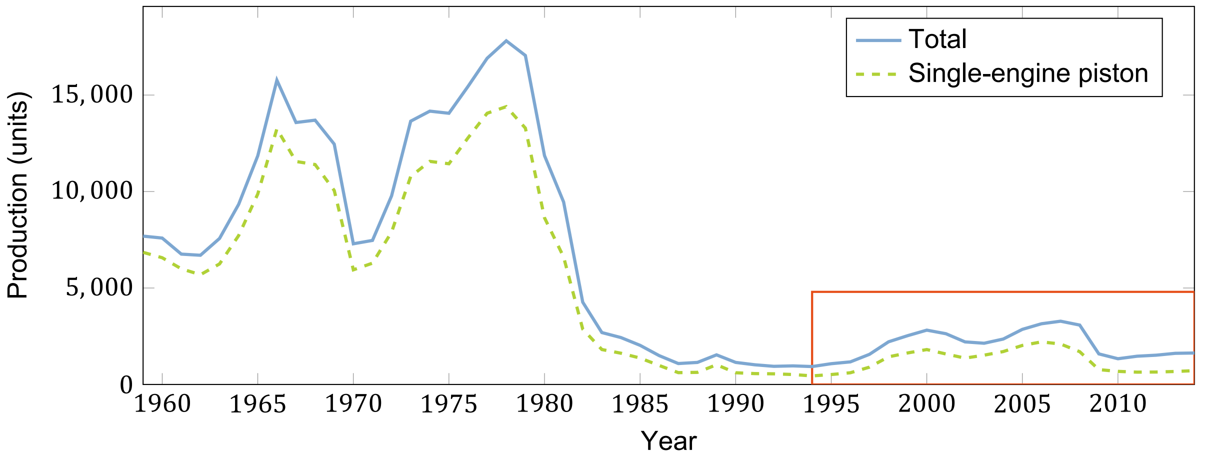

Figure 4.5: U.S.-manufactured general aviation airplane shipments (1959–2014) [4, p. 20]. The rectangle encapsulates the years shown in Figure 4.4 for the entire world.

The number of piston aircraft actively flying in the US is expected to decrease by 0.4% per year (7.7% in total) for the period 2013-2034. All other aircraft categories are expected to have an increase in demand, even up to 3.0% per year for business jets [4, p. 25]. Nevertheless, older aircraft are continuously phased out, so there will still be a demand for new aircraft.

Cessna sold 3,176 units of the 172S between 2000 and 2014 (averaging at 212 per year) [4, p. 18]. Figure 4.6 gives an overview of the annual production of Cessna's 172 and 182 models. As discussed in Section 4.4, the number of aircraft sales dropped after the financial crisis in 2008. For Cessna, this meant the number of 172S sales reduced to circa 100 per year, with a sudden increase to 155 in 2014. If the economy continues to recover, sales are likely to go up, continuing the (small) positive trend of the past four years. Given that the Cessna Morphlight has better characteristics than the currently available competition, first time buyers or owners of different classes of aircraft might be interested. Based on this and the average number of sales over the past decade, selling circa 100-200 aircraft per year seems like a plausible aim.

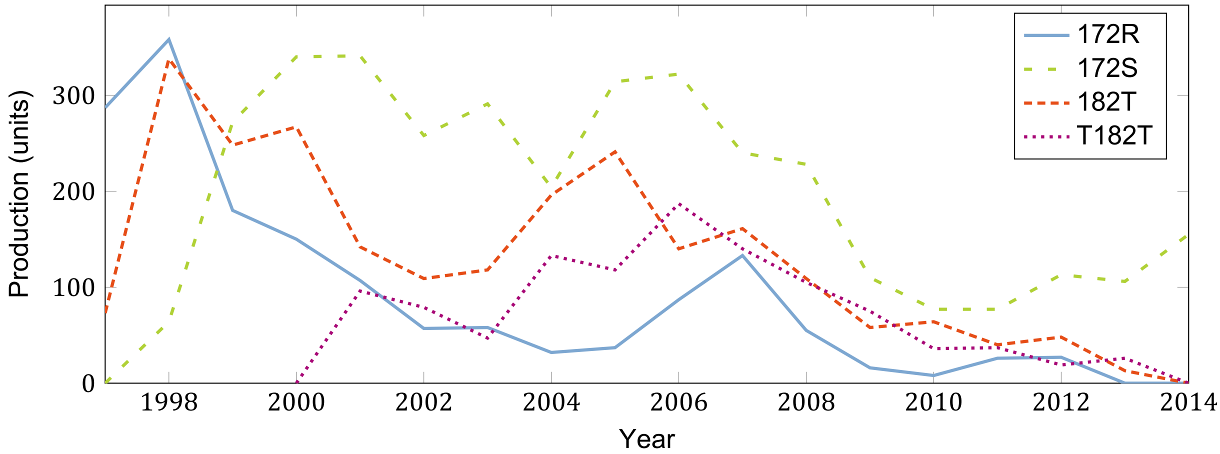

Figure 4.6: Cessna 172 and 182 shipments from the start of the production of the 172S (1997) until 2014 [4, 9]

5 Sustainable Development

This chapter shows how sustainability is taken into account during the design of the Cessna Morphlight. A sustainable aircraft operates efficiently, reducing its environmental impact. An increase in efficiency can be gained by actively adapting the shape of aerodynamic surfaces. Regardless of the aircraft's mission, drag can be reduced. Complex systems are required however for proper shape control, which may result in a heavier and less reliable design. The following precautions have been taken or can be taken to avoid this.

- Requirements on the system are verified and validated, avoiding unachievable requirements and an over designed or less reliable product.
- Snowball effects are avoided through thorough structural load and weight estimations.
- A simple design, which keeps the number of moving parts to a minimum, will limit the weight and power consumption, and maximise reliability.
- Morphing concepts are only used on the wing, tail and landing gear to limit cost and complexity.

The first major decision touching upon the sustainability requirement is the choice of material. A logical option would be to use the main material which is utilised in the Cessna 172: aluminium. Recycling aluminium is straightforward and cost efficient. Carbon fibre would lead to a lighter structure, but is more complex to recycle. The fibres, still possessing their original strength, can be extracted to 99% purity by wet degradation of the polymer matrix, discarding the polymer as waste. A more efficient method is to use a thermoplastic matrix; the fibres and polymer can be separated with minimal degradation. Composite components can be easily repaired or reformed. The thermoplastic behaviour must be taken into account for all flight conditions. After dismantling the aircraft, the material of the tires can be re-used in the production of tractor tires and windows can be melted and applied for a different use. Electronics can be stripped down to component level as well and used in the assembly of other systems.

Another big source of pollution is the engine. In 2002 it was estimated that 45% of the yearly emitted lead in the United States came from the usage of leaded avgas (100LL) [10]. In order to reduce emission, a different engine is used that does not consume 100LL. Few airfields supply unleaded avgas fuels at the moment, so the engine shall run on the more commonly available Diesel or Jet A-1.

Finally, Cessna's production facilities are located at a significant distance from each other. Structural manufacturing facilities are situated in Chihuahua, Mexico, while the assembly line is located in Independence, Kansas. Centralisation would greatly reduce transportation emissions. Further sustainability can be gained through usage of solar energy, hydropower, or wind energy by production and assembly facilities.

II

Design

This part of the report describes the design steps that are performed to develop an aircraft that meets the requirements as determined in Part I. The design phase includes an initial investigation into the potential design options in Chapter 6. The second part of the design phase is the selection of a suitable aircraft configuration. This is described in Chapter 7. With the global aircraft configuration determined, the aircraft can be designed in detail. This is described in Chapters 8 through 15.

6

Design Options

In this chapter the different design options for the Cessna Morphlight are analysed and possible configurations are considered. The potential means of morphing, benefits and drawbacks are described.

Sweep

A variable sweep wing is called a swing wing. Pivoting of the left and right wing around individual pivot points is a method of changing wing sweep. The advantage of a swept wing is primarily in high speed performance. The disadvantages of sweep are mainly on aerodynamic performance and structural weight. Finally, sweep has a negative effect on stall characteristics. Because of the disadvantages of using variable sweep on a low speed aircraft this design option will not be considered in the further design.

Span

Increasing the wing span results in a higher aspect ratio as well as a larger wing planform area. A higher aspect ratio has the beneficial effect that the lift over drag ratio increases, which provides for a longer loiter time and a larger range. It also results in a lower roll angular acceleration and thus in poor manoeuvrability, which is usually not preferred, and a lower maximum speed. The induced drag of an aircraft with a high aspect ratio is lower than for a low aspect ratio, however parasitic drag increases. A higher wing planform area causes higher lift as well as more parasitic drag.

The importance of span morphing can be supported with the use of the following derivation. The drag has two components, the profile and the induced drag, as in Equation (6.1). In steady symmetric flight, the lift will equal the weight. Therefore, C_L can be rewritten as in Equation (6.2). The induced drag can be rewritten as in Equation (6.3).

$$C_D = C_{D_0} + C_{D_i} \quad (6.1) \qquad C_L = \frac{2W}{\rho V^2 S} \quad (6.2) \qquad C_{D_i} = \frac{{C_L}^2}{\pi A e} \quad (6.3)$$

For the range, the optimum flight condition is $\left(\frac{C_L}{C_D}\right)_{max}$ [11]. When substituting Equations (6.1)-(6.3) in this condition, and differentiation with respect to the airspeed and equating this to zero yields the optimum speed for range, as in Equation (6.4).

$$V_{range,opt} = \frac{\sqrt{2 \cdot W}}{b^{3/4} \cdot \sqrt[4]{\pi \cdot c \cdot C_{D_0} \cdot e} \cdot \sqrt{\rho}} \quad (6.4) \qquad \left(\frac{C_L}{C_D}\right)_{max} = \frac{1}{2} \cdot \frac{\sqrt{\pi \cdot b \cdot e}}{\sqrt{c \cdot C_{D_0}}} \quad (6.5)$$

Now this optimum speed can be substituted in the condition for $\left(\frac{C_L}{C_D}\right)_{max}$. The result is shown in Equation (6.5). Here it can be seen that a higher span increases the ratio, which increases the range.

The span extension can be done telescopically, consisting of one or more spanwise sections that slide into each other like a telescope. The advantage is the relative simplicity and rigidity of the structure.

Chord

Increasing the chord length will decrease the thickness ratio, thus improving the high speed airfoil performance. The chord extension enlarges the wing surface resulting in an increase in lift and load factor capability, though it also increases parasitic drag. When the wing plan area is kept constant, enlarging the chord results in a decrease in parasitic drag, which is beneficial when flying at a higher airspeed. This is due to the decrease in wing aspect ratio. Decreasing the chord length will improve the range, as shown by Equation (6.5), and the turn rate and decrease the engine requirements [12].

Twist

Wing twist can be used to prevent tip stall and to improve the wing lift distribution [12]. The twisting motion can be achieved by using a pivot connection to adjust the incidence angle of either the entire wing, or only a section of the wing. The wing incidence angle is mainly used to assure a level cabin in cruise flight. Twisting of the wing tip is used to adjust the lift distribution over the wing.

Dihedral

Increasing the wing dihedral increases the rolling moment capability and improves the lateral stability, while decreasing the maximum speed [12]. It is expected that changing the dihedral is not beneficial for the Morphlight.

Camber

The most common way to accomplish camber morphing is by using a discrete trailing edge flap. This method is conceptually simple and has been proven over the years, however it does not come without its drawbacks. The sharp, discrete change in camber leads to a high increase in drag over the baseline airfoil and early flow separation at the trailing edge limiting the maximum lift coefficient. This is overcome by using slotted Fowler flap trailing edge high lift devices. These use a gap to reattach airflow. The camber of an airfoil has a direct effect on the C_l and C_d coefficients.

Thickness

The optimum wing thickness depends on the flight speed and other requirements. A small thickness is better for drag at a higher airspeed, while a high thickness results in a lower structural weight, because of a larger bending inertia of the wing. Thicker wings are able to obtain a higher maximum lift coefficient. The wing thickness usually varies from the root to the tip. The advantages of this are a reduced structural weight and more available fuel volume.

Fuselage

The possible fuselage morphing concept is the landing gear retraction, which is done by most medium and high speed aircraft. Landing gear retraction is also implemented in the Cessna 172RG Cutlass, which rotates the nose landing gear forward into the fuselage and the main landing gear rearwards. This reduces aerodynamic drag, but will also increase weight due to the implementation of moving parts. A retractable landing gear adds about 1.4% of the maximum take-off weight to the total aircraft weight [13]. This can be considered as a feasible option for the Morphlight.

Engine

For propeller aircraft the propeller pitch can be changed to increase engine performance under different flight conditions. In order to reach the requirement limiting the fuel on take-off to 2.5 litres, fuel saving measures are investigated. An engine change is desired. Engine options include a more efficient conventional engine, a hybrid engine – consisting of a conventional engine assisted by an electric motor, and an electric power unit.

7

Configuration Trade-off

When the different design options for the morphing are analysed an optimal combination of those options has to be selected. To find the optimal configuration first fifteen different configurations are chosen. Then using a preliminary trade-off the five best configurations are selected. This is explained in Section 7.1. From these five promising configurations, a more detailed trade-off is made which is described in Section 7.2 in order to find the best configuration of the remaining five. Finally two different layouts for all the morphing systems are created and from those layouts again the best one is selected using a trade-off. This process is explained in Section 7.3

7.1. Preliminary Trade-off

The research of the design options provided some preliminary knowledge about the performance of each different different design option. For example changing the sweep of the wing will not be beneficial because of the low cruise speed the Morphlight will fly at. On the other hand, some other morphing options seem more promising than other options. Span morphing will be better for the performance than changing the dihedral or thickness. Using this preliminary knowledge the first fifteen combinations of morphing concepts are created and these can be seen in Table 7.1. The configurations are chosen in such a way that the most promising morphing concepts are used in more configurations than the less promising concepts. This is to reduce the amount of configurations in the trade-off. Therefore there are more configurations that use a combination of span and chord than there are configurations using a combination of gull and thickness.

In this preliminary trade-off the categories on which each configuration is rated are range, endurance, take-off distance, landing distance and weight. Using preliminary equations to estimate these values finally five configurations are selected. The trade-off process is mostly based on eliminating the configurations that are not likely to meet all performance requirements. As can be seen in Table 7.1, these five configurations have been highlighted: 3, 6, 9, 11 and 13. These will be used in the detailed trade-off.

7.2. Detailed Trade-off

After the selection of the five most promising configurations a more in depth trade-off is performed to find the best configuration. When looking at Table 7.1 it can be seen that configurations 6 and 11 are the same as configurations 9 and 13 respectively, but then with twist added. From the design option research it can be concluded that twist morphing can be added relatively easily by simply twisting a small section of the wingtips. Therefore configurations 6 and 11 are not considered in the trade-off for simplicity. Later during the design it will be investigated whether twist will be added or not.

Also, when looking one step ahead to the selection of different layouts for each configurations, it is concluded that there are two completely different ways to morph the span of an aircraft. One concept uses an extending structure covered by a zero Poisson's ratio skin that will stretch to provide the extra

Table 7.1: Fifteen configurations using different morphing concepts, the five highlighted configurations are chosen as the best configurations

Configurations	Span	Chord	Twist	Dihedral/ Gull	Camber	Thickness
1	x	x				
2	x	x		x		
3	x	x	x		x	
4	x	x				x
5	x		x			
6	x		x		x	
7	x			x		
8	x			x	x	
9	x				x	
10	x					x
11		x	x		x	
12		x		x	x	
13		x			x	
14		x				x
15			x		x	x

required outer skin when extending a wing. The other concept uses a telescopic extension, using for example metal sheets sliding over each other to provide the extra required skin. These two concepts differ significantly with respect to each other in terms of performance, weight, cost and risk. For this reason in this trade-off these are treated as two different concepts. In this trade-off the configurations using the zero Poisson skin will be denoted with the character A and the configurations using telescopic extension with the character B. The zero Poisson ratio skin is explained in more detail in Appendix A.

7.2.1. Trade-Off Method, Criteria and Weights

The criteria in this trade-off are different than those of the preliminary trade-off. In this selection the performance, weight, cost and risk/RAMS are evaluated in more detail and a relative importance between the criteria is considered as well. Furthermore, in the performance criterion, range, endurance, take-off and landing distance and cruise characteristics are grouped. The weights of the four criteria are determined by using the analytic hierarchy process (AHP). Each project member determined the relative importance between the criteria, after which the points were averaged, summed and normalised as can be seen in Table 7.2.

Table 7.2: Configuration trade-off criteria weights

	Performance	Weight	Cost	Risk/RAMS	Sum	Normalised sum
Performance	1	1.632	2.489	2.195	7.315	0.378
Weight	0.613	1	2.208	2.439	6.259	0.324
Cost	0.402	0.453	1	1.252	3.106	0.161
Risk/RAMS	0.456	0.410	0.799	1	2.665	0.138

From Table 7.2 it can be seen that performance is ranked as the most important. This is in line with the requirements, because the largest increase in performance is required. The second most important criterion is the weight, since the weight of the improved aircraft is required to be approximately the same as the reference aircraft. It is therefore essential that the morphing wing does not increase the weight more than what could realistically be saved on other parts of the aircraft. The cost criterion is not rated as high, because the cost is allowed to increase over the reference aircraft. Nonetheless, it is important that the cost of the systems stay within a reasonable bound. Finally, the risk/RAMS criterion was also not rated as high as performance and weight, because all morphing concepts are mostly of an experimental nature. Therefore, any morphing aircraft design will have risk associated to the morphing concepts, but that will have to be accepted in order to meet the performance requirements.

7.2.2. Trade-off Table and Configuration Selection

The performance of each configuration is assessed by using preliminary calculations for the design options combined in one configuration. The weight of a configuration is assessed according to how many mechanisms are needed and also if the required mechanisms are complex and heavy. For example, chord and camber morphing combined can be done with a flap system, which is relatively simple, however a telescopic span extension system is relatively heavy. The cost is estimated based on the required materials, how much research will have to be done and how many mechanisms are required. The risk is related to the design maturity of the options. The ratings for each criterion, ranging from 0 to 20, are entered into Table 7.3.

First it is determined if the configuration exceeds, meets or almost meets the requirements or if it is unacceptable for the given criteria. This is indicated by the colours in Table 7.3. Afterwards a rating is given between 1 and 20, which is used to calculate which configuration is best. Points will be around 15, 10 and 5 for the green, blue and yellow boxes respectively. In this way, small differences between configurations can be identified.

Table 7.3: Trade-off for morphing configuration; A indicates the use of zero Poisson skins for span morphing, B indicates telescopic wing span morphing. All performance is assessed with 20% camber

Configuration	Performance (38%)	Weight (32%)	Cost (16%)	Risk/RAMS (14%)
Span-camber-A	(12) 84% span morphing required	(10) Nominal	(6) Expensive materials and research for zero Poisson skin	(7) Material tested only on small scale. Span morphing has relatively easy maintenance. Average failure risk
Span-camber-B	(10) 84% span morphing required; camber morphing only over part of wing	(8) Heavy mechanisms: telescopic span mechanism is heavy	(11) Nominal	(10) Extrapolated from current design. Span morphing has relatively easy maintenance. Average failure risk
Span-camber-chord-A	(18) 50% span morphing and 24% chord morphing required	(8) Many mechanisms	(4) Expensive materials and research for zero Poisson skin	(5) Material tested only on small scale. Most morphing systems: failure more likely
Span-camber-chord-B	(15) 50% span morphing and 24% chord morphing required; camber morphing only over part of wing	(6) Many and heavy mechanisms: telescopic span mechanism is heavy	(9) Many mechanisms	(8) Extrapolated from current design. Most morphing systems: failure more likely
Chord-camber	(0) 130% chord morphing required: unrealistic	(15) Simple system	(15) Simple system	(12) Extrapolated from current design. Chord maintenance more complex. Least morphing systems: failure less likely

Green	Excellent, exceeds requirements	White	Correctable deficiencies
Blue	Good, meets requirements	Red	Unacceptable

The total scores for the configurations are displayed in Table 7.4. It can be seen that the configuration with span, camber and chord morphing, using the zero Poisson skin concept, is rated best.

Table 7.4: Final score for configurations

Configuration	Score
Span-camber-A	9.708
Span-camber-B	9.523
Span-camber-chord-A	10.730
Span-camber-chord-B	10.167
Camber-chord	8.931

7.3. Concept Trade-off

The result of the detailed trade-off is that the configuration that combines span chord and camber morphing using zero Poisson skin will be used on the Morphlight. In the detailed trade-off in Section 7.2 already a distinction is made between morphing using zero Poisson skins and telescopic extension mechanisms. This substantially reduces the concept trade-off and only two concepts will be considered in this trade-off. The two chosen concepts are described in Section 7.3.1 and in Section 7.3.2 the best one is selected using a trade-off.

7.3.1. Possible Concepts

In this section the two possible concepts are explained in detail.

Concept 1: Span and chord morphing combined

In this concept, span, chord and camber morphing is used on the same location of the wing. The camber and chord is morphed using Fowler flaps. These Fowler flaps also extend spanwise using a zero Poisson skin. The inner part of the wing will house the fuel tank and is not extended spanwise. This inner part however will be fitted with a Fowler flap as well. The ailerons of this concept will also extend spanwise together with the main structure of the wing. Preliminary drawings can be seen in Figures 7.1 and 7.2.

(a) Span and chord retracted

(b) Span and chord extended

Figure 7.1: Concept 1 for the wing layout. Green indicates high lift devices and orange shows the aileron. The entire wing on the right side of the vertical line can morph its span. The wing root wing is on the left of the figure.

(a) Fowler flap retracted (b) Fowler flap extended

Figure 7.2: Fowler flaps will be used for chord and camber morphing. Near the root they will not be span morphing, for the other section they will be.

Concept 2: Span and chord morphing separated

Concept 1 uses multiple morphing concepts on the same location of the wing. However this is not yet used in existing designs, therefore the second concept will not make use of multiple morphing options om the same location of the wing. As can be seen in Figure 7.3 the root section of the wing (left side in Figure 7.3) will not be span morphing and it will be fitted with Fowler flaps as well as slats or some other leading edge high lift devices. Leading edge devices will be required to still meet the average chord increase since in this concept the flaps do not extend spanwise. In this section the fuel will be stored as well. Next to this there will be a span morphing section of the wing and finally the section closest to the tip will not be span morphing and the aileron will be fitted here.

(a) Span and chord retracted

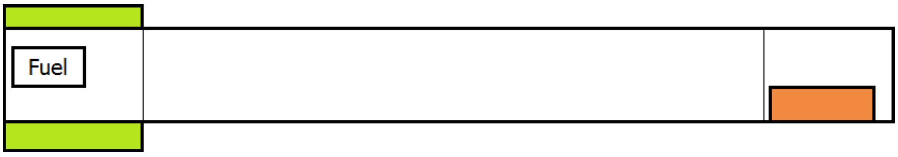

(b) Span and chord extended

Figure 7.3: Concept 2 for the wing layout. Green indicates high lift devices and orange shows the aileron. The part between the vertical lines can morph its span. The wing root is on the left of the figure.

(a) Fowler flap and slat/Krueger flap retracted

(b) Fowler flap and slat/Krueger flap extended

Figure 7.4: Fowler flaps and slats/Krueger flaps will be used for chord and camber morphing. These will only be used near the root and will not be span morphing.

7.3.2. Trade-off Table and Concept Selection

The same trade-off method is used as in Section 7.2.2 and the resulting table can be seen in Table 7.5.

Table 7.5: Trade-off for wing layout concept

Concept	Performance (38%)	Weight (32%)	Cost (16%)	Risk/RAMS (14%)
Concept 1	(10) Nominal	(8) Fowler flaps are heavy; flaps over entire wing	(5) Expensive zero Poisson materials on both wing and flaps; complex	(7) Complex flap system; multiple morphing concepts at same location
Concept 2	(3) Not enough chord morphing achievable; high drag at transition	(9) Large HLDs at root; rest relatively simple	(10) Zero Poisson material not on flaps; large flaps	(10) Large HLDs at root; morphing concepts separated

Green	Excellent, exceeds requirements	White	Correctable deficiencies
Blue	Good, meets requirements	Red	Unacceptable

Table 7.6: Final score for concepts

Concept	Score
Concept 1	8.143
Concept 2	7.040

The scores resulting from the trade-off can be seen in Table 7.6. Concept 1 wins and will be used further on during the project. The main problem for concept 2 is that the span morphing section of the wing will be quite large to achieve the required span increase, leaving only a small section of the wing for the chord morphing. To reach a reasonable average chord increase on such a small section of the wing is considered not feasible. Furthermore the transition drag will be large as well. These are the main reasons for the lower score of concept 2.

8
Performance Analysis

This chapter describes the performance analysis of the Cessna Morphlight. First, in Section 8.1, an explanation is given of an optimisation tool which calculates the amount of morphing needed to meet the requirements. Sections 8.2 and 8.3 provide the verification and validation of the optimisation tool. In Section 8.4 the results of the performance optimisation are discussed. Section 8.5 gives a sensitivity analysis of the performance parameters. The payload-range diagram can be found in Section 8.6. The climb performance is determined in Section 8.7. The flight envelope is provided in Section 8.8. In Section 8.9 the estimated noise characteristics are provided and the emissions during different phases of flight are shown.

8.1. Performance Optimisation

This section introduces and gives the outline of the optimisation tool. The underlying equation used in the optimisation tool are also explained in this section.

8.1.1. Introduction to the Optimisation Tool

Morphing allows for a variable aircraft configuration during flight. Different configurations are desired for different missions. Optimising a morphing wing planform for a design mission profile is documented in literature, for example in [14], but no programs are readily available and accessible. Therefore a design optimisation tool is developed. Not only the basic planform, but also the morphing amounts should be optimised by the program. The tool will be able to combine the requirements for different missions and return a basic planform, including morphing bounds, that is optimised for all requirements.

The basic underlying ideas of the program can be used for any morphing aircraft design. The tool developed in this project is suited to a propeller type aircraft with a certain engine. For other projects, the same tool could be used with different inputs, bounds, and constraints. The tool therefore also has an educational purpose. For example, the current tool can be developed more, adapted to a different type of aircraft with different requirements, or used for completely new projects.

The level of detail of the program is defined by the wishes of the user. Additional functionality can be included if required or desired. For this project, reasonably accurate performance estimators were required, especially for the detail design phase. During this project, the weight of the wing was not included in the performance optimisation. Instead, realistic bounds on the reference planform and the morphing bounds were introduced so the program would not yield unfeasible solutions. Ideally, the weight of the wing should be incorporated in the performance optimisation [14]. However, the weight of the wing could not be estimated both accurately and quickly at the time of development. Thus, performance analysis and structural analysis were performed separately.

8.1.2. Outline of the Optimisation Tool

The aim of the optimisation tool is to calculate the best configuration, within the solution space constrained by the bounds on the input parameters and the top level requirements. The requirements on range, endurance, cruise speed, landing and take-off distance are included in the performance optimiser. Since these requirements are conflicting in terms of performance parameters, finding an optimum solution within a certain set of bounds is expected.

The main program is written as a Python[1] script, and makes use of the SciPy[2] optimisation module. The governing equations are developed using Maple[3] and then converted for use in Python.

For the optimisation process, the equations for range, landing distance, and so on, are expressed in terms of the morphing parameters. In this way the optimisation process will also take into account the amount of morphing. An example is shown in Equation (8.1), in which the span is expressed in terms of a fixed value and an amount of morphing that is allowed. An overview of the input and output variables of the optimisation tool is shown in Table 8.1.

$$b = b_{fix}\left(1 + b_{morph}\right) \tag{8.1}$$

The optimisation is performed on both the fixed reference span and the morphing amount. Both parameters are bounded to represent a realistic range of what can be achieved with morphing. For example, it is easier to get a large percentage of span extension than a chord extension. The morphing bounds are set such that the program is only allowed to increase the fixed span. The definition of the direction of the morphing is arbitrary. When used consistently, the selected definition does not matter. For example, with a span allowed to increase by 50%, $b_{morph} \in [0, 0.5]$. With another choice of reference span, the maximum span for example, bounding b_{morph} to $[-1/3, 0]$ describes the same problem.

The morphing amounts are variable during flight. Therefore, these can be optimised over the course of the mission. However, the fixed reference planform, the span and chord, can only be optimised once. These have to make sure that all performance requirements can be met including the morphing. In order to enable this, the program is set up such that the mission performance (for example landing) depends on the fixed reference span and chord and is a function of the variable morphing amounts. Then, the morphing during the mission is optimised for each mission and the global reference planform is optimised only once.

The global optimisation is defined as a minimisation of the negative sum of all performance increments. A negative sum is used because SciPy only offers a minimisation function. The largest increment in performance would yield the most negative result, which is found by the minimisation optimiser. This is shown by Equation (8.2), in which $\vec{X}$ contains the variable parameters, comprised of the reference parameters (b, c, and so on) and the morphing allowances (as in b_{morph}). The amount of morphing is variable for each flight phase. Weights can be added to the individual fractions if a higher performance in a certain area is deemed more important than another.

$$\vec{X}_{opt} = \min\left(-\left[\frac{s_{L_0}}{s_L\left(\vec{X}\right)} + \frac{s_{TO_0}}{s_{TO}\left(\vec{X}\right)} + \frac{R\left(\vec{X}\right)}{R_0} + \frac{E\left(\vec{X}\right)}{E_0} + \frac{V_{cruise}\left(\vec{X}\right)}{V_{cruise_0}}\right]\right); \quad \vec{X} = \vec{X}_{fix} \cup \vec{X}_{morph} \tag{8.2}$$

The minimisation is subjected to constraints, which are determined by the requirements. For example, the landing distance is required to be less than 300 m, so s_{L_0} was set at 300 m. The results for the optimisation are constrained such that $\vec{X}_{opt}$ satisfies the condition that $s_L\left(\vec{X}\right) \leq s_{L_0}$. Similar constraints are applied for the other requirements. The range, endurance, and cruise speed have to be increased, but the take-off and landing distance have to be decreased. Therefore, all terms are related to their constraints such that an increase in performance yields a result greater than 1. This is why the parameters for take-off and landing distance in Equation (8.2) are inverted compared to the others. The

[1] https://www.python.org/
[2] http://www.scipy.org/
[3] https://www.maplesoft.com/products/maple/

Table 8.1: Input and output variables for performance optimisation tool

Input	Description	Unit	Output	Description	Unit
b_{upper}, c_{upper}, e_{upper}	Upper morphing bounds for span, chord and Oswald factor	[%]	b_{fix}, c_{fix}	Optimised fixed reference span and chord	[m]
b_{lower}, c_{lower}, e_{lower}	Lower morphing bounds for span, chord and Oswald factor; usually set to zero	[%]	$b_{morph_{cruise}}$, $c_{morph_{cruise}}$, $e_{morph_{cruise}}$	Optimised morphing fractions for cruise condition	[%]
$b_{fix_{upper}}$, $c_{fix_{upper}}$	Upper bound for fixed reference span and chord	[m]	$b_{morph_{range}}$, $c_{morph_{range}}$, $e_{morph_{range}}$	Optimised morphing fractions for range condition	[%]
$b_{fix_{lower}}$, $c_{fix_{lower}}$	Lower bound for fixed reference span and chord	[m]	$b_{morph_{endurance}}$, $c_{morph_{endurance}}$, $e_{morph_{endurance}}$	Optimised morphing fractions for endurance condition	[%]
e_{fix}	Reference Oswald factor	[-]	$b_{morph_{TO}}$, $c_{morph_{TO}}$, $e_{morph_{TO}}$	Optimised morphing fractions for take-off condition	[%]
W	Weight at conditions to be evaluated	[N]	$b_{morph_{L}}$, $c_{morph_{L}}$, $e_{morph_{L}}$	Optimised morphing fractions for landing condition	[%]
ρ	Air density at conditions to be evaluated	[kg/m^3]	R	Maximum range	[km]
$C_{L_{max_0}}$, $C_{L_{max_L}}$, $C_{L_{max_{TO}}}$	Maximum lift coefficient in clean, landing, and take-off configuration	[-]	E	Maximum endurance	[h]
C_{D_0}, $C_{D_{0_{range}}}$, $C_{D_{0_{endurance}}}$, $C_{D_{0_L}}$, $C_{D_{0_{TO}}}$	Zero lift drag coefficient in all configurations	[-]	V_{cruise}	Cruise speed at 75% power	[km/h]
h_{scr}	Obstacle height for take-off and landing	[m]	$V_{optimum}$	Optimum cruise speed	[km/h]
$P_{max_{cruise}}$, $P_{max_{TO}}$	Maximum power for cruise and take-off	[W]	s_L, s_{TO}	Landing and take-off distance	[m]
$P_{setting_{cruise}}$	Power setting during cruise	[%]	$s_{L_{ground}}$, $s_{TO_{ground}}$	Ground run of landing and take-off distance	[m]
η_j , η_{TO}	Propulsive efficiency during cruise and take-off	[-]	R_{cruise}	Range at cruise speed	[km]
μ_{brake}	Maximum friction coefficient during braking	[-]	F_{res}	Reserve fuel	[L]
μ_{ground}	Friction coefficient with wheels rolling on runway	[-]	h_{range}, $h_{endurance}$	Range and endurance altitude	[m]
$\bar{C}_{L_L}$, $\bar{C}_{L_{TO}}$	Average lift coefficient when rolling on the ground	[-]			
$t_{delay_{TO}}$, t_{delay_L}	Rotation time at liftoff or touchdown	[s]			
t_{res}	Loitering time for reserve fuel	[s]			
n_{nose}	Load on nose wheel when braking	[-]			
n_A	Load factor during flare	[-]			
n_{LOF}	Load factor during take-off transition	[-]			
c_P	Specific fuel consumption data	[N/s]			
F_{tot}, F_{TO}, F_{climb}	Total fuel capacity, fuel for start-up, taxi and take-off, fuel for climb	[N]			

determination of endurance, range, cruise speed, landing distance and take-off distance is explained in Sections 8.1.3 through 8.1.7.

8.1.3. Endurance

The maximum endurance is the flight condition for which the aircraft can stay in the air the greatest amount of time. In order to maximise the endurance, the fuel flow (F) must be minimised. This can be seen in Equation (8.3) [11] and is illustrated in Figure 8.6. The fuel flow is integrated from W_2, the weight at the end of cruise, to W_1, the weight at the start of cruise. W_2 includes the reserve fuel needed for 45 minutes of loitering (REQ-CON-REG-2), which is calculated with the same endurance equation and multiplied with a safety factor of 2 to ensure the aircraft can stay in the air in all possible states of morphing. The contingency fuel of 5% of the total trip fuel is also included in W_2. The reserve and contingency fuel is saved for later, for the calculation of range. If at every integration step the fuel flow is minimised, the resulting endurance will be maximised. This is the approach of the endurance optimiser: optimising the configuration for each integration step within the given bounds.

$$E = \int_{W_2}^{W_1} \frac{dW}{F} \tag{8.3}$$

The fuel flow is calculated by multiplying the specific fuel consumption (c_P) and the brake power. The specific fuel consumption varies for different values of brake power, which can be seen in Figure 8.1.

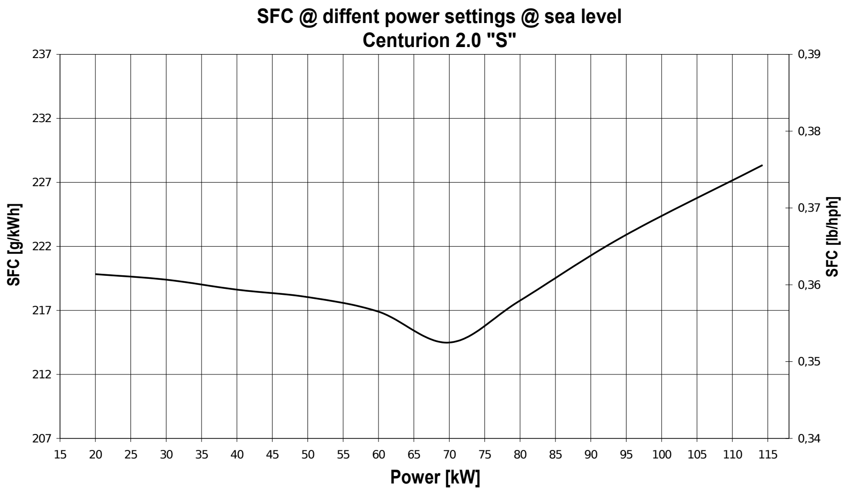

Figure 8.1: Specific fuel consumption of Continental Centurion 2.0 at sea level[4]

For maximum endurance, the speed is variable during the length of the mission. The altitude during the mission has to be larger than 2000 m, as stated by REQ-FUNC-PERF-7 in Table 2.1. The maximum mission altitude is 3048 m, which is the highest continuous operating altitude for an aircraft without oxygen supply, according to SPO.OP.195 of the European Aviation Safety Agency regulations [15]. For the endurance mission, the altitude is chosen as a constant altitude, which makes it easier for a pilot to operate and the altitude is usually limited by air traffic control.

To prevent the program from choosing the stall speed as optimum speed to fly a maximum endurance, a constraint is applied stating that the minimum speed shall be larger than 1.2 times the stall speed.

The amount of morphing is also variable for every integration step, which leads to an optimum configuration during the entire mission. The pilot cannot morph the aircraft continuously and the morphing is not automatic, which could cause the endurance to decrease slightly. However, the endurance analysis showed that the configuration during endurance always includes maximum morphing, thus the pilot does not have to adjust the amount of morphing during the maximum endurance cruise. Instead, the airspeed is variable, which the pilot can vary relatively easily. This is shown for the entire mission in Figure 8.5. In this figure it can be seen the endurance speed is selected at 1.2 times the stall speed, as the constraint defines. The optimum endurance speed would be lower, but the constraint overrides this point.

8.1.4. Range

The maximum range is the flight condition for which the aircraft can cover the greatest amount of distance. Contrary to the endurance, the flight speed does matter for the range. Here the ratio of speed and fuel flow (V/F) is maximised to give the best result. This point of maximum V/F is shown

[4]`http://www.continentaldiesel.com/typo3/index.php?id=102` [cited 22 April 2015]

in Figure 8.6 for a specific configuration. The maximum range is calculated using Equation (8.4) [11]. Because airspeed now matters, the point for maximum range will typically be at a higher airspeed than that for endurance.

Analogous to the endurance calculation, the fuel flow is determined by multiplying the specific fuel consumption and the brake power. Just as with the endurance computation, the speed and amount of morphing are variable during the mission. The altitude is kept constant for the same reasons as for the endurance. The minimum height is 305 m according to REQ-CON-REG-3 and the maximum height is 3048 m again. Also the minimum speed is 1.2 times the stall speed.

$$R = \int_{W_2}^{W_1} \frac{V}{F} dW \tag{8.4}$$

The optimisation program also optimises the range at every integration step, following the same procedure as for the endurance. Similar to the endurance configuration, the span is maximised and the chord minimised during the entire mission. The altitude is chosen as high as allowable, which is as expected. The airspeed is slightly higher than that for endurance, which is also as expected. This is shown in Figure 8.5

The range in the cruise configuration is also determined with Equation (8.4).

8.1.5. Cruise Speed

The cruise speed is defined to be at 75% power (REQ-FUNC-PERF-11) and at 2600 m altitude (REQ-FUNC-PERF-6). The program makes sure that the average speed over the entire cruise mission meets the requirement of 250 km/h. The only variable parameters for cruise are span and chord morphing and the reference span and chord dimensions. With the final results, the speed is slightly lower at the start of cruise and slightly higher at the end of cruise.

There also exists an optimum cruise speed, as defined by the 'Carson speed.' This speed is not the optimal speed for maximum range. Rather, it is a 'next best' airspeed corresponding to minimum additional fuel consumption for an increment of the speed speed (or decrease in flight time) [16]. In other words, this speed balances fuel consumption with flight time. The Carson speed represents the "least wasteful way of wasting fuel" [16, p. 3].

Whereas for endurance the parameter $1/F$ is maximised and for range the parameter V/F is minimised, the optimum cruise speed is the point at which the product of speed and range is maximised. This speed can be defined as the optimum cruise speed, if range and speed are weighed equally. This means the Carson speed is the point at which the parameter V^2/F is maximised, or the inverse of that parameter is minimised, as shown by Equation (8.5).

$$\frac{\partial \left(\frac{F}{V^2} \right)}{\partial V} = 0 \tag{8.5}$$

The optimum point can be found by drawing the tangent between the F/V curve and the airspeed V. This is shown in Figure 8.6 by the dashed line. The characteristics of the engine are such that the optimum cruise speed is at about 65% power. This makes the optimum cruise speed fairly low. However, because the engine is more efficient than the engine of the Skyhawk, the fuel consumption at a higher power setting is still lower.

8.1.6. Landing Distance

The landing manoeuvre consists of an airborne distance, including a landing flare, and a ground distance. The airborne distance is the horizontal distance between the screen location and the end of flare. The full landing manoeuvre can be seen in Figure 8.2 and the landing flare is shown in Figure 8.3. During the flare, the vertical speed is removed by applying a vertical acceleration.

The landing approach, the part between the screen location and the start of flare, is calculated using Equation (8.6) [11]. γ_{dA} is the slope of descent path, which is at most equal to the glide angle. h_t is the

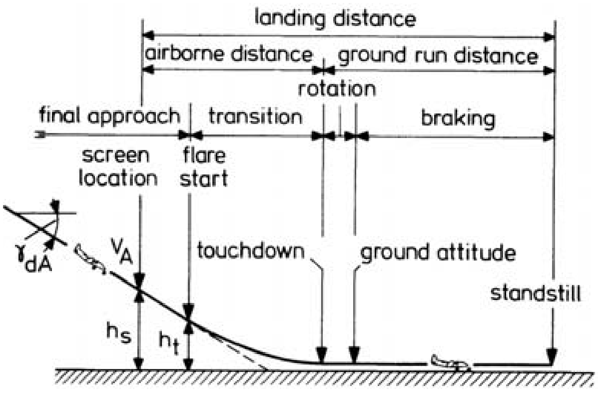

Figure 8.2: Landing manoeuvre [11]

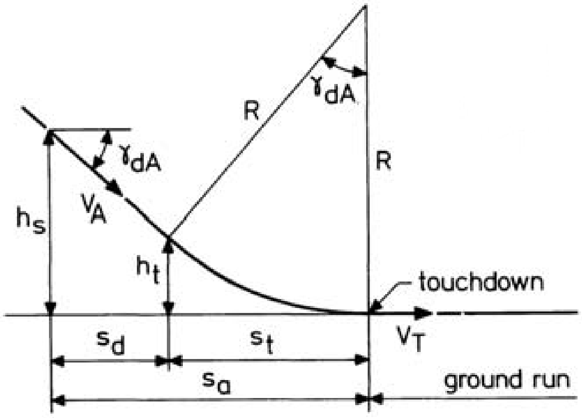

Figure 8.3: Landing flare analysis [11]

height at the start of the flare. The flare distance is calculated using Equation (8.7), in which R is the radius of curvature of the flare. The approach speed, V_A, is defined as $1.3V_{S_{landing}}$ per the regulations. The radius of curvature is determined by the load factor during the flare, n_A. Using a value of about 1.08 as the flare load factor is suggested in [17], which proved to yield accurate results for the Morphlight.

$$s_d = \frac{h_s - h_t}{\tan(\gamma_{dA})} \quad (8.6) \qquad s_t = R\gamma_{dA} = \frac{V_A^2}{g(n_A - 1)}\gamma_{dA} \quad (8.7)$$

After touchdown the aircraft needs two seconds to rotate to its ground attitude, after which the braking starts [18]. The ground distance is calculated using Equation (8.8), in which the acceleration is given by Equation (8.9). The friction force (see Equation (8.10)) depends on μ, the friction coefficient, for which an average of 0.65 is chosen, slightly lower than the average maximum amount indicated in [19]. Only the main wheels have brakes, so only the normal force on the main gear can be used for braking. This effect is included by removing the load on the nose wheel, n_{nose}. The magnitude of the nose gear load depends on the deceleration rate. With an average deceleration of $0.35g$ [19], the nose gear load factor is about 35% [20].

$$s_b = \int_{V_T}^{0} \frac{VdV}{a} \quad (8.8) \qquad a = (T - D - D_g)\frac{g}{W} \quad (8.9) \qquad D_g = \mu(1 - n_{nose})(W - L) \quad (8.10)$$

8.1.7. Take-off Distance

Analogous to the landing distance, the take-off distance consists of the ground run distance and an airborne distance, including flare. The ground run is calculated using Equation (8.11) [11]. The lift-off speed is $1.2V_S$ and the average acceleration is taken as the acceleration at a speed of $V_{LOF}/\sqrt{2}$. A rotation time of one second instead of two seconds is added, since a liftoff rotation is quicker than a touchdown rotation.

The airborne distance also consists of a flare, which means that Equations (8.6) and (8.7) are used again. Only this time, the V_A is replaced by V_{LOF} and the descent angle, γ_{dA}, is replaced by the flight path angle, γ_C. The flight path angle is calculated using the maximum rate of climb, which results in Equation (8.12). The load factor during the flare is taken as 1.15, which is in line with [11] and [17].

$$s_g = \frac{V_{LOF}^2}{2\bar{a}} \quad (8.11) \qquad \gamma_C = \left(\frac{T - D}{W}\right)_C \quad (8.12)$$

8.2. Verification

The optimisation tool and the underlying performance calculations are verified by supplying test cases for which an analytical solution could also be obtained. When the error between the analytical solution and the solution provided by the Python program is smaller than 0.1%, the program is considered verified.

Extra attention is given to the conversion from Maple to Python, since errors occurred in some cases when dividing by a term that consists of a sum of multiple components, for example $1/(1+x)$ and also the natural logarithm of a fraction. Simplifying the equations in Maple solves the problem in some cases. Maple is not used for natural logarithms. Where needed, these equations are directly inserted into Python. For future reference, conversions from Maple to Python, or any other programming language, should be checked carefully.

Furthermore, the optimisation tool is verified by plotting the optimum speeds for endurance, range and cruise as can be seen in Figure 8.6. By analysing these plots, it is checked whether the program chooses the correct optimum condition. It can be concluded that the optimisation tool is highly sensitive to the initial guess, which is needed to start the optimisation. When this initial guess is too high or too low, the program chooses the initial guess as optimum. This problem is solved by checking the solution of the optimisation with the plots.

The optimisation used the SLSQP (sequential least squares) method because it is able to handle both bounds and constraints on the input data. This allowed for the most simple description of the optimisation problem. However, convergence is not very reliable due to the way the method works. First, it ignores all bounds and constraints to try a solution. Then it checks if it meets the bounds and constraints. This introduces a problem if the objective function only holds for some finite domain. This can be solved by adapting the objective functions and all underlying functions so they force the optimiser to stay within its bounds. Also penalties can be included if a constraint is not met. When these improvements are implemented, more optimisation methods can be used that are more reliable or quicker to converge. This is not used in this project in the interest of time. The program using SLSQP yields a solution very close to the optimum.

8.3. Validation

The performance estimators described in Sections 8.1.3 through 8.1.7 are validated to ensure they yield representative results that can be used for the design. Validation is done by assessing the performance of the reference aircraft with the performance program. The results are then compared.

Endurance
The endurance is difficult to validate because the Skyhawk has no real endurance. Instead, Cessna only specifies an endurance at maximum range, which is not the maximum possible endurance. When looking at the average speed of the maximum range mission, as determined with the program, it matches closely with the value specified by Cessna. Since the endurance calculator follows essentially the same procedure as the range, the endurance can be considered valid.

Range
The calculated range of the Skyhawk has an undershoot of 2%, which is an acceptable validation value. This result depends on the fuel consumption data, for which conflicting sources exist. Different data is available for the 180-horsepower engine and the 160-horsepower engine. Either the number of data points is too limited or the c_P shows unrealistic behaviour. For the engine of the Morphlight the data is available (Figure 8.1) and the result for range can be expected to be much more reliable.

Cruise Speed
At 75% power, the cruise speed estimated for the Cessna Skyhawk was 4% too high, which is an acceptable margin for validation. This speed does not line up with the Carson speed, but this may be due to a different definition of the cruise speed by Cessna. Selecting the cruise speed of the Morphlight also at 75% is a valid approach.

Landing
The landing distance assessed for the Skyhawk gives and error in the airborne phase of about 1%. The landing distance is also compared to the equation used in the preliminary design, which yields results within 1%. The glide slope of the Skyhawk is about 6 degrees, which is in line with typical values [20]. The largest influencing factor is C_{D_0}, which can be significantly larger with the flaps fully deployed.

The ground run also has an error of about 1%. This included a delay time of 2 seconds. Also the average deceleration is between $0.3g$ and $0.35g$, which is in line with [19] where $0.35g$ is typical for conventional brakes.

The results for the landing distance of the Morphlight are also validated by looking at several descriptive coefficients. The glide slope of the Morphlight is about 8 degrees, slightly higher than the Skyhawk, mainly due to the larger flaps and the speedbrakes. This is still a reasonable angle. The average deceleration is about $0.37g$, which also matches the initial assumption.

Take-off
Initially, the error in the ground run of the Skyhawk was large. Introducing a delay time of 1 second accounts for rotating the aircraft before liftoff. Due to this the error reduces to about 1%.

The airborne distance is underestimated by less than 5%, which is an acceptable margin. For the Morphlight, the airborne distance is much less than the requirement, so the error margin is more than accounted for.

8.4. Performance Optimisation Results

The results of the optimisation tool are described in this section. As explained in Section 8.1 the optimisation tool returns values for the fixed span and chord and the amount of morphing. The optimised values for span, chord and the amount of morphing are shown in Table 8.2. The program tends to select the maximum allowable amounts of morphing, because that gives the greatest performance potential.

The limits on the morphing are based on the maximum feasible amount of morphing. The zero Poisson skin allows for a maximum increase in the span of 100%, but the span cannot be morphed over the entire span, because of the fuselage, the fuel tanks, and the strut. Therefore a feasible limit is set at 50% of the entire span that is allowed to morph. The chord morphing limits come from the flaps, which are also not on the entire wing. This means the flaps extend farther than the global increase in chord shown in Table 8.2. Based on the extension capability of the flaps and the size of the ailerons, a maximum chord extension of 17.5% is possible.

Twist morphing to change the Oswald factor, e, is not worth the additional weight and complexity for the slight increase of performance, thus twist morphing is not added to the aircraft. Camber morphing is also not added to this table, since this value is not optimised via the Python program. Fowler flaps are used for camber morphing, thus the maximum change in $C_{L_{max}}$ is used in calculations and no optimisation is needed. This maximum change is determined by the size and type of flap system.

Table 8.2: Optimised values for span and chord including morphing bounds

Parameter	Value	Unit
Span	10.0	m
Chord	1.0	m
Span morphing bound	50	%
Chord morphing bound	17.5	%

Table 8.3: Optimised morphing amounts for every mission. Note that the morphing amounts are limited by the bounds.

Mission	Span morphing	Chord morphing	Flaps
Endurance	50%	0%	0 deg
Range	50%	0%	0 deg
Cruise	0%	0%	0 deg
Take-off	50%	17.5%	7 deg
Landing	50%	17.5%	45 deg

The optimisation tool also returns the maximum range, endurance, cruise speed and minimum landing and take-off distance. Figure 8.4 shows the performance of the Cessna Morphlight compared to the requirements and the Cessna Skyhawk. It can be seen that all performance requirements are met. The take-off and landing ground distances and cruise speed are the critical requirements for which morphing is needed. A high cruise speed is reached with a small wing area, but a large wing area is needed for short take-off and landing distances. Due to the large amount of morphing, requirements for range and endurance are easily reached. The exact values for all performance indicators can be found in Table 19.1.

Figure 8.4 also shows the Morphlight with the engine from the Skyhawk. It can be seen that with this engine the aircraft is not able to meet all requirements. Due to the inefficient nature of the Skyhawk engine at low power settings, the maximum range and endurance are much less compared to the Morphlight. The maximum range requirement cannot be met and also the take-off ground distance cannot be reached. These reasons justify the improved, more efficient engine.

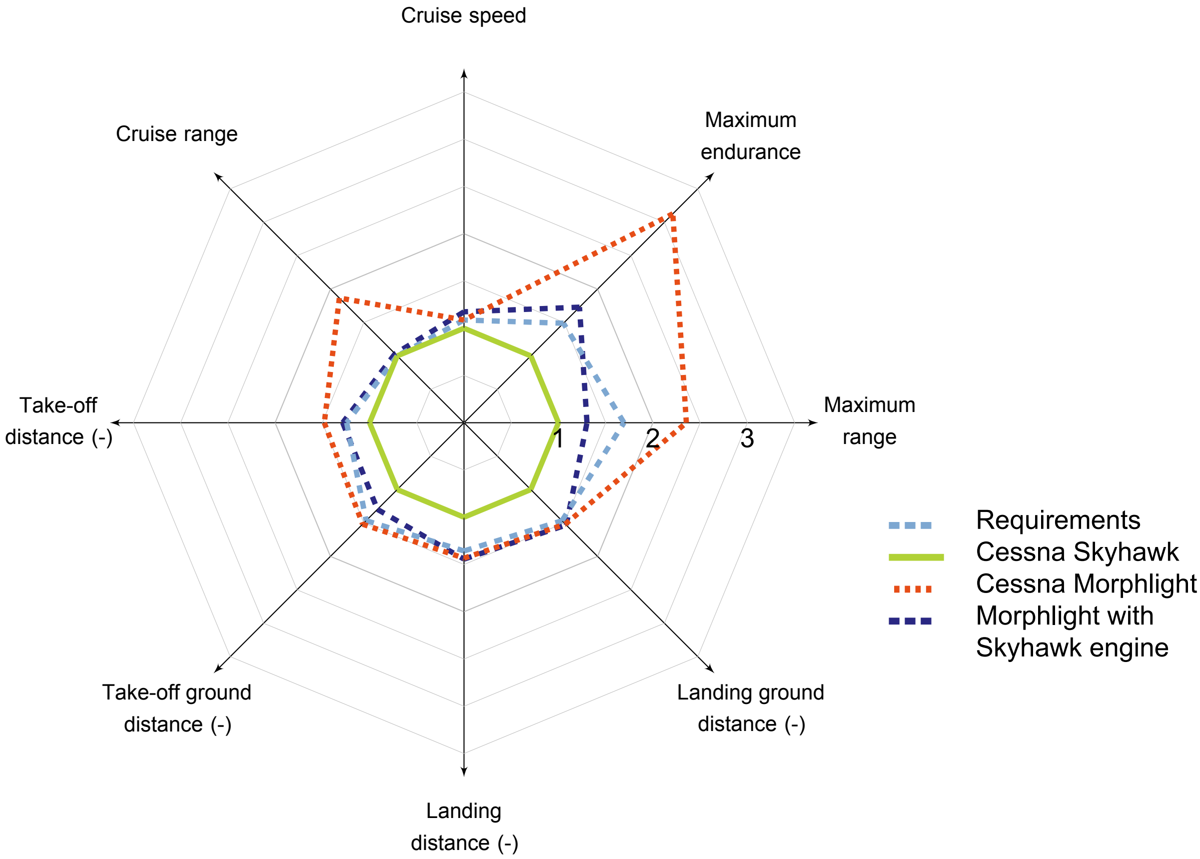

Figure 8.4: Radial diagram showing the performance of the Morphlight and the requirements with respect to the Skyhawk as base value.

The amount of morphing for every part of the mission is variable. The optimiser could also vary the amount during the cruise, range, and endurance missions. However, the optimum configuration always has either the minimum or the maximum amount of morphing. This is shown in Table 8.3. For the take-off and landing manoeuvres, the configuration has to be constant as stipulated in the regulations. For the range and endurance, the aircraft flies at such a low speed that decreasing the induced drag is most important. For the cruise mission, the induced drag is relatively low, so reducing the wing area is most important.

The optimum airspeed for range and endurance is variable over the course of the flight. At a higher weight, the aircraft has to fly faster to maintain the same optimum condition. These optimum speeds, along with the stall speed, are indicated in Figure 8.5. It can be seen that the endurance condition is limited by the constraint stating the airspeed should be at least 1.2 times the stall speed. The optimum speed for endurance would actually be lower, as indicated in Figure 8.6, where it is just to the right of the stall speed. This figure also shows that the maximum range is achieved at the minimum ratio of fuel flow and airspeed.

To investigate the increase in performance due to morphing, the performance is determined for the fully extended and fully retracted configurations, without morphing capabilities (except flaps). The radial diagram in Figure 8.7 shows the calculated performance compared to the Cessna Morphlight. It can be seen that the performance for the extended configuration is less when comparing cruise speed. In this case, the cruise speed requirement cannot be met. Also, the range and endurance are slightly

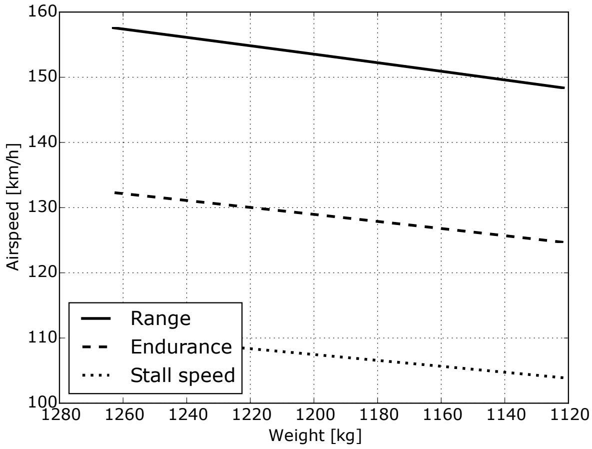

Figure 8.5: Decrease in airspeed during flight for range and endurance configuration

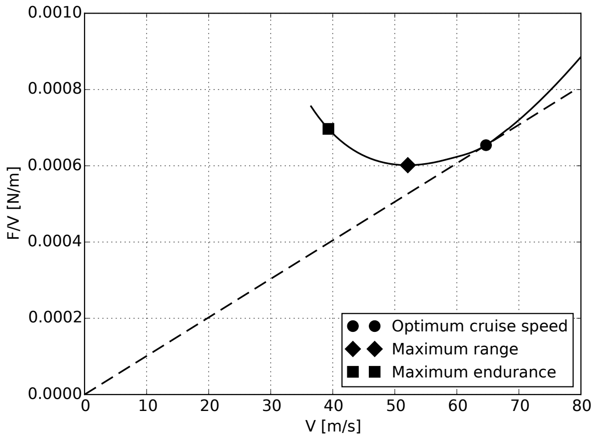

Figure 8.6: Indication of optimum speeds for endurance, range, and cruise. (Cruise configuration shown)

less, since the chord is fully extended, which decreases the aspect ratio and thus lowers the range and endurance. A fully retracted configuration shows a large decrease in performance when comparing take-off and landing distances. It can be concluded that morphing is needed to reach the requirements for cruise speed and take-off and landing distance.

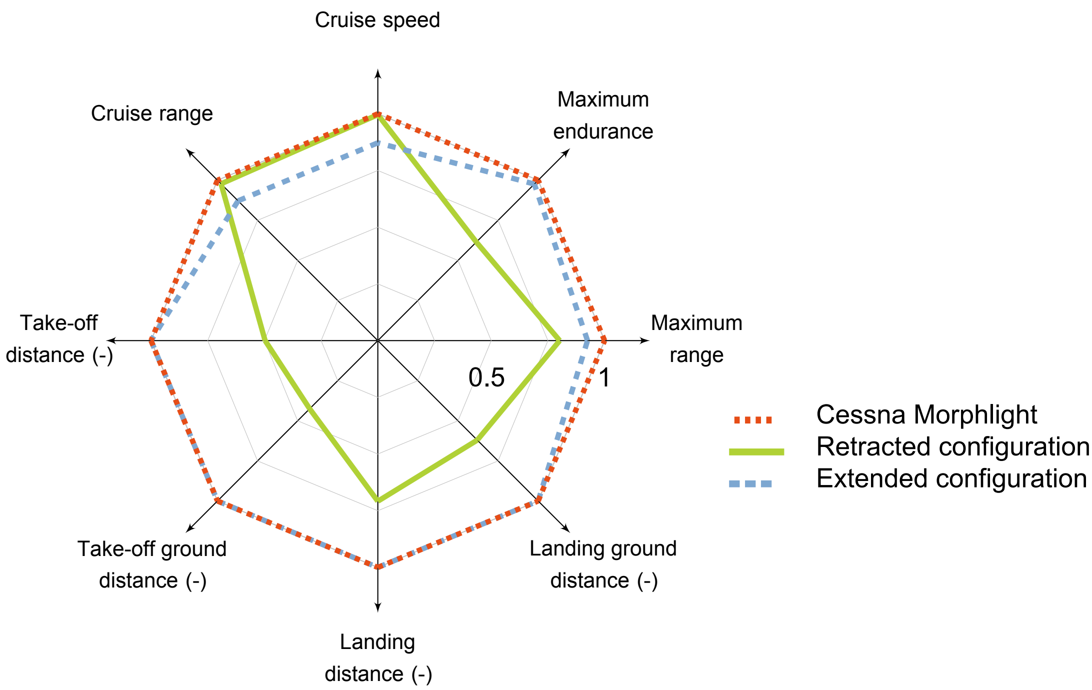

Figure 8.7: Radial diagram showing the performance of the retracted and extended configuration compared to the morphing configuration as a base value.

8.5. Sensitivity Analysis

A sensitivity analysis is performed to investigate the influence of a small change in an input variable to the performance parameters. The final solution is taken as the point around which to determine the sensitivity. Table 8.4 shows the change in performance due to a 1% change in input variable. The input variables consist of the reference planform, the morphing amounts, weights, aerodynamic parameters, and propulsion characteristics.

The effect of MTOW on the take-off ground distance is greatest. This is because the ground distance is quadratically dependent on the weight. It can also be seen the maximum power and the propulsive efficiency have the same effect on the cruise speed and take-off distance. This is due to the definition of available power, which is $P_{max} \cdot \eta$. Another interesting point is that the effect of MTOW on range and endurance is less than the effect of OEW. This is due to the fact that the MTOW also includes the fuel. Increasing the MTOW thus also increases the amount of fuel on board, reducing the negative effects of increasing weight. Finally, it can be seen that the planform area cannot be increased, because then the cruise speed would decrease.

Table 8.4: Sensitivity analysis on performance parameters. All input parameters changed by 1%. Sensitivity expressed in percent. The effect of MTOW on take-off ground distance has largest sensitivity

Parameter	Range	Endurance	Cruise speed	Landing distance	Landing ground distance	Take-off distance	Take-off ground distance
b_{fix}	0.49	1.11	-0.11	-0.47	-0.80	-1.13	-1.44
c_{fix}	-0.49	-0.12	-0.38	-0.62	-0.84	-0.99	-1.37
b_{morph}	0.16	0.37	-	-0.16	-0.27	-0.38	-0.49
c_{morph}	-	-	-	-0.09	-0.13	-0.15	-0.21
OEW	-0.62	-0.93	-0.17	0.33	0.49	1.12	1.44
Payload	-0.30	-0.45	-0.08	0.16	0.24	0.54	0.69
MTOW	-0.10	-0.61	-0.27	0.55	0.83	1.91	**2.45**
$C_{L_{max}}$	-	0.26	-	-0.49	-0.78	-1.06	-1.44
e_{fix}	0.49	0.61	0.13	0.07	0.02	-0.07	-0.04
C_{D_0}	-0.49	-0.38	-0.38	-0.16	-0.13	0.05	0.04
P_{max}	-	-	0.51	-	-	-0.80	-0.99
η	0.99	0.99	0.51	-	-	-0.80	-0.99

8.6. Payload-Range Diagram

A payload-range diagram shows how payload and range can be interchanged. By taking less payload on board, the range can be increased, and vice versa.

The payload-range diagram was developed using the range equation (Equation (8.4)) from Section 8.1.4. When some payload is removed, the weights at the beginning and end of the cruise phase, W_1 and W_2, change. The difference in the weights W_1 and W_2 is the fuel burned during cruise. This amount is almost the same with a different take-off weight. With a lower take-off weight, slightly less fuel will be used to climb to the cruise altitude. In general, with less payload, the amount of usable fuel becomes a larger fraction of the total weight, which effectively can increase the range.

The payload-range diagram for the Cessna Morphlight (Figure 8.8) is slightly different than that of a typical aircraft. This is due to REQ-FUNC-PERF-12, which states the maximum range be attained with the maximum payload on board. In order to get the maximum range, the maximum amount of fuel is taken on board. In this case, no additional fuel can be added if some payload is removed because the maximum fuel capacity is limited. Notice that there will always be payload on the aircraft. This is because the pilot(s) is/are considered to be part of the payload for this type of aircraft. In order to fly at all, a pilot is required to operate the aircraft. Only theoretically could the range be higher.

8.7. Climb Performance

The climb performance of the Cessna Morphlight is assessed by means of the rate of climb. This parameter varies with altitude, which is shown in this section. It also varies with the morphing state of the aircraft. This is also investigated in this section.

The steady rate of climb is defined by the excess power divided by the weight of the aircraft. This is shown in Equation (8.13). The available power and required power are defined in Equations (8.15) and

(8.16). The required power depends on the morphing state, which influences S and A during the climb. The rate of climb can only be assessed for flight speed greater than the stall speed, and is only useful if it is greater than zero. The stall speed can be determined with Equation (8.14), where S, $C_{L_{max}}$, and ρ have to be changed according to the current morphing configuration and the altitude.

$$RC = \frac{P_a - P_r}{W} \tag{8.13}$$

The rate of climb is assessed for the take-off configuration, with the span and chord fully extended (Figure 8.10), for the cruise configuration, with the span and chord at its minimum lengths (Figure 8.9), and for the maximum range and endurance configurations, which have the span at its maximum length but the chord at its minimum (Figure 8.11). The lower limit on the speed is the stall speed, which increases with altitude. It can also be seen the rate of climb decreases with altitude, as expected. In fact, the aircraft has best climb performance in its take-off configuration, as the maximum power is higher at take-off and the wing area is largest at take-off. In the maximum range and endurance configuration, with the wing span fully extended, the climb performance is still better than in the cruise configuration. The cruise configuration shows the worst climb performance. This is due to having the smallest wing area during cruise.

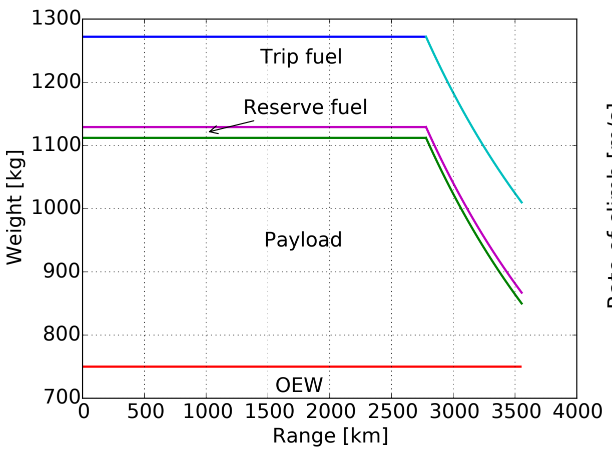

Figure 8.8: Payload-range diagram for the Cessna Morphlight

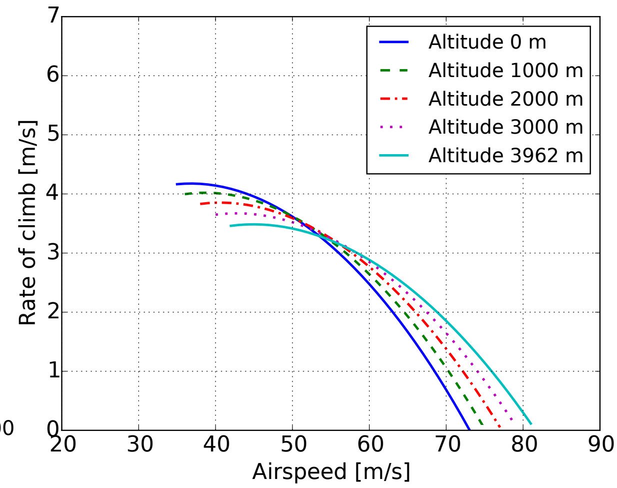

Figure 8.9: Rate of climb in cruise configuration

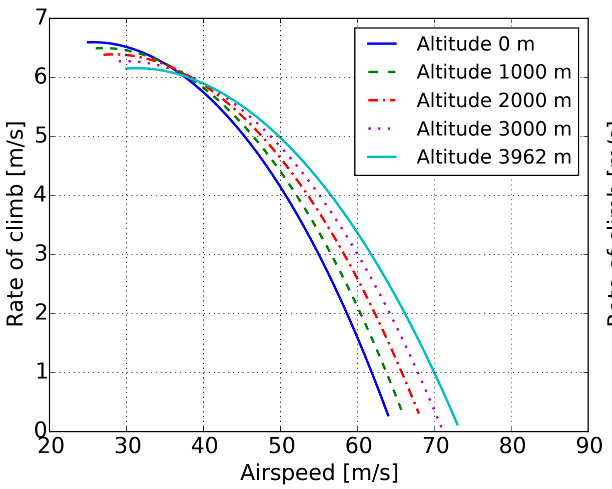

Figure 8.10: Rate of climb in take-off configuration

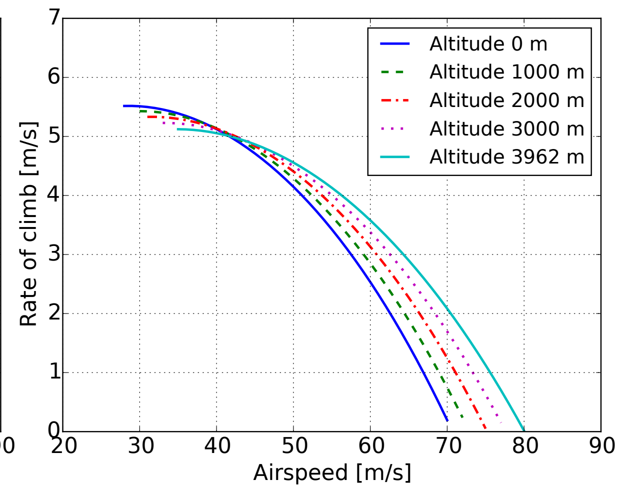

Figure 8.11: Rate of climb in maximum range configuration

Compared to the Cessna Skyhawk, the climb performance of the Cessna Morphlight is increased. The climb rate of the Skyhawk is 3.7 m/s at sea level [21]. To compare this value to the climb performance of the Morphlight, the climb rate in range configuration with take-off power is taken. The climb rate for this configuration is 5.2 m/s, which is an increase in performance of 40%. The Morphlight loses less climb performance at altitude, because the new engine does not suffer from a decreased output at the altitudes the Morphlight flies[5].

8.8. Flight Envelope

The aircraft's flight envelope determines the range of allowable speeds at all possible flight altitudes. Several performance limitations are possible, such as available engine power, structural characteristics, and stall speed.

The stall speed can be determined in several aircraft configurations. The stall speed is determined for take-off and landing configuration, which is defined as V_S by Equation (8.14). The stall speed varies with altitude as the air density decreases. The area for take-off and landing configuration are equal, since maximum morphing is needed in both take-off and landing. The $C_{L_{max}}$ for landing and take-off are different, since more flaps are used during landing.

$$V_S = \sqrt{\frac{2W}{\rho S C_{L_{max}}}} \tag{8.14}$$

Another speed limitation is determined by the engine. With a given amount of maximum power, the maximum speed in level flight, V_H, is obtained when the maximum available power is equal to the minimum required power. The available power is assumed to be constant with airspeed. The available power is shown in Equation (8.15). The required power is given by Equation (8.16). The maximum speed will be obtained in the cruise configuration, with a corresponding wing area S_{cruise}.

$$P_a = \eta_j P_{br_{max}} \tag{8.15}$$

$$P_r = DV = C_{D_0} \frac{1}{2} \rho V^3 S_{cruise} + \frac{2W^2}{\pi A e \rho V S_{cruise}} \tag{8.16}$$

The maximum relevant altitude is 3962 m, which is the maximum altitude the aircraft is allowed to fly without oxygen supply for a maximum of 30 minutes, which can be found in SPO.OP.195 of the European Aviation Safety Agency regulations [15].

The operational speed limits follow from the regulations described in Certification Specifications 23 [1]. The maximum operating manoeuvring speed, the maximum flaps extended speed, the never exceed speed, the maximum structural cruising speed and the maximum operating speed can be found in Figure 8.12.

Several observations can be made related to Figure 8.12. First of all, the cruise speed is lower than the maximum attainable speed, so the aircraft is able to get to the desired cruise speed at the desired altitude. In addition, the maximum operating speed coincides with the maximum structural cruise speed. They are both higher than the maximum level speed, so during normal operations, it would be very difficult to get to these speeds. Even if the pilot would not be paying attention at full power, the aircraft would not immediately go into overspeed, but only in the case of a prolonged nose down attitude. This introduces an additional margin of safety into the Morphlight.

8.9. Estimated Noise and Emission Characteristics

According to measurements from the Federal Aviation Administrations, the noise of a flyover at 450 m distance is 71.7 dB for the Cessna 172 [22], which is only slightly louder than a vacuum cleaner. However, since the Cessna 172 is fairly old, newer aircraft will likely be more silent. The expectation is that the noise for the Cessna Morphlight is lower, since a modern engine is installed. In addition, three propeller blades are used instead of two, which reduces the noise as well. Equation (8.17) shows the blade pass frequency (BPF), in which ω is the rotational velocity in rpm and B_p is the number of blades. When increasing the number of blades, the frequency increases. High frequencies contain less energy and are damped out faster than low frequencies. Thus the noise decreases when using a three-blade

[5] `http://www.continentaldiesel.com/typo3/index.php?id=102` [cited 22 April 2015]

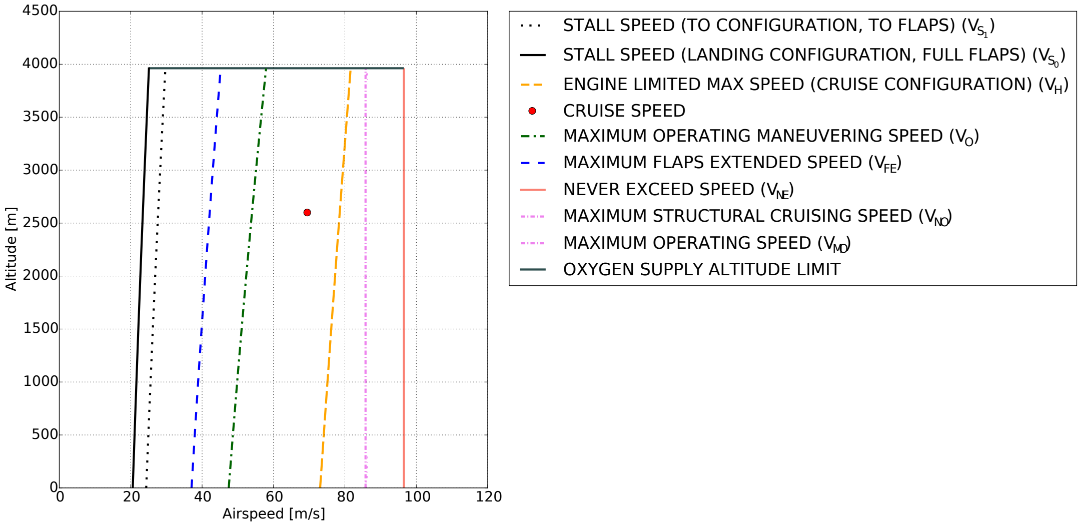

Figure 8.12: Flight envelope for the Cessna Morphlight in terms of operational limitations

propeller instead of a two-blade propeller. The calculation of the noise of the Cessna Morphlight is complex and beyond the scope of this project.

$$BPF = \frac{\omega B_p}{60} \tag{8.17}$$

Table 8.5 shows the emission of Carbon Monoxide (CO), Nitrogen Oxides (NO_X), Total HydroCarbons (THC), Sulfur Oxides (SO_X) / CO_2 and includes the fuel burn of the engines during the different phases of the flight. The new engine only consumes 1.92 litres of fuel from start to take-off compared to 3.57 litres of the old engine. This indicates the old engine is unable to meet the take-off fuel consumption requirement (REQ-CON-SUST-1), but the new engine is able to meet it.

Table 8.5: Emissions for the Continental CD-155 [23]

Mode	**Power**	**Time**	**CO**		**NO_X**		**THC**	
		min	kg/h	kg	kg/h	kg	kg/h	kg
Taxi/Idle	IDLE	4.0	0.064	0.0043	0.07	0.0048	0.026	0.0017
Take-off	100%	0.3	0.151	0.0008	0.54	0.0027	0.173	0.0009
Climbout	75%	4.98	0.088	0.0073	0.53	0.0438	0.141	0.0117
Run up	60%	1.0	0.068	0.0011	0.42	0.0070	0.109	0.0018
Approach	40%	6.00	0.073	0.0073	0.29	0.0291	0.083	0.0083
Taxi	25%	12.0	0.06	0.012	0.14	0.0288	0.048	0.0096
Start to take-off	-	13.3	-	0.0139	-	0.0385	-	0.0123

Mode	**CO_2**		**Fuel flow**		
	kg/h	kg	kg/h	kg	L
Taxi/Idle	10.08	0.67	3.2	0.213	0.267
Take-off	68.73	0.34	21.6	0.108	0.135
Climbout	55.97	4.65	17.6	1.461	1.826
Run up	43.25	0.72	13.6	0.227	0.283
Approach	33.02	3.30	10.4	1.04	1.3
Taxi	19.02	3.80	6	1.2	1.5
Start to take-off	-	4.87	-	1.533	1.917

9

Aerodynamics

As with any other aircraft, proper study of the aerodynamics is essential for the Cessna Morphlight. Aerodynamics contributes significantly to the design of an aircraft as it has a direct effect on the performance, stability, structure and much more. This chapter covers the aerodynamic analysis of the aircraft. Starting with the selection procedures taken to select the new airfoil, including CFD validation, continuing with a comparison between wing planforms and an investigation on the possible use of a raked wing tip.

9.1. Aerodynamic Tools

To most accurately estimate the aerodynamic properties of the aircraft, several already existing aerodynamic analysis tools are used. Each of them having different functionalities, meant to be used for different purposes. This section gives a short description of these tools.

- **JavaFoil**[1]
  JavaFoil is a 2D airfoil analysis tool. It allows the user to rapidly generate airfoils belonging to different series and subsequently use the panel method to estimate the lift and drag polar of these airfoils. JavaFoil also allows users to design custom airfoils with a given pressure distribution.
- **XFLR5/XFoil**[2]
  XFLR5 is an analysis tool for airfoils, wings and planes. It uses XFoil in the background to analyse 2D airfoils, and then uses these results with range of methods namely, lifting linetTheory, horseshoe vortex VLM, ring vortex VLM and panel method, to estimate the aerodynamic properties for 3D wings and complete aircraft configurations.
- **Digital DATCOM**[3]
  Digital DATCOM is a stability and control aerodynamics tool developed by the United States Airforce, encompassing a set of empirical and semi-empirical methods commonly known as the DATCOM method. It is used to estimate aerodynamic properties such as static aerodynamic coefficients, coefficients derivatives, control derivatives, and so on, based on a given aircraft configuration and flight condition. It is meant to be used to analyse the static and dynamic stability and controllability of an aircraft.
- **Tornado VLM**[4]
  Tornado VLM uses the Vortex Lattice method to, just as DATCOM, estimate a wide range of aerodynamic parameters for a given wing and optionally tailplane configurations at different flight conditions.

[1] `http://www.mh-aerotools.de/airfoils/javafoil.htm`
[2] `http://www.xflr5.com`
[3] `http://www.pdas.com/datcom.html`
[4] `http://tornado.redhammer.se/`

- **Ansys Fluent**[5]
  Fluent is a computational fluid dynamics program developed by Ansys to analyze flow around a body by numerically solving Navier-Stokes equations. In this project it is used for two dimensional simulations of several airfoils.

9.2. Airfoil Selection

The Cessna 172S Skyhawk has been using the same airfoil shape since its conception more than 60 years ago. Since then, advances in technology and research in the field of aerodynamics have resulted in new tools to analyse and design airfoils. It is thus interesting to investigate whether a different airfoil is better suitable to the Cessna Morphlight.

9.2.1. Airfoil Comparison

Several airfoils used in comparable, but newer aircrafts are tested in XFLR5/XFoil. The airfoils are compared in cruise and take-off conditions, but the results obtained are comparable to each other, thus only the cruise flight condition is be considered here. This flight condition consists of an airspeed of 69.4 m/s, reference chord length of 1.00 m and atmospheric conditions at 2,600 m altitude resulting in a Reynolds number of $3.8 \cdot 10^6$. These results are shown in Figure 9.1.

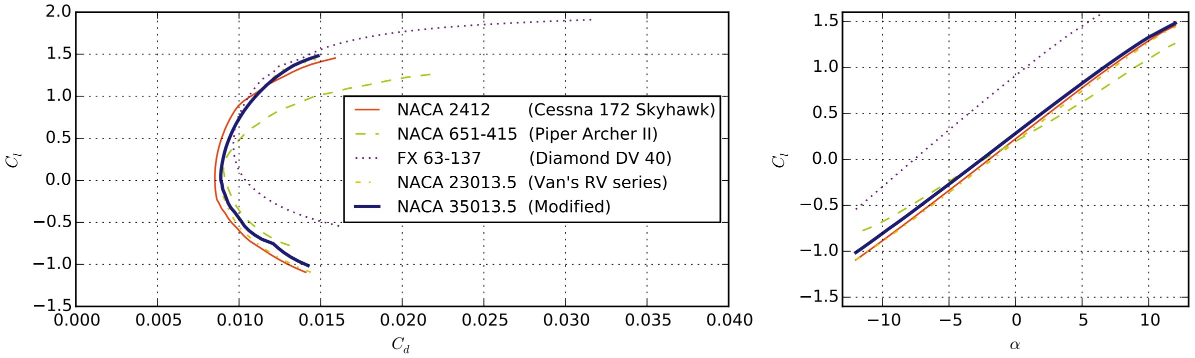

Figure 9.1: Lift and drag polars of the airfoils being considered.

Low drag is desired in the target flight regimes (C_l of 0.4-0.6 in cruise and C_l of 1.1-1.4 for maximum range and endurance), while also having a high $C_{l_{max}}$ for takeoff and landing. The NACA35013.5 has a higher $C_{l_{max}}$ and lower C_m and initial research also showed lower drag, compared to the NACA2412. Because of its thicker profile it is structurally more favorable. However, further research into the airfoils showed that the NACA35013 has a higher drag than the NACA2412, it is therefore recommended for further research to be done and possibly change the main wing airfoil back to the NACA2412.

9.2.2. Verification using Computational Fluid Dynamics

The results in Section 9.2 are verified using CFD. Two dimensional simulations for both NACA 2412 and NACA 35013.5 are done for different angles of attack.

When analysing an airfoil using CFD it is challenging to find the correct drag coefficient. To be able to capture the drag correctly the boundary layer around the airfoil should be meshed with sufficient detail. To determine the height of the first layer that is meshed the following approach is used[6].

The thickness of the first layer can be calculated using Equation (9.1). The y^+ from this equation can be determined using the graph in Figure 9.2, where u^+ is the non-dimensional parallel velocity. For this case a y^+ of 30 is used. The value of the frictional velocity U_τ is determined using Equations (9.3), (9.4)

[5] http://www.ansys.com/Products/Simulation+Technology/Fluid+Dynamics/Fluid+Dynamics+Products/ANSYS+Fluent

[6] http://www.computationalfluiddynamics.com.au/tips-tricks-cfd-estimate-first-cell-height/ [cited 18 June 2015]

and finally (9.5) for the skin friction coefficient, the wall shear stress and the frictional velocity respectively. The Reynolds number in Equation (9.3) is determined using Equation (9.2). These calculations resulted in a height of the first layer Δy_1 of $1.9 \cdot 10^{-4}$.

$$\Delta y_1 = \frac{y^+ \mu}{\rho U_\tau} \qquad (9.1) \qquad\qquad Re = \frac{\rho V L}{\mu} \qquad (9.2)$$

$$C_f = \frac{0.058}{Re^{0.2}} \qquad (9.3) \qquad \tau_w = \frac{1}{2} C_f \rho U^2 \qquad (9.4) \qquad U_\tau = \sqrt{\frac{\tau_w}{\rho}} \qquad (9.5)$$

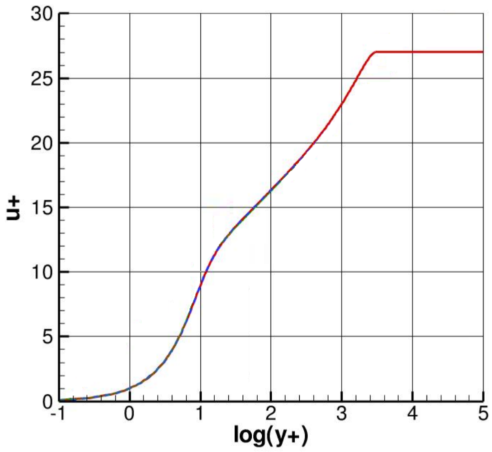

Figure 9.2: Graph used to determine y^+ using the non-dimensional parallel velocity[7].

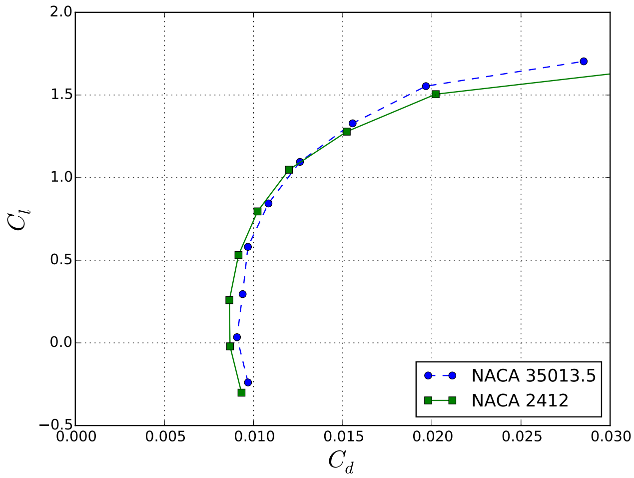

Figure 9.3: Comparison between airfoils using CFD

The coordinates for both airfoils are obtained using JavaFoil which are then used to create the mesh in the Ansys ICEM mesher. For the analysis of multiple angles of attack, a new mesh has to be created for each angle. This can be achieved very easily using the ICEM replay function. This function repeats every step taken by the user, but uses another input file. To make a new input file the coordinates have to be transformed from the body reference system to the aerodynamic reference frame using Equation (9.6).

$$\begin{bmatrix} x_a \\ y_a \end{bmatrix} = \mathbb{T}_{ab} \cdot \begin{bmatrix} x_b \\ y_b \end{bmatrix} = \begin{bmatrix} \cos\alpha & \sin\alpha \\ -\sin\alpha & \cos\alpha \end{bmatrix} \cdot \begin{bmatrix} x_b \\ y_b \end{bmatrix} \qquad (9.6)$$

The simulations are done using the same conditions as in Section 9.2 and resulted in Figure 9.3. As can be seen Figure 9.3 is very similar to Figure 9.1 proving that the results provided in Section 9.2 are correct.

9.2.3. Validation of Computational Fluid Dynamics

The results of the CFD analysis are used to verify the JavaFoil results of Section 9.2, however the CFD results from Fluent should be validated as well. This is done using the two dimensional NACA0012 validation by NASA's Langley Research Center[8].

This validation is performed using a Mach number of 0.15, a temperature of 300 Kelvin and a Reynolds number of 6 million. At a temperature of 300 Kelvin the air density is 1.161 kg/m^3, the speed of sound is 347.202 m/s and using Equation (9.2) it is calculated that the dynamic viscosity for this case is $1.011358 \cdot 10^{-5}$ kg/m/s. These values are used as input for Fluent.

[7] `http://turbmodels.larc.nasa.gov/flatplatesa.html` [cited 18 June 2015]
[8] `http://turbmodels.larc.nasa.gov/naca0012_val.html` [cited 16 June 2015]

For the validation NASA slightly altered the definition of the airfoil so that the airfoil closes with a sharp trailing edge. The revised definition can be seen in Equation (9.7).

$$y = \pm 0.594689 \cdot \left(0.298223\sqrt{x} - 0.127125x - 0.357908x^2 + 0.291985x^3 - 0.105175x^4\right) \tag{9.7}$$

Using Equation (9.7) the coordinates of the airfoil are calculated which are then used to create the mesh in the Ansys ICEM mesher. The same method as in Section 9.2.2 is used to transform the airfoil's coordinates for the different angles of attack using Equation (9.6). NASA recommended to use a far-field that is about 300 chord lengths far from the airfoil. However it is chosen to use only 100 chord lengths as distance to reduce the computation time. It is assumed that this decision will not affect the results very much, however the drag may be calculated slightly larger due to the smaller far-field.

In the validation case NASA provided several plots which can be used for comparison, namely a C_l - C_d plot and plots with the pressure coefficient for $\alpha = 0$, 10 and 15. These plots have been reproduced using Fluent and can be seen in Figures 9.4, 9.5, 9.6 and 9.7.

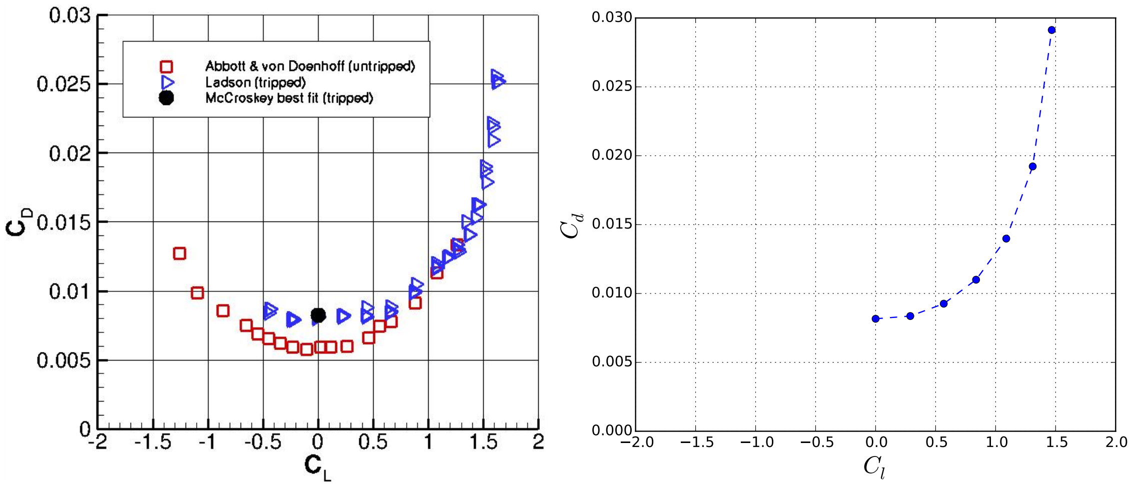

(a) NASA validation data. (b) CFD results.

Figure 9.4: C_l - C_d Comparison between the validation data by NASA and the calculated results using CFD.

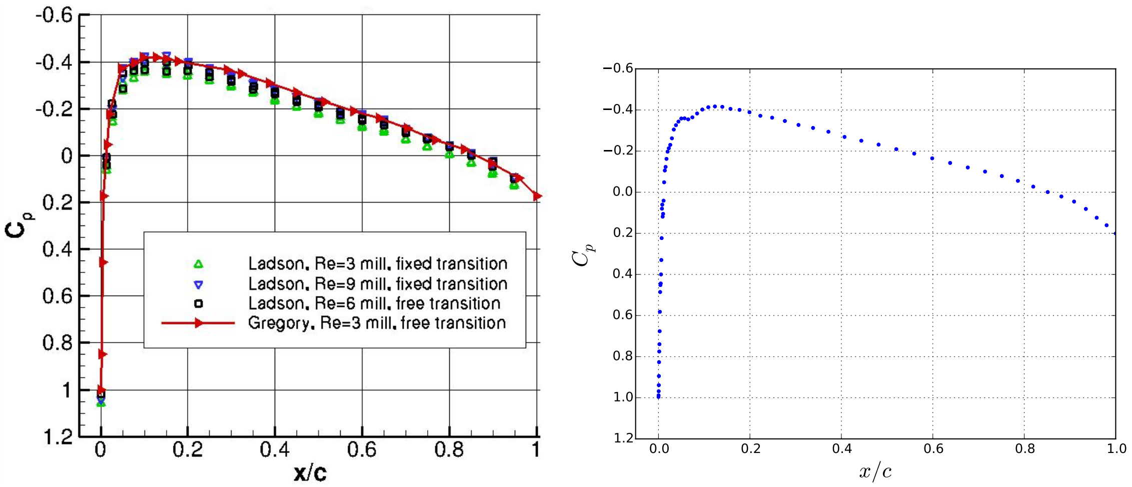

(a) NASA validation data. (b) CFD results.

Figure 9.5: Comparison between the validation data by NASA and the calculated results using CFD at $\alpha = 0$.

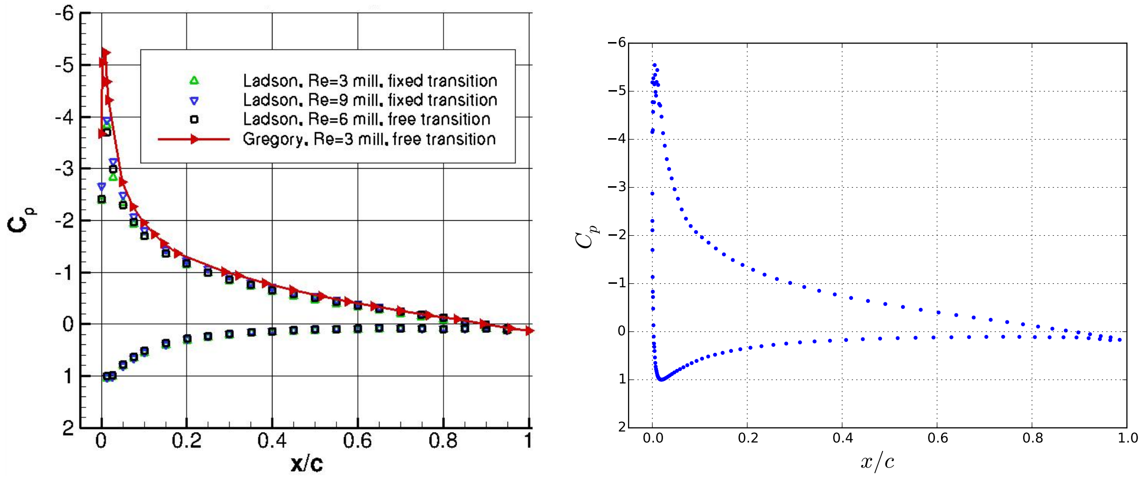

(a) NASA validation data. (b) CFD results.

Figure 9.6: Comparison between the validation data by NASA and the calculated results using CFD at $\alpha = 10$.

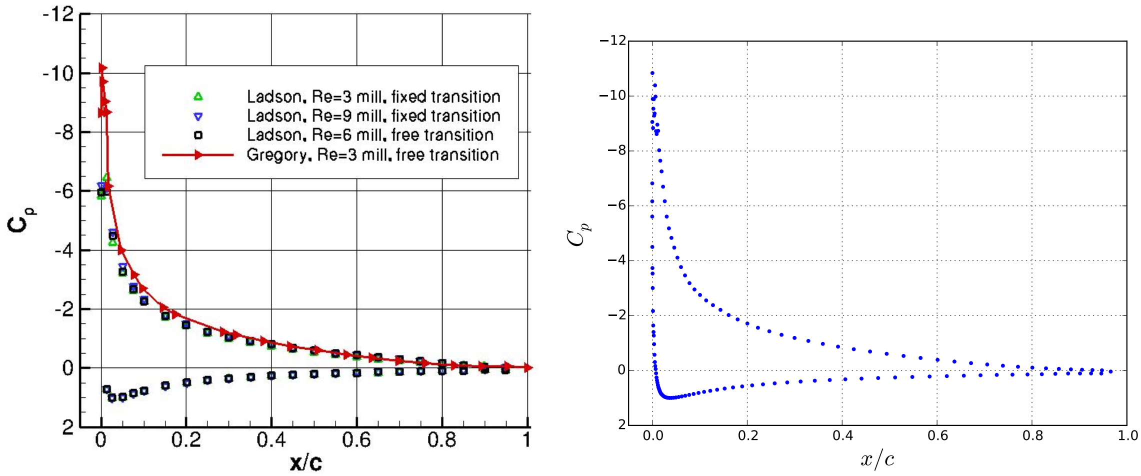

(a) NASA validation data. (b) CFD results.

Figure 9.7: Comparison between the validation data by NASA and the calculated results using CFD at $\alpha = 15$.

As can be seen in Figures 9.4, 9.5, 9.6 and 9.7 the CFD gave quite good results. The C_p plots (Figures 9.5, 9.6 and 9.7) of the validation data compared to the CFD data are similar for all three angles of attack. When looking at the drag polars in Figure 9.4 the tripped polar should be used for comparison, because in Fluent the fully turbulent K-ω-SST model is used. As can be seen the polar is the same as the validation data for low angles of attack, however when the angle of attack is increased the drag becomes slightly larger than the validation results. This is expected because the used far-field is smaller than recommended by NASA. These results validate the results given in Section 9.2.3, however it is assumed that for these results the drag is overestimated at large angles of attack as well.

9.3. Wing Planform Analysis

To come up with the most aerodynamically efficient wing design a set of wings is analysed with XFLR5. The main parameters of interest in this analysis are the effects of taper and the combination of wing sections with different taper ratios. Table 9.1 contains the results for the Morphlight with retracted span. The same analysis with the extended span yielded comparable results. Despite that more planforms where taken into consideration, they all fell into one of the four layouts shown in Figure 9.8, thus for the preliminary design of the wing these four planforms are compared with each other. The flight conditions at which the wings are analysed consist of an airspeed of 69.4 m/s, C_L of 0.55 and ground level atmospheric conditions.

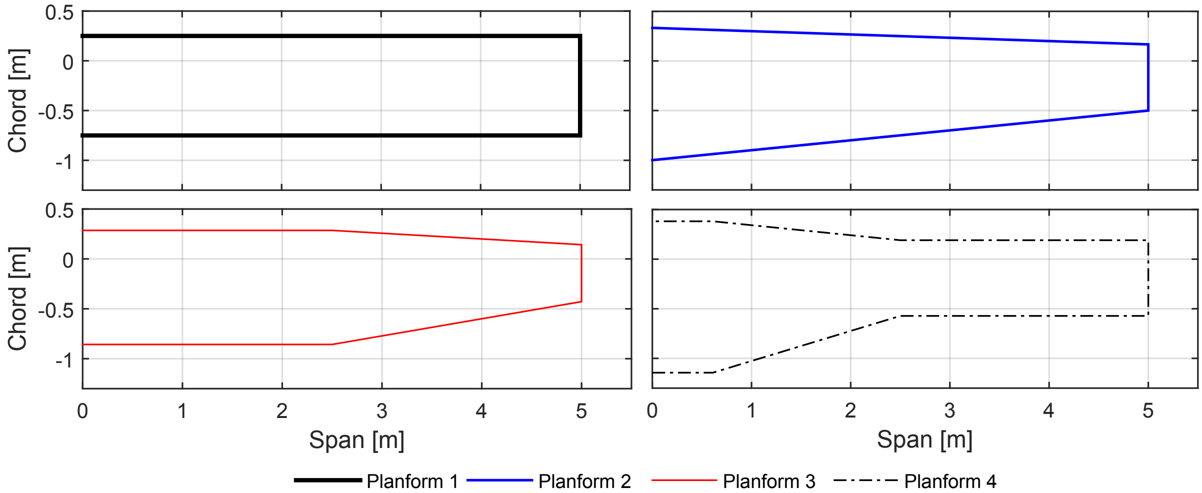

Figure 9.8: Four planform layouts analysed. The layouts are shown with a taper ratio of 0.5 for the retracted configuration, while the wing of the Cessna Morphlight has a higher taper ratio. The quarter-chord line is chosen to be on the line for which $y = 0$.

Table 9.1: Comparison between possible planforms.

	C_D	L/D
Planform 1	0.016448	33.43962792
Planform 2	0.016196	33.95764386
Planform 3	0.016367	33.59815482
Planform 4	0.016381	33.56473964

As expected, planform 2 has the highest L/D ratio since it is fully tapered and is the best among the options at approximating an elliptical lift distribution. On the other hand, planform 1, being a straight wing, has the lowest L/D ratio. Combinations of tapered and straight sections such as planforms 3 and 4 are in the middle of these and do not differ from each other significantly. However wings similarly shaped to planform 3 are in general more efficient, since they better approximate an elliptical distribution near the wing tips where dynamic drag is most significant. Figure 9.9 shows the lift distribution of these four planforms.

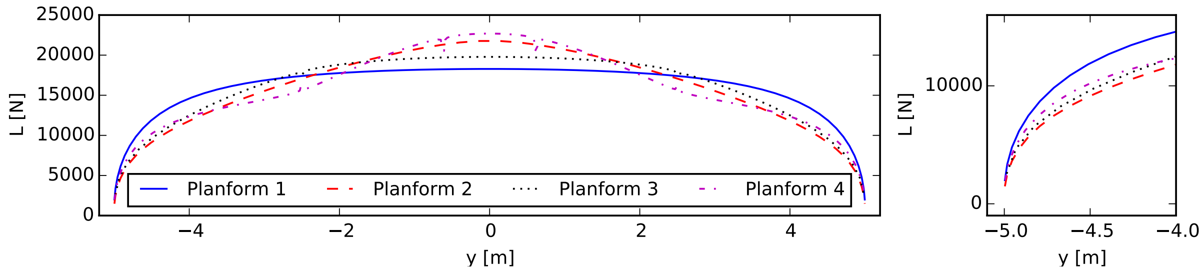

Figure 9.9: Lift distributions of the four planforms of interest.

9.4. Wing Rake

This section investigates the aerodynamic improvement of raked wings by adding a raked wing section to the tip of the extended Morphlight planform, as shown in Figure 9.10. Figure 9.11 shows the lift distribution of the raked and non-raked wing planforms, while Table 9.2 contains the aerodynamic coefficients of the wings. As its clear from Table 9.2, the L/D ratio of the wing can be improved improved with 1.83% by adding the raked section to the wing tip. It' to be noted though, that part of this improvement is caused by the extended wingspan.

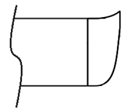

Figure 9.10: Raked wing tip.

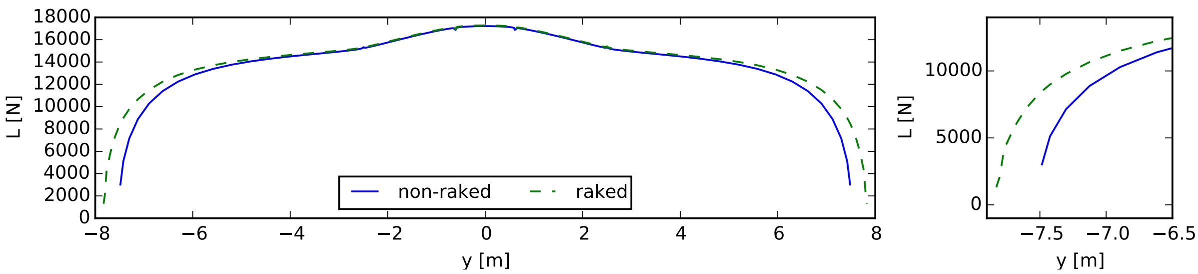

Figure 9.11: Lift distributions of a raked and non-raked wing at $\alpha = 2.5 : \mathrm{deg}$ and $V = 69.4\ [m\ s^{-1}]$ at ground level.

Table 9.2: Comparison between possible planforms.

	C_L	C_{D_i}	C_{D_v}	C_D	L/D
Non-raked	0.495059	0.005312	0.009817	0.015129	32.72251966
Raked	0.499759	0.00515	0.009848	0.014998	33.32170956

9.5. Validation using Computational Fluid Dynamics

To see if the results are useful and can be trusted the they are compared to results obtained using CFD. Using Fluent a two dimensional analysis is done for NACA 35013.5, then using the lifting line theory the aerodynamic coefficients and the lift distribution is calculated for the three dimensional wing. The two dimensional results calculated by Fluent are already validated in Section 9.2.3. The numerical results and the difference can be seen in Table 9.3, the lift distribution can be seen in figure 9.12.

Table 9.3: Comparison of XFLR5 results with CFD.

	C_L	C_{D_i}	C_{D_v}	C_D	**L/D**
XFLR5	0.499759	0.00515	0.009848	0.014998	33.3217
CFD	0.502663	0.00542	0.009584	0.015003	33.5042
Difference	0.5777%	4.98%	2.755%	0.0333%	0.5447%

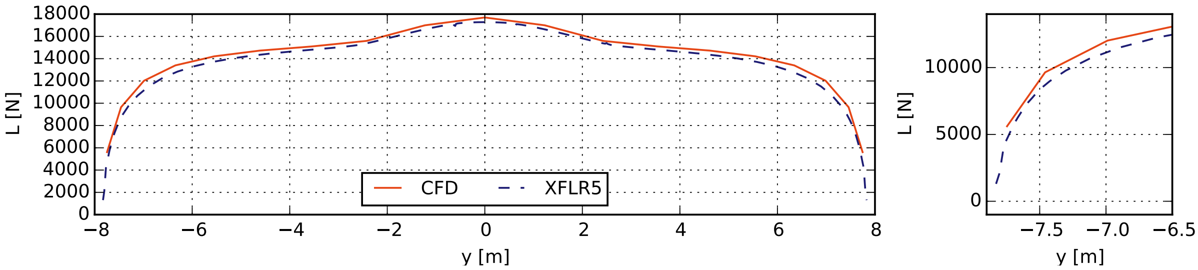

Figure 9.12: Lift distribution comparison between XFLR5 and CFD

As can be seen in Table 9.3 the largest difference is in the lift coefficient. When looking at figure 9.12 it can be seen the the lift distribution resulting from the CFD analysis is slightly larger, this also confirms the larger lift coefficient resulting from the CFD in table 9.3. This discrepancy is probably due to difference in the panel method approach and the lifting line theory. The other coefficients however are very similar. Therefore it is concluded that the XFLR5 results are valid. There is a small remark, this case is done for an angle of attack of 2.5 degrees. In Section 9.2.3 it is shown that for large angles of attack the drag is overestimated in the CFD results. For this case that will not be a problem, however for large angles of attack it is assumed that the drag will be too large.

10

Stability and Control

For any aircraft, being stable and controllable is essential. Both characteristics are strongly related to the size of the stabilisers and control surfaces. A large tail increases weight and drag, so optimising the size of the tail is an important aspect of the design. Stability and control characteristics can be split up in a static and dynamic aspect. Sections 10.1, 10.2 and 10.3 discuss the static characteristics of the longitudinal, lateral and directional stability, respectively. The elevator control force is discussed in Section 10.4 and finally Section 10.5 treats the dynamic stability.

10.1. Longitudinal Stability and Control

In this section the longitudinal stability and control are investigated. Since the weight and balance of the aircraft are driving parameters for determining the required tail size, this is determined first in Section 10.1.1. With the operational centre of gravity (cg) range available, the horizontal stabiliser is sized by means of a scissor plot in Section 10.1.2.

10.1.1. Balance

To determine the operational cg range which should be ensured by the tail, first the most critical load cases should be analysed. As explained in Section 10.1.2 the extended configuration demands the highest loads from the tail. Therefore only the balance of this configuration will be presented. In this section the followed approach is discussed.

To find the cg of the empty aircraft, first all component weights and positions are determined. The weights can be found in Chapter 18, while the moment arms of all components are determined from the Skyhawk manual [21] or through measurements. Furthermore a few assumptions are made regarding the cg position of the wing, tail and fuel. First of all, the cg location of the wing is assumed to be at 40% of the root chord. The cg of the tail is at 42% of the chord at 38% span. These assumptions can be justified by the method presented in Roskam [13]. Finally the fuel is located behind the wingbox at 35% to 65% of the mean aerodynamic chord (MAC). These locations are determined from Figure 13.5. Furthermore it is assumed that the fuel moment arm will remain the same during flight because the wing does not feature large taper. Finally, by multiplying the arms with the component weights, the cg location can be determined.

To determine the most forward and aft cg locations during operation, a weight and balance program is made in Python[1] in which several configurations of payload, fuel and luggage division are compared. From this it can be determined that the most forward cg location occurs with only the two front seats occupied, with almost no fuel and no additional luggage. The most aft location is with the aircraft fully loaded including luggage in the most aft baggage compartment. Moreover, the adjustable seat position of the pilot is considered in determining the limits. Finally it is checked whether the aircraft in any loading

[1] `https://www.python.org`

condition can tip over when on the ground. Because the most aft limit never exceeds the position of the main wheels at 55% of the chord, the aircraft will not be able to tip over. The determined cg limits can be seen in Table 10.1.

Table 10.1: Operational centre of gravity limits for the Skyhawk and Morphlight (extended configuration)

Limit	**Centre of gravity position [% MAC]**	
	172S	Morphlight
Empty	19	18
Forward	18	18
Aft	36	46

This approach is validated by the allowed cg locations of 15% to 36% MAC, provided by the manufacturer in the Skyhawk information manual [21, p. 6-16]. Comparing this allowed margin to the found limits it can be stated that they are very close. Furthermore, it should be noted that the investigated load cases are examples of likely occupations. Every other load case for normal use can be adapted to fall within the envelope, by shifting some weights or adding ballast.

Following the same approach for the Morphlight, its operational centre of gravity limits are determined as well. The results can be seen in Table 10.1. By comparing the values it can be seen that the aft limit of the Morphlight is located further on the chord than that of the Skyhawk. This can be explained by the fact that the chord of the Morphlight is smaller, resulting in a relative backwards shift of position on the chord. In absolute distance however, the Morphlight cg locations are more to the front. This can be seen when looking at the forward limit which is for both aircraft at 18% of the MAC. The absolute forward shift can be explained by the fact that the leading edge position of the wing is kept fixed while a smaller chord is considered, moving the cg of the wing and therefore also fuel to the front.

10.1.2. Horizontal Stabiliser Sizing

The horizontal stabiliser should be designed to ensure both stability and controllability during every phase of the flight and for all configurations of morphing. The landing configuration featuring the extended span and chord results in the most demanding constraints. This is because in landing the wing has its largest surface area and thus generates the most lift. Furthermore during landing the flaps are fully deployed which generates an additional pitch down moment. All of this requires a larger pitch up moment from the tail and is thus more demanding regarding stability and controllability. Therefore only this configuration is considered in sizing the horizontal tail.

To determine the minimum required surface area, both the stability and controllability requirements are assessed. For the aircraft to be stable, it is required that the neutral point is located behind the cg. The neutral point location can be found by evaluating around which point the variation of moments due to a change in angle of attack is zero. By following the approach in [24] the location of the neutral point as percentage of the MAC can be determined by Equation (10.1). From this equation it can be seen that a larger tail moves the neutral point more aft and thus improves the stability.

$$\bar{x}_{np} = \bar{x}_{ac} + \frac{C_{L\alpha_h}}{C_{L_{\alpha_w}}}\left(1 - \frac{d\epsilon}{d\alpha}\right)\frac{S_h l_h}{S\bar{c}}\left(\frac{V_h}{V}\right)^2 \tag{10.1}$$

Concerning the controllability, it is assessed whether the horizontal tail is able to trim the aircraft into moment equilibrium. This capability of the tail is dependent on the tail area and also the cg location, which changes the effective tail arm. A schematic overview of this moment equilibrium can be seen in Figure 10.1. To assess the controllability the same way as stability, the allowed cg position can be determined as function of the horizontal tail area as in Equation (10.2) [25].

$$\bar{x}_{cg} = \bar{x}_{ac} - \frac{C_{m_{ac}}}{C_{L_{A-h}}} + \frac{C_{L_h}}{C_{L_{A-h}}}\frac{S_h l_h}{S\bar{c}}\left(\frac{V_h}{V}\right)^2 \tag{10.2}$$

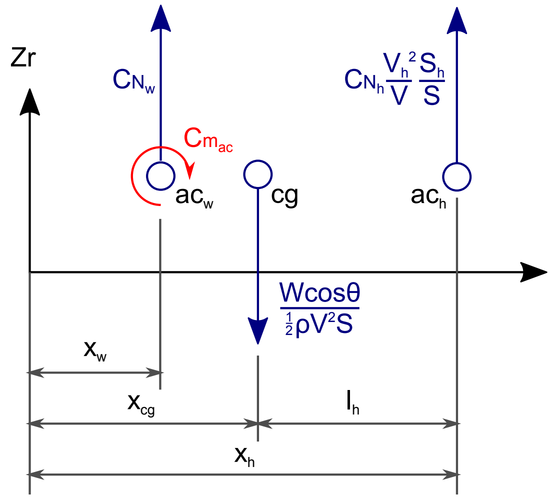

Figure 10.1: Non-dimensional moment contributions of the wing and tail around the center of gravity.

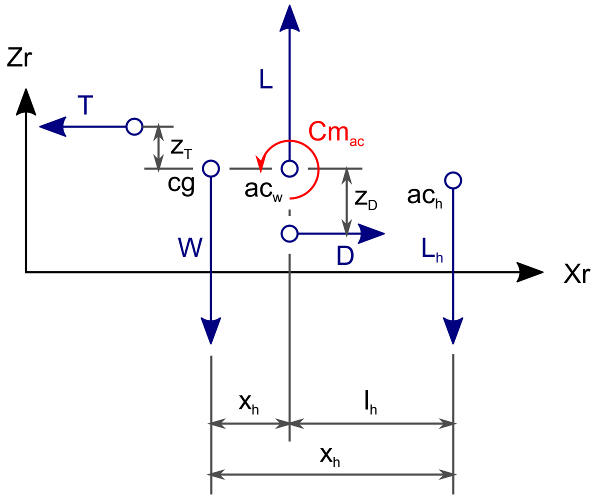

Figure 10.2: Overview of generated moments during take-off

Important parameters influencing the stability and controllability of the aircraft are the position of the aerodynamic centre, lift slopes of the wing and tail and finally the moment around the aerodynamic centre, $C_{m_{ac}}$. The followed approach to determine these parameters is discussed here. To start with, the aerodynamic centre of the main wing plus fuselage $x_{ac_{wf}}$ is determined with the method in [20]. First by using a carpet plot, the wing aerodynamic centre can be found to be at 23% of the MAC. Then a destabilising effect of the fuselage has to be added which can also be found from [20]. This approach results in an aerodynamic centre at 20% of the MAC. The value for $C_{m_{ac}}$ is determined by adding the contribution of the wing, fuselage and most importantly the flaps as in Equation (10.3). Finally the lift slopes are determined with DATCOM and the panel method in XFLR5. These coefficient were validated with the Torenbeek method [20]. An overview of the determined parameters can be seen in Table 10.2.

$$C_{m_{ac}} = C_{m_{ac_w}} + C_{m_{ac_f}} + C_{m_{ac_{flaps}}} \tag{10.3}$$

Table 10.2: Aerodynamic parameters influencing stability and controllability of the Skyhawk and Morphlight.

		C172S	**Morphlight**
$C_{L_{\alpha_h}}$	[rad^{-1}]	3.27	3.27
$C_{L_{\alpha_w}}$	[rad^{-1}]	4.25	4.83
$C_{m_{ac}}$	[-]	−0.17	−0.28
MAC	[m]	1.49	1.17
$x_{ac_{wf}}$	[% MAC]	19	20

To assess both the stability and controllability requirements at the same time a scissor plot is made. Here the required horizontal tail area can be found as function of the desired allowable cg range. This range can be formulated as a requirement specified by the operational cg range stated in Section 10.1.1.

The scissor plots in Figure 10.3 are created by plotting Equations (10.1) and (10.2), where the former gives the stability curve indicated by the most right lines. The latter gives the controllability curve which points left and is indicated by an unmarked line. Furthermore a stability margin of 5% is plotted just left of the stability curve. This margin is intended to make sure that the tail will just be slightly larger to ensure stability.

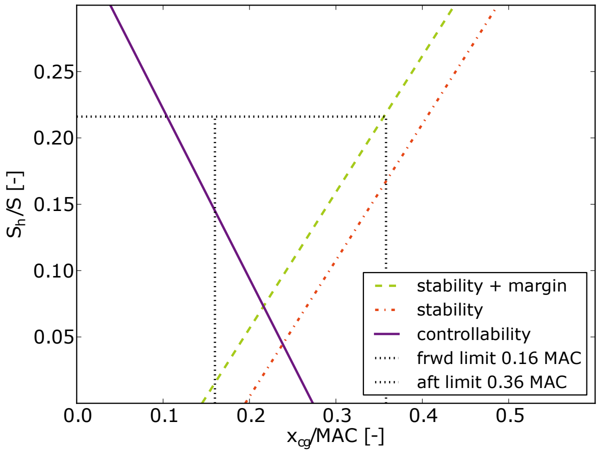

(a) Scissor plot of the Skyhawk

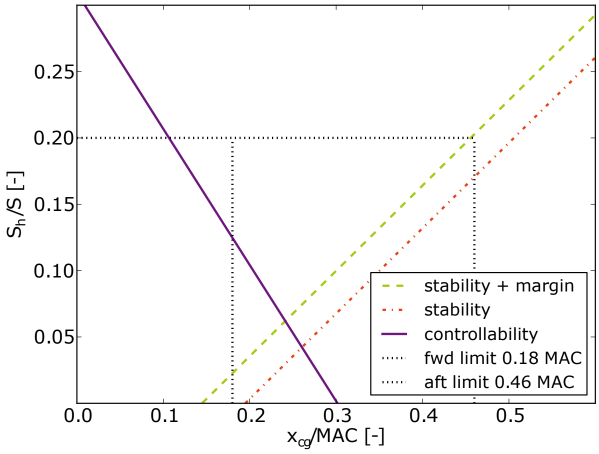

(b) Scissor plot of the Morphlight

Figure 10.3: Scissor plots of the Cessna Skyhawk and Morphlight.

Results of Horizontal Stabiliser Sizing

Looking at the two plots in Figure 10.3 one can see that for the Morphlight the absolute allowable range is shifted to the right. This can be explained by the fact that the MAC is smaller therefore every point shifts to the back. Furthermore, regarding the two controllability curves, the Morphlight shows a line starting further right which indicates that the controllability requirement becomes more stringent. This is the direct effect of the increased flapped area of the Morphlight which has a destabilising effect. This is expressed in the more negative $C_{m_{ac}}$ which shifts the curve right as can be seen in Equation (10.2).

Concerning the operational cg range specified in Section 10.1.1 the minimum allowed cg range for the Skyhawk should be within 0.18 and 0.36 of the MAC. According to [21, p. 6-16] however the limits are slightly more to the front at 0.16 MAC. Therefore these limits are indicated. The horizontal dotted line represents the actual size of the tail which proves to be of sufficient size as can be seen in the plot. For the Morphlight the cg limits were taken at 0.18 and 0.46 MAC as determined from Table 10.1. This is assumed to be valid since this method produced sufficiently accurate limits for the Skyhawk. By reading off the required tail size on the vertical axis it can be seen that this aft limit results in a tail size of 20% of the wing area which corresponds to 3.52 m^2. Comparing this to the tail size of the original Skyhawk (3.54 m^2) the horizontal tail is essentially the same.

10.1.3. Elevator Sizing

The function of the elevator is to adjust or maintain the attitude of the aircraft. This may either require a positive lift force to pitch the aircraft down, or a negative lift force to generate a pitch up moment.

By analysing the different flight situations it is determined that the highest loads from the tail are required during take-off. This is because during take-off the aircraft needs to generate sufficient pitch up moment to rotate and maintain this attitude. Furthermore the deployed flaps in this stage of the flight will result in a significant negative pitching moment around the aerodynamic centre ($C_{m_{ac}}$) which will require even more pitch up moment from the tail. Finally, the lift generated by the main wing can also contribute to the pitch down moment of the aircraft. This moment is dependent on the cg position with respect to the aerodynamic centre. With the cg located in front of the aerodynamic centre the main wing will effectively generate a pitch down moment which again will have to be compensated by the tail. An overview of these moment contributions can be seen in Figure 10.2.

For sizing the elevator, the main influencing parameter is the maximum required lift from the tail. This maximum, though negative, C_{L_h} can be determined by the pitch up moment required from the tail to rotate the aircraft. By looking at Figure 10.2 the moment equilibrium can be derived as in Equation (10.4).

$$L_h \cdot x_h = T \cdot z_t + L \cdot x_L + D \cdot z_D + I_{yy} \cdot \ddot{\theta} \tag{10.4}$$

The pitch up moment required from the tail can be determined by adding all the pitch down moments on the right hand side. These consist of a contribution of the thrust, lift, moment around the aerodynamic centre and the drag. Additionally an angular acceleration is required to rotate the aircraft as is indicated by the last term. The moment arms are determined from measurements where the drag is assumed to act 0.15 m below the cg which results in the most critical situation. Furthermore the inertia term is found from [13] and the required angular acceleration to rotate is found to be 9 deg/s^2 [26]. Then with the found tail lift, L_h, the maximum lift coefficient of the tail can be found to be -0.66 [-].

The actual elevator sizing is done on basis of a method presented in [26]. This method determines the required elevator chord ratio as function of the found lift coefficient and maximum possible deflection. It defines an elevator effectiveness factor τ_e, which is the angle of attack of the elevator over its maximum deflection. The elevator angle of attack consists of an angle originating from the horizontal stabiliser at take-off, α_h, and the angle required by the elevator, α_e, which can be found by Equation (10.5). This elevator angle is linearly dependent on the required lift coefficient. When τ_e is determined according to Equation (10.6), the method gives a direct relation between τ_e and the required fraction of the tail chord which should be occupied by the elevator, c_e/c_h.

$$\alpha_e = C_{L_h}/C_{L_{\alpha_h}} \tag{10.5}$$

$$\tau_e = \frac{\alpha_h + \alpha_e}{\delta_{max}} \tag{10.6}$$

Results of Elevator Sizing

Using the approach described in this section, the maximum negative value for C_{L_h} is found to be -0.66. This is assumed achievable since the maximum lift coefficient of the tail is found to be -0.686 with the panel method in XFLR5. This value for C_{L_h} results in a chord ratio of 0.34 of the total tail chord. Compared to a ratio of 0.36 of the actual Skyhawk this approach can be considered validated. For the Morphlight the lift coefficient of the tail is required to be -0.67, corresponding to a required chord ratio of 0.342. Therefore, also because the horizontal stabiliser area is the same, it can be concluded that the current elevator is of sufficient size to be applied to the Morphlight.

10.2. Lateral Stability and Control

10.2.1. Aileron Sizing

Featuring a varying span, the need for an aileron resizing arises for the Cessna Morphlight. The aircraft manoeuvrability shall be similar to the Cessna 172S in every possible configuration.

In order to size the ailerons, the method described by S. Gudmundsson is used [27]. This method starts by determining the aileron authority derivative $C_{L_{\delta_a}}$ for the three-dimensional wing. This is calculated with the wing span, b, wing chord, c, surface area, S, and the two dimensional aileron lift coefficient, $C_{l_{\delta_a}}$, as inputs. The wing stations are defined as spanwise wing locations. $C_{l_{\delta_a}}$ is defined as the two dimensional change in lift coefficient with aileron deflection. The simplified equation for a tapered wing is shown in Equation (10.7).

$$C_{L_{\delta_a}} = \frac{C_{l_{\delta_a}} c_r}{Sb} \left(\left({b_2}^2 - {b_1}^2\right) + 4\frac{(\lambda - 1)}{3b}\left({b_2}^3 - {b_1}^3\right) \right) \tag{10.7}$$

The second derivative to be determined is the roll damping derivative, C_{l_p}. The effect is due to the asymmetric angle of attack of the left and right wing during a rolling manoeuvre. This coefficient is found using Equation (10.8) which is simplified for a tapered wing.

$$C_{l_p} = -\frac{\left(C_{l_\alpha} + C_{d_0}\right) \cdot c_r \cdot b}{24S}(1 + 3\lambda) \tag{10.8}$$

The final step is to determine the steady state roll rate, p, which is determined by Equation (10.9) for a given aileron deflection δ_a. The roll rate is dependent on the airspeed, where a lower airspeed gives a lower roll rate. Therefore, the ailerons were sized for a low speed condition, where $V = 28$ m/s. This is close to the stall speed for all aircraft, and provides a good reference point.

$$p = -\frac{C_{L_{\delta_a}}}{C_{l_p}}\delta_a\left(\frac{2V}{b}\right) \tag{10.9}$$

From (10.9) it can be seen that the roll rate is negatively influenced by a large wing span. Therefore, the aileron area has to be increased to ensure a roll rate similar to the Skyhawk. In spanwise direction however there is not sufficient space to place more ailerons considering the large area occupied by the trailing edge devices. This problem was resolved by increasing the chordwise length of the ailerons, making the change in lift larger when the aileron is deflected. The ailerons take up 35% of the wing chord.

Table 10.3 shows the roll rate of the old Cessna and the roll rates of the new Cessna Morphlight in the two span conditions, being fully extended and fully retracted. The parameters used to calculated the roll rates are stated as well. As one can see the roll rate of the new aircraft is slightly reduced to 46.5 deg/s. In the extended state the roll rate is reduced to 40 deg/s.

Table 10.3: Aileron size and roll rate

Aircraft	b [m]	c [m]	S [m^2]	b_1 [m]	b_2 [m]	$C_{l_{\delta_a}}$ [1/deg]	$C_{L_{\delta_a}}$ [1/rad]	C_{l_p} [1/rad]	δ_a [deg]	p [deg/s]
Cessna 172S Skyhawk	11	1.466	16.1	2.57	5.35	0.065	0.57	-0.8594	20	49.6
Cessna Morphlight (retracted)	10	1.000	10.0	3.34	4.90	0.072	0.64	-1.1572	20	46.5
Cessna Morphlight (extended)	15	1.175	17.6	4.27	7.40	0.072	0.69	-0.9644	20	40.0

The dimensions b_1 and b_2 given in Table 10.3 are measured from the aircraft centre line. A margin of 10 cm is taken at the wingtip in order to have sufficient space for a navigation light and for the aileron attachment.

10.3. Directional Stability and Control

10.3.1. Vertical Tail Sizing

This section discusses a fast method, presented by Torenbeek, to estimate the vertical tail size required to ensure sufficient directional stability [20]. The prime parameter describing directional stability is C_{n_β}. For aircraft of the class of the C172 with (a single) fuselage mounted engine(s), stability is generally driving the vertical tail sizing [28]. Therefore, the controllability is not considered in this analysis. Equations (10.10) and (10.11) are used to compute the effect on the yawing moment caused by the presence of the fuselage and propeller, respectively.

$$C_{n_{\beta_f}} = -k_\beta \frac{S_{fs} l_f}{Sb}\left(\frac{h_{f_1}}{h_{f_2}}\right)^{1/2}\left(\frac{b_{f_2}}{b_{f_1}}\right)^{1/3} \tag{10.10}$$
$$k_\beta = 0.3\frac{l_{cg}}{l_f} + 0.75\frac{h_{f_{max}}}{l_f} - 0.105$$

$$C_{n_{\beta_p}} = -0.053 B_p \sum \frac{l_p D_p^2}{Sb} \tag{10.11}$$

Most of the parameters are similar for the Skyhawk and Morphlight, except for the wingspan and wing area, which vary with morphing, and the centre of gravity location. The centre of gravity is taken at the aft location, corresponding to the smallest tail arm (and thus largest tail area required). The definitions of the dimensions are given in Figure 10.4.

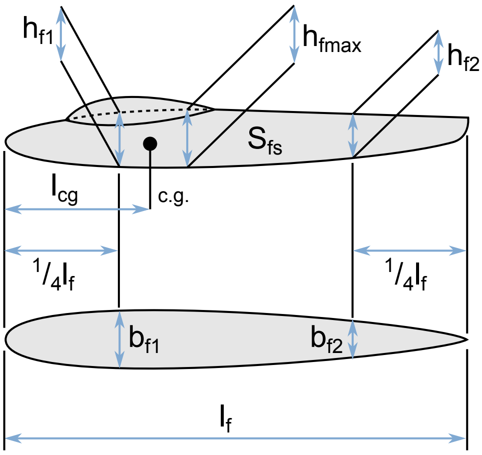

Figure 10.4: Fuselage geometry in relation to the yawing moment due to sideslip [20].

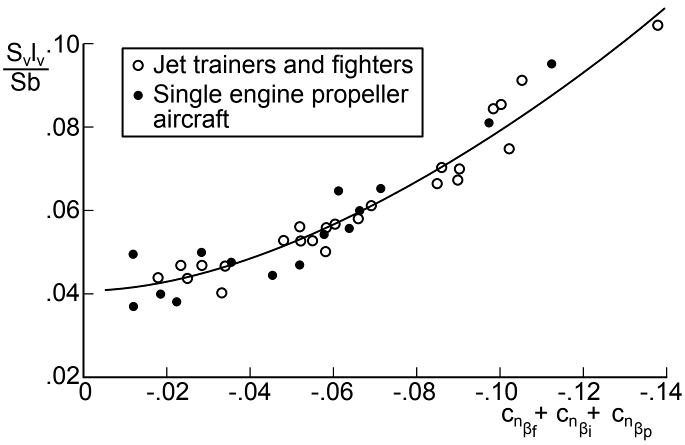

Figure 10.5: Rapid estimation of vertical tail volume for aircraft with fuselage-mounted engines [20].

Since the Skyhawk and Morphlight have a high wing configuration, $C_{n_{\beta_i}} = -0.017$ [20]. Now the total coefficient can be computed with Equation (10.12). The required tail volume can then be derived from Figure 10.5.

$$C_{n_\beta} = C_{n_{\beta_f}} + C_{n_{\beta_i}} + C_{n_{\beta_p}} \tag{10.12}$$

To validate the computation method, the required surface for the Cessna 172S was calculated and compared to the actual area found in literature. The Torenbeek method gives a vertical tail surface area of 1.86 m^2, a 10% overestimation of the actual 1.68 m^2. This is considered acceptable for a first estimate of the tail size. For the Morphlight, the required vertical tail size is found to be 2.31 m^2.

10.3.2. Rudder Sizing

The most critical task for the rudder of a singe engine normal category general aviation aircraft is to allow the pilot to maintain the course of the aircraft during a crosswind landing [26]. According to FAR Part 23 section 233, general aviation aircraft must be able to cope with 90° crosswinds of up to 25 knots ($V_w = 12.9$ m/s) [29]. This requirement can be used to verify whether the rudder is properly sized.

In a crosswind landing, the aircraft flies under a certain crab angle. To maintain this crab angle χ, the aircraft flies with a sideslip angle β, with respect to the relative wind. This offset causes the wind to push on the side area of the entire aircraft. As the centre of pressure and the centre of gravity generally do not coincide, this generates a yawing moment. To balance this moment, the tail should provide a sideforce. The tail can generate this force by a deflection δ_R of the rudder.

To derive the required deflection of the rudder, the moments and forces can be summed. The approach used by Sadraey [26] was found to have the angles defined erroneously, so an adapted solution is derived based on the same principles. By summing the side forces and yawing moments shown in Figure 10.6, Equations (10.13) and (10.14) can be derived. The side force due to the wind, F_w, is expressed in terms of the side profile area, S_s, and the side profile drag coefficient, C_{D_Y}. The forces and moments caused by having the aircraft at a sideslip angle come from the terms C_{Y_β} and C_{n_β}. The influence of the rudder is included by the coefficients of δ_R.

$$\sum Y = 0: \quad \frac{1}{2}\rho V_w^2 S_s C_{D_Y} + \frac{1}{2}\rho V_T^2 S \left(C_{Y_\beta}\beta + C_{Y_{\delta_R}}\delta_R\right) = 0 \tag{10.13}$$

$$\sum N = 0: \quad -\frac{1}{2}\rho V_w^2 S_s C_{D_Y} d_c \cos\beta + \frac{1}{2}\rho V_T^2 S b \left(C_{n_\beta}\beta + C_{n_{\delta_R}}\delta_R\right) = 0 \tag{10.14}$$

A critical aircraft speed equal to the minimum flight speed ($U_1 = 1.1V_S$) is used. For the Morphlight, this, together with the crosswind speed requirement, equates to a true relative wind speed $V_T = \sqrt{U_1^2 + V_w^2} =$

Table 10.4: Rudder deflections and sideslip angles for crosswind landings of the Cessna 172S and Morphlight

	172S	**Morphlight**
β	12.7°	10.0°
δ_R	7.9°	6.1°

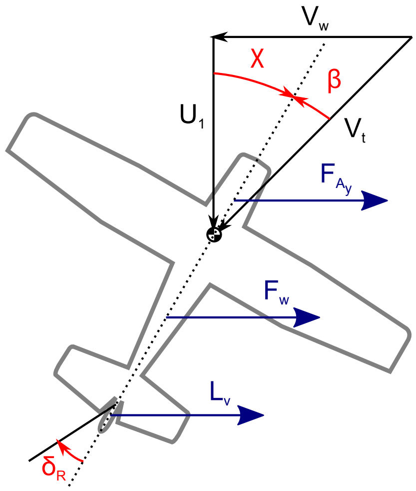

Figure 10.6: Angles and forces for the rudder equations

30.1 m/s. This allows the control derivatives to be computed, from which the rudder deflection and sideslip angle follow.

The results of the rudder sizing analysis for both the Skyhawk and the Morphlight are listed in Table 10.4. For both aircraft, the required rudder deflection is significantly less than the maximum of about 17°, so the aircraft can safely land in a 25-kt crosswind. The margin ensures the pilot can still manoeuvre with a change in wind or for evasive manoeuvres. The Morphlight requires less rudder deflection due to its increased vertical tail size, which is determined in Section 10.3.1.

10.4. Elevator Control Force

To keep the elevator at the desired deflection, the pilot has to exert a force on the controls to counteract the aerodynamic moment on the elevator hinge. This force is linearly dependent on the dynamic pressure and therefore becomes very large at high speeds. For this reason a trim tab is installed at the end of the elevator to alleviate the moments on the hinge and thus reduce the control force required by the pilot. When the required control force is zero with a certain trim tab setting, the aircraft is trimmed for a corresponding trim speed. The required trim tab angle varies with airspeed. To guarantee controllability in all conditions, it is required that the aircraft can be trimmed over the entire velocity range for all allowed cg positions.

There are regulations regarding allowable maximum forces which are required to control the aircraft. For the elevator control, the maximum permissible force for a long period (more than a few minutes) is 4.5 kg, while 35 kg is allowed for a short period [1]. Since short periods are harder to analyse, only the long period forces are checked. The control system can be split in aileron, elevator and rudder, each having specific maximum forces. Only the elevator forces are considered, as these are the most demanding.

The required control forces can be determined by the approach outlined in [24] where control force is given by Equation (10.15). The force depends on the elevator hinge moment coefficient, C_{h_e}, the dynamic pressure and the gear ratio between the effective elevator deflection and the applied deflection on the stick. Furthermore the hinge moment coefficient can be expanded to Equation (10.16), since it depends on the local angle of attack α_h, the elevator deflection δ_e, and the trim tab deflection δ_{t_e}. Furthermore, since a symmetrical airfoil (NACA 0012/009) is used for the tail, C_{h_0} is zero.

$$F_e = -\frac{d\delta_e}{ds_e}\frac{1}{2}\rho V_h^2 S_e \bar{c}_e \cdot C_{h_e} \tag{10.15}$$

$$C_{h_e} = C_{h_0} + C_{h_\alpha} \cdot \alpha_h + C_{h_\delta} \cdot \delta_e + C_{h_{\delta_t}} \cdot \delta_{t_e} \tag{10.16}$$

To find the hinge moment coefficient, the angles α_h and δ_e should be determined as a function of the velocity since the relationship between control force and velocity is investigated. First of all, α_h is a function of the angle of attack and the downwash gradient where the angle of attack can be found according to the equation of vertical equilibrium. The elevator deflection can be determined from the equation for moment equilibrium (10.17) which can be solved for δ_e (10.18). Here C_{m_α} is found from Equation (10.19). The used lift coefficients of the wing and tail, downwash and local airflow at the tail can be found in Table 10.5. The lift coefficients were determined with DATCOM and validated with the panel method in XFLR5. Furthermore for the downwash gradient several values were found in literature ranging from 0.41 according to Roskam [30] to 0.49 from DATCOM. An average value of 0.45 was used in the calculations.

$$C_m = C_{m_0} + C_{m_{\delta_e}} \cdot \delta_e + C_{m_\alpha} \cdot (\alpha - \alpha_0) \tag{10.17}$$

$$\delta_e = -\frac{1}{C_{m_{\delta_e}}} \cdot \{C_{m_0} + C_{m_\alpha} \cdot (\alpha - \alpha_0)\} \tag{10.18}$$

$$C_{m_\alpha} = C_{N_{\alpha w}} \cdot \frac{x_{cg} - x_{ac}}{\bar{c}} - C_{N_{\alpha_h}} \cdot \left(1 - \frac{d\epsilon}{d\alpha}\right) \cdot \left(\frac{V_h}{V}\right)^2 \cdot \frac{S_h \cdot l_h}{S \cdot \bar{c}} \tag{10.19}$$

Before the Skyhawk and the Morphlight can be analysed, first this approach is validated for the Cessna 152. This aircraft is used as reference since experimental and theoretical control force data can be found in literature [31] and this aircraft is similar to the Skyhawk. By using the same cg location, weight, gearing ratio and downwash as provided in [31] and geometry data of the Cessna 152, the starting point of the control force plot (V = 0) is only is 1% off. Furthermore, also the trim tab deflection required to trim at a given airspeed matches. Therefore the approach is validated. It should be noted however that the hinge moment coefficients for the Cessna 152 are not provided in the literature therefore the same values are used as determined for the Skyhawk. These coefficients, C_{h_α}, C_{h_δ}, and $C_{h_{\delta_t}}$ are determined with DATCOM and can be found in Table 10.5.

Applying this approach to the Skyhawk and Morplight gives control force plots as can be seen in Figures 10.7 and 10.8. Furthermore the used coefficients can again be found in Table 10.5. To determine the maximum control force and trim tab deflection, also the most forward position of cg is considered (15% MAC) since this results in the largest required tail force as explained in Section 10.1.3.

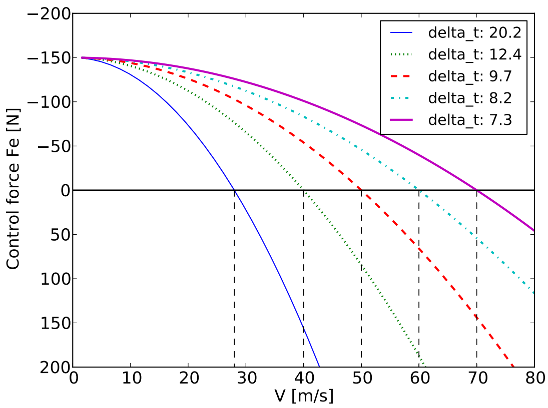

Figure 10.7: Elevator control force curve for the Cessna Skyhawk at $x_{cg}/\bar{c} = 0.15$ where the most left curve corresponds to the largest trim tab deflection.

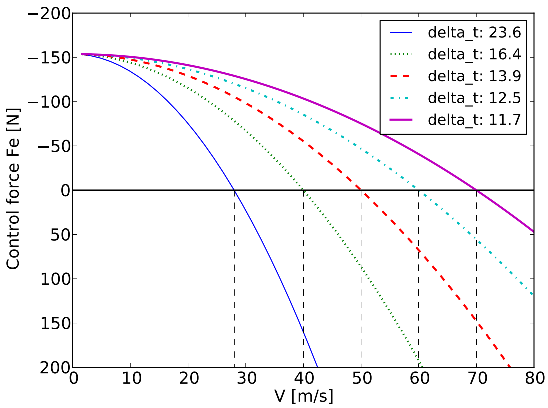

Figure 10.8: Elevator control force curve for the Morphlight at $x_{cg}/\bar{c} = 0.15$ where the most left curve corresponds to the largest trim tab deflection.

By looking at the control force plots it can be seen that both aircraft can be trimmed for the whole range of velocities with a maximum required trim tab deflection of 23.6°. This is within the specified limits of the deflection ranging from -23° to +28° and therefore this requirement is met. The pilot can thus trim the aircraft at any airspeed in such a way that the required control force is less than 4.5 kg. It can

[2] `http://tigert.1g.fi/kuvat/Simulators/Flightgear/C172-dimensions` [cited 28 May 2015]

Table 10.5: Parameters for the Cessna 152, 172S and Morphlight.

Parameter		C152	C172S[32]	Morphlight
C_{h_α}	[deg^{-1}]	-0.0057	-0.0057	-0.0057
C_{h_δ}	[deg^{-1}]	-0.0115	-0.0115	-0.0115
$C_{h_{\delta_t}}$	[deg^{-1}]	-0.01	-0.01	-0.01
$C_{N_{w_\alpha}}$	[deg^{-1}]	0.074	0.074	0.084
$C_{N_{h_\alpha}}$	[deg^{-1}]	0.057	0.057	0.057
i_h	[deg]	-2.5	-2	-2
S_e	[m^2]	0.94	1.35	1.35
S_h	[m^2]	2.58	3.5	3.5
$\left(\frac{V_h}{V}\right)^2$	[-]	0.85	0.85[33]	0.85
$\frac{d\delta_e}{ds_e}$	[deg/m]	4.92	4.945[2]	4.945
$\frac{d\epsilon}{d\alpha}$	[-]	0.45	0.45	0.45

be seen however that the Morphlight requires a larger trim tab angle to trim at the stall speed of 28 m/s. This is due to the effect of the flaps which create a large pitch down moment which has to be compensated by the tail.

A sensitivity analysis is performed to determine the effect of some estimated parameters. First of all, as stated before, the whole allowable centre of gravity range is investigated for its effect on the controllability. From this it can be concluded that the most forward cg position requires the largest forces of the pilot. Secondly, the parameter which determines the effectiveness of the trim tab, $C_{h_{\delta_t}}$, was analysed for a range of values. The trim tab should be designed such that this coefficient is just large enough to enable the pilot to trim the aircraft at all possible velocities. In this analysis the required value was found to be -0.01 which is in the same order as the elevator effectiveness C_{h_δ}. Considering the trim tab is smaller than the elevator but has a larger arm with respect to the hinge this is assumed to be valid.

In the control force curves, the trim speed can be found at the point where the control force is zero, $V_{F_e=0} = V_{trim}$. At this trim speed, the slope of the curve determines the elevator control force stability of the aircraft. If $\left(\frac{dF_e}{dV_e}\right)_{F_e=0} > 0$, the aircraft has control force stability. This means that with increasing speed the required push force will be larger. The natural response of the pilot is to bring the aircraft back to its trim speed. This is desired, since it makes it much easier and more pleasant for the pilot to control the aircraft. As there is a (small) non zero friction force involved in the actual system, there is a small range of trim speeds for a certain condition. The elevator control force stability should actually be slightly positive to account for this. According to U.S. military regulations, this yields $\left(\frac{dF_e}{dV_e}\right)_{F_e=0} > 0.041$ kg/(km/h) [24]. At 250 km/h, $\left(\frac{dF_e}{dV_e}\right)_{F_e=0} = 0.143$ kg/(km/h) for the Morphlight. Because the value is positive, the Morphlight has elevator control force stability. The stability margin is also sufficiently large to account for friction in the system.

Because the Morphlight is control force stable, it is implied the aircraft is also statically stable. This means the aircraft, after encountering a disturbance, will try to restore the condition it was flying before the disturbance. This is favourable for the pilot, as he will not have to correct all the time.

From this analysis it can be concluded that the original trim tab of the Skyhawk is sufficiently effective to be applied on the Morphlight.

10.5. Dynamic Stability

One of the key requirements of the Cessna Morphlight is that it should have similar dynamics and handling characteristics to the Cessna 172S. To ensure this, a suitable wing, tailplane and control surface configuration have to be selected, thus part of the selection process involves properly analysing the dynamic stability and the aircraft's sensitivity to control inputs. This section covers all details around the numerical simulation tool, from the theory behind the simulations to a short explanation behind the verification process taken. Section 10.6.3 contains the dynamic stability results for the Cessna Morphlight and compares these to the Skyhawk to form a final conclusion.

In order to evaluate the dynamic stability of the aircraft, a state space Linear Time Invariant (LTI) system is used. The aerodynamic coefficients and mass properties used in this system are obtained using a range of aerodynamics tools. The following sections go through a detailed explanation of the numerical simulation tool.

10.5.1. Equations of Motion and LTI-System

To model any system a set of governing equations representing the system is required. In the case of most vehicles such as an aircraft, these would be the Equations of Motion (EOM). To simplify the problem, these equations have been simplified by taking assumptions and linearising them. Equations (10.20) and (10.21) are the linearised EOM for symmetric and asymmetric motions for aircraft [24].

$$\begin{bmatrix} C_{X_u} - 2\mu_c D_c & C_{X_\alpha} & C_{Z_0} & C_{X_q} \\ C_{Z_u} & C_{Z_\alpha} + (C_{Z_{\dot\alpha}} - 2\mu_c)D_c & -C_{X_0} & C_{Z_q} + 2\mu_c \\ 0 & 0 & -D_c & 1 \\ C_{m_u} & C_{m_\alpha} + C_{m_{\dot\alpha}} D_c & 0 & C_{m_q} - 2\mu_c K_Y^2 D_c \end{bmatrix} \begin{bmatrix} \hat{u} \\ \alpha \\ \theta \\ \frac{q\bar{c}}{V} \end{bmatrix} = \begin{bmatrix} -C_{X_{\delta_e}} \\ -C_{Z_{\delta_e}} \\ 0 \\ -C_{m_{\delta_e}} \end{bmatrix} \delta_e \tag{10.20}$$

$$\begin{bmatrix} C_{Y_\beta} + \left(C_{Y_{\dot\beta}} - 2\mu_\beta\right) D_b & C_L & C_{Y_p} & C_{Y_r} - 4\mu_b \\ 0 & -\frac{1}{2}D_b & 1 & 0 \\ C_{l_\beta} & 0 & C_{l_p} - 4\mu_b K_X^2 D_b & C_{l_r} + 4\mu_b K_{XZ} D_b \\ C_{n_\beta} + C_{n_{\dot\beta}} D_b & 0 & C_{n_p} + 4\mu_b K_{XZ} D_b & C_{n_r} - 4\mu_b K_Z^2 D_b \end{bmatrix} \begin{bmatrix} \beta \\ \varphi \\ \frac{pb}{2V} \\ \frac{rb}{2V} \end{bmatrix} = \begin{bmatrix} -C_{Y_{\delta_a}} & -C_{Y_{\delta_r}} \\ 0 & 0 \\ -C_{l_{\delta_a}} & -C_{l_{\delta_r}} \\ -C_{n_{\delta_a}} & -C_{n_{\delta_r}} \end{bmatrix} \begin{bmatrix} \delta_a \\ \delta_r \end{bmatrix} \tag{10.21}$$

With the governing equations known, the next step is to create a model representing the system. A relatively simple way to achieve this is by rewriting the EOM into state space form and thus obtain a state space Linearized Time Invariant system (LTI-system). The non-dimensionalised EOM are rewritten into a dimensionalised LTI-system. This derivation process is shown below.

Symmetrical Equations of Motion

The first step is to dimensionalise the state variables by rearranging the equation of motion as in Equation (10.22). In Equation (10.23) the D_c terms are separated and substituted by $\frac{\bar{c}}{V}\frac{d}{dt}$. The last step for now is to rearrange the equation such that the $\frac{d}{dt}$ terms are moved to the state vector resulting in Equation (10.24) containing three matrices, which are subsequently used to create the state space model.

$$\begin{bmatrix} \frac{1}{V}\left(C_{X_u} - 2\mu_c D_c\right) & C_{X_\alpha} & C_{Z_0} & \frac{\bar{c}}{V} C_{X_q} \\ \frac{1}{V} C_{Z_u} & C_{Z_\alpha} + (C_{Z_{\dot\alpha}} - 2\mu_c)D_c & -C_{X_0} & \frac{\bar{c}}{V}\left(C_{Z_q} + 2\mu_c\right) \\ 0 & 0 & -D_c & \frac{\bar{c}}{V} \\ \frac{1}{V} C_{m_u} & C_{m_\alpha} + C_{m_{\dot\alpha}} D_c & 0 & \frac{\bar{c}}{V}\left(C_{m_q} - 2\mu_c K_Y^2 D_c\right) \end{bmatrix} \begin{bmatrix} u \\ \alpha \\ \theta \\ q \end{bmatrix} = \begin{bmatrix} -C_{X_{\delta_e}} \\ -C_{Z_{\delta_e}} \\ 0 \\ -C_{m_{\delta_e}} \end{bmatrix} \delta_e \tag{10.22}$$

$$\begin{gathered} \begin{bmatrix} -\frac{2}{V}\mu_c \frac{\bar{c}}{V}\frac{d}{dt} & 0 & 0 & 0 \\ 0 & (C_{Z_{\dot\alpha}} - 2\mu_c)\frac{\bar{c}}{V}\frac{d}{dt} & 0 & 0 \\ 0 & 0 & -\frac{\bar{c}}{V}\frac{d}{dt} & 0 \\ 0 & C_{m_{\dot\alpha}}\frac{\bar{c}}{V}\frac{d}{dt} & 0 & \frac{2\bar{c}}{V}\mu_c K_Y^2 \frac{\bar{c}}{V}\frac{d}{dt} \end{bmatrix} \begin{bmatrix} u \\ \alpha \\ \theta \\ q \end{bmatrix} + \\ + \begin{bmatrix} \frac{1}{V} C_{X_u} & C_{X_\alpha} & C_{Z_0} & \frac{\bar{c}}{V} C_{X_q} \\ \frac{1}{V} C_{Z_u} & C_{Z_\alpha} & -C_{X_0} & \frac{\bar{c}}{V}\left(C_{Z_q} + 2\mu_c\right) \\ 0 & 0 & 0 & \frac{\bar{c}}{V} \\ \frac{1}{V} C_{m_u} & C_{m_{\alpha_c}} & 0 & \frac{\bar{c}}{V} C_{m_q} \end{bmatrix} \begin{bmatrix} u \\ \alpha \\ \theta \\ q \end{bmatrix} + \begin{bmatrix} C_{X_{\delta_e}} \\ C_{Z_{\delta_e}} \\ 0 \\ C_{m_{\delta_e}} \end{bmatrix} \delta_e = 0 \end{gathered} \tag{10.23}$$

$$
\begin{bmatrix}
-\frac{2}{V}\mu_c\frac{\bar{c}}{V} & 0 & 0 & 0 \\
0 & (C_{Z_{\dot{\alpha}}} - 2\mu_c)\frac{\bar{c}}{V} & 0 & 0 \\
0 & 0 & -\frac{\bar{c}}{V} & 0 \\
0 & C_{m_{\dot{\alpha}}}\frac{\bar{c}}{V} & 0 & \frac{2\bar{c}}{V}\mu_c K_Y^2\frac{\bar{c}}{V}
\end{bmatrix}\dot{\bar{x}} +
$$
$$
+\begin{bmatrix}
\frac{1}{V}C_{X_u} & C_{X_\alpha} & C_{Z_0} & \frac{\bar{c}}{V}C_{X_q} \\
\frac{1}{V}C_{Z_u} & C_{Z_\alpha} & -C_{X_0} & \frac{\bar{c}}{V}\left(C_{Z_q} + 2\mu_c\right) \\
0 & 0 & 0 & \frac{\bar{c}}{V} \\
\frac{1}{V}C_{m_u} & C_{m_{\alpha_c}} & 0 & \frac{\bar{c}}{V}C_{m_q}
\end{bmatrix}\bar{x} + \begin{bmatrix}
C_{X_{\delta_e}} \\ C_{Z_{\delta_e}} \\ 0 \\ C_{m_{\delta_e}}
\end{bmatrix}\delta_e = 0 \tag{10.24}
$$

Asymmetrical Equations of Motion

The derivation of the asymmetrical equation of motion follows the same process as the derivation of symmetrical equation of motion. First dimensionalising the states, then separating and substituting the D_b terms and then rearranging to get the final three matrices (Equation (10.25)).

$$
\begin{bmatrix}
\left(C_{Y_{\dot{\beta}}} - 2\mu_\beta\right)\frac{\bar{c}}{V} & 0 & 0 & 0 \\
0 & -\frac{1}{2}\frac{\bar{c}}{V} & 0 & 0 \\
0 & 0 & -4\mu_b K_X^2\frac{\bar{c}b}{2V^2} & 4\mu_b K_{XZ}\frac{\bar{c}b}{2V^2} \\
C_{n_{\dot{\beta}}}\frac{\bar{c}}{V} & 0 & 4\mu_b K_{XZ}\frac{\bar{c}b}{2V^2} & -4\mu_b K_Z^2\frac{\bar{c}b}{2V^2}
\end{bmatrix}\dot{\bar{x}} +
$$
$$
+\begin{bmatrix}
C_{Y_\beta} & C_L & \frac{b}{2V}C_{Y_p} & \frac{b}{2V}\left(C_{Y_r} - 4\mu_b\right) \\
0 & 0 & \frac{b}{2V} & 0 \\
C_{l_\beta} & 0 & \frac{b}{2V}C_{l_p} & \frac{b}{2V}C_{l_r} \\
C_{n_\beta} & 0 & \frac{b}{2V}C_{n_p} & \frac{b}{2V}C_{n_r}
\end{bmatrix}\bar{x}_a + \begin{bmatrix}
C_{Y_{\delta_a}} & C_{Y_{\delta_r}} \\
0 & 0 \\
C_{l_{\delta_a}} & C_{l_{\delta_r}} \\
C_{n_{\delta_a}} & C_{n_{\delta_r}}
\end{bmatrix}\bar{u}_a = 0 \tag{10.25}
$$

State Space LTI-System

The derivations above result in three matrices in the form of Equation (10.27). To create the state space representation of the LTI-system (Equation (10.26)) for the numerical simulation, the first step is to fill the C_1, C_2 and C_3 matrices with the input data. The A and B matrices required for the state space representation are then computed numerically using Equation (10.28) using simple numerical matrix inversion and multiplication functions available in Python numerical algebra libraries.

Since the states of the system are the outputs of interest the C matrix for both systems is an identity matrix and the D matrix is a zero matrix of the appropriate size.

$$
\begin{aligned}
\dot{\bar{x}} &= A\bar{x} + B\bar{u} \\
\bar{y} &= C\bar{x} + D\bar{u}
\end{aligned} \tag{10.26}
$$
$$
C_1\dot{\bar{x}} + C_2\bar{x} + C_3\bar{u} = 0 \tag{10.27}
$$
$$
\begin{aligned}
A &= -C_1^{-1}C_2 \\
B &= -C_1^{-1}C_3
\end{aligned} \tag{10.28}
$$

10.5.2. Aerodynamics Model

To obtain accurate results the input data used in the model has to be accurate. The aerodynamics model consisting of more than 30 of the input parameters has a significant effect on the system and thus it is imperative that these parameters are all estimated correctly. The main source of these aerodynamic parameters is Digital DATCOM. The main reason for this is because, unlike the other tools available, it can relatively easily provide a complete set of the aerodynamic inputs. However Digital DATCOM does have problems estimating some coefficients, namely the yawing moment coefficients. These coefficients are thus calculated using Tornado VLM.

10.5.3. Mass Properties

The mass and other mass properties such as the cg position and mass moment of inertia have a significant effect on the dynamic behaviour of the aircraft. Unlike mass and cg location, the mass moment of inertia is at this stage of the design only relevant for the dynamic analysis of the aircraft, thus the estimate of mass moment of inertia is done here.

Equations (10.29), (10.30) and (10.31) are used to estimate the mass moment of inertia of the aircraft. Parameters R_x^2, R_y^2 and R_z^2 are constants which depend on the type of aircraft being designed. Further information about these estimates can be found in [34].

$$I_{xx} = \frac{b^2 W \bar{R}_x^2}{4g} \quad (10.29) \qquad I_{yy} = l^2 W \bar{R}_y^2 \quad (10.30) \qquad I_{zz} = \left(\frac{b+l}{2}\right)^2 \frac{W \bar{R}_z^2}{4g} \quad (10.31)$$

10.5.4. Numerical Program Structure

The numerical simulation program makes use of the object oriented programming paradigm to structure its code using object of different types. This allows the user to rapidly adapt the program to suit its individual needs at a particular moment with minimal to no modifications to the core code inside the simulation library.

The core of the simulation is split in 5 main classes or object types. Each one of these classes can be used to create objects performing a specific subset of tasks. There is no limit on the number of objects of the same type that can exists parallel to each other, thus this allows to easily create an unlimited number of configurations to compare with each other at the same time.

The main 5 classes are:

- **IDATCOM**
  It serves as the interphase between Python and Digital DATCOM. It creates the input files for Digital DATCOM, then runs it and reads in the results. These files are created based on geometry parameters given to the object.
- **Aero**
  It uses an IDATCOM object to create a table of aerodynamic coefficients necessary for the state space model.
- **MassProperties**
  It calculates the non-dimentional masses and mass moment of inertia.
- **StateSpaceModel**
  It uses objects of all the classes mentioned above to create a state space model of the aircraft. The class possesses separate methods that perform the simulations on the generated state-space models and the results are subsequently stored in the state-space model obeject itself.
- **StateSpaceModelPlotter**
  Used to plot the results stored in StateSpaceModel objects. Multiple StateSpaceModel objects can be given to be plotted one on top of each other.

Verification of the Numerical Tool

A necessary step in assuring confidence in the results obtained from any numerical simulation is to check whether each component of the simulation is behaving the way it is meant to according to the theory chosen to solve the problem. This is commonly known as verification. This section focuses on the verification process of the overall numerical simulation by comparing analytical and numerical results for the Cessna Ce500 Citation.

Analytical Solution
It is possible to derive Equation (10.32) [24]. To calculate the eigenvalues corresponding to each eigenmotion, Equation (10.32) can be substituted into the equations of motion (Equations (10.20) and (10.21)). The characteristic equation can then be obtained by taking the determinant of the matrix and it can then be solved for λ_c to obtain the non-dimensional eigenvalues. The damping factors, time constants, and other characteristics, can be calculated from the eigenvalues. The results of these calculations are shown in the following sections.

$$D_c x = \frac{\bar{c}}{V} \frac{d}{dt} \left(A_x e^{\lambda_c \frac{V}{\bar{c}} t} \right) = \lambda_c x \qquad (10.32)$$

Numerical Solution
To numerically calculate the eigenvalues of the system, the inputs for the Cessna Ce500 Citation are

passed to the numerical simulation tool. After the state space systems have been created the eigenvalues can be calculated by using numerical methods available in NumPy[3], a scientific computing library for Python. These results are shown below.

Comparison Between Models
Table 10.6 shows the results from the analytical and numerical solutions for the Cessna Ce500. The errors in the table are the percentages between the absolute value of the complex eigenvalues. As expected the errors in between the two are small and can be attributed to floating point representation errors.

Table 10.6: Damping factor (ς), natural frequencies (ω_0) and errors in eigenvalues between the analytical and numerical solution of the dynamic stability tool.

	Analytical		**Numerical**		**Error [%]**
	ς	ω_0	ς	ω_0	
Symmetric	0.7182	1.6153	0.7182	1.6153	$8.70e-09$
	0.7182	1.6153	0.7182	1.6153	$8.70e-09$
	0.0441	0.1957	0.0441	0.1957	$1.18e-07$
	0.0441	0.1957	0.0441	0.1957	$1.18e-07$
Asymmetric	1.0000	2.2331	1.0000	2.2331	$5.96e-09$
	0.1045	1.7831	0.1045	1.7831	$6.46e-09$
	0.1045	1.7831	0.1045	1.7831	$6.46e-09$
	−1.0000	0.0764	−1.0000	0.0764	$3.30e-08$

10.6. Results of Stability and Control

10.6.1. Static Stability Results

For the horizontal stabiliser the required area is determined to be 3.52 m^2. This is slightly smaller than that of the original Skyhawk with a surface area of 3.54 m^2. The vertical tail of the Morphlight requires an area of 2.31 m^2, circa 37% larger than the Skyhawk.

The results of the static stability analysis are given in Table 10.7.

Table 10.7: Required horizontal and vertical tail size for the Morphlight (extended). Computed values for the Cessna 172S are included for reference.

	$\mathbf{S_h}$ [m^2]	$\frac{\mathbf{S_h}}{\mathbf{S}}$ [-]	$\mathbf{S_v}$ [m^2]
C172S	3.54	0.212	1.86
Morphlight	3.52	0.20	2.31

10.6.2. Control Surfaces Results

By analysing the control surfaces it can be determined that the elevator and rudder are of sufficient size to be applied to the Morphlight. The ailerons however are required to be larger since the extended configuration of the Morphlight experiences more damping in roll and therefore is slower. A resolution for this is found in increasing the chord fraction to 35% of the total chord, thereby ensuring a decent roll rate comparable to the Skyhawk.

10.6.3. Dynamic Stability Results

This section contains the dynamic simulation results for the Cessna Morphlight and compares these with simulation results for the Cessna 172S Skyhawk.

[3]http://www.numpy.org/

Simulation Results

Figures 10.9 to 10.12 show the time response to different inputs and Table 10.6 compares the dimensional eigenvalues, damping factors and natural frequencies of the different motions.

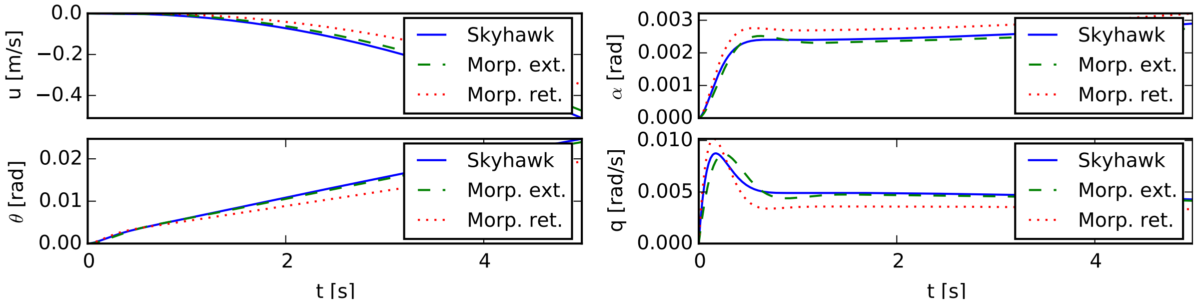

Figure 10.9: Step elevator input of -0.005 rad

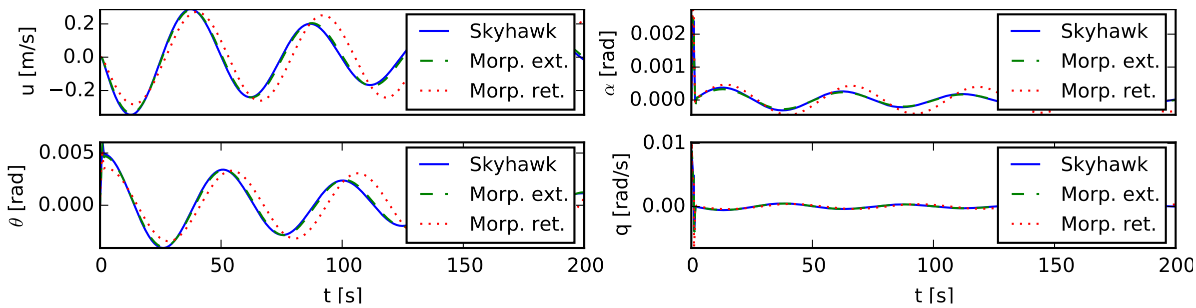

Figure 10.10: Pulse elevator input of -0.005 rad for 1 s

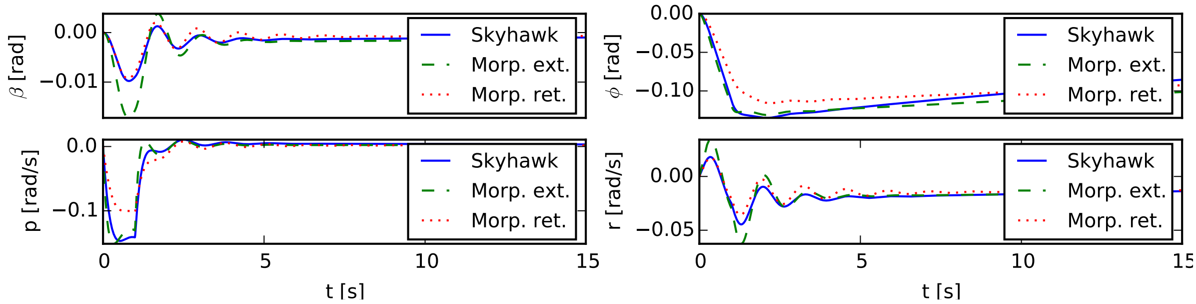

Figure 10.11: Pulse aileron input of -0.025 rad for 1 s

Looking at Table 10.8 it may be noted that the Morphlight, in both its retracted and extended configurations is slightly less dampened that the Cessna Skyhawk for symmetrical motion.

For short period oscillations (first and second symmetric eigenvalues), the retracted configuration has a slightly higher natural frequency while for long period oscillation (third and fourth symmetric eigenvalues) it has lower natural frequency.

Unlike in its retracted configuration, the Morphlight in its extended configuration has a lower undamped natural frequency for the short period oscillations compared to the Skyhawk. The natural frequency for the long period oscillations are approximately the same as the Skyhawk.

As expected the Morphlight in its extended configuration is more damped for asymmetric motion compared to both the Skyhawk and retracted Morphlight. This is due to the larger wingspan. However due to its larger ailerons and position further from the aircraft's centre, the extended Morphlight is more sensitive to aileron inputs. Due to their high wing configuration all three of the aircraft configurations are stable for spiral motion (fourth asymmetric eigenvalue).

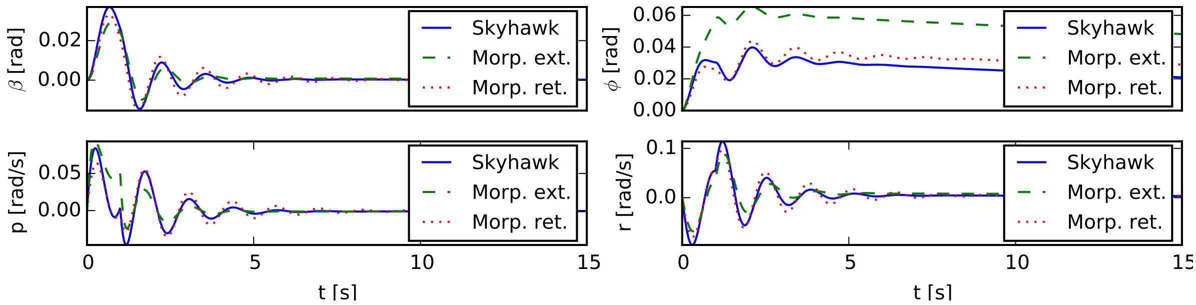

Figure 10.12: Pulse rudder input of 0.025 rad for 1 s

Table 10.8: Eigenvalues, damping factors and natural frequencies for Cessna 172S Skyhawk and the Cessna Morphlight with retracted and extended span.

	Skyhawk				Morphlight retracted				Morphlight extended			
	ξ	η_0	ς	ω_0	ξ	η	ς	ω_0	ξ	η	ς	ω_0
Symmetric	−7.08	4.46	0.85	8.36	−6.36	5.55	0.75	8.44	−3.84	4.98	0.61	6.29
	−7.08	−4.46	0.85	8.36	−6.36	−5.55	0.75	8.44	−3.84	−4.98	0.61	6.29
	−0.01	0.13	0.06	0.13	0.00	0.12	0.01	0.12	−0.01	0.13	0.05	0.13
	−0.01	−0.13	0.06	0.13	0.00	−0.12	0.01	0.12	−0.01	−0.13	0.05	0.13
Asymmetric	−0.85	4.76	0.18	4.84	−0.50	4.82	0.10	4.85	−1.04	4.55	0.22	4.67
	−0.85	−4.76	0.18	4.84	−0.50	−4.82	0.10	4.85	−1.04	−4.55	0.22	4.67
	−4.71	0.00			−2.92	0.00			−8.46	0.00		
	−0.03	0.00			−0.02	0.00			−0.02	0.00		

Conclusions and Recommendations

By looking at the time responses in Figures 10.9 to 10.12 it can be seen that the Cessna Morphlight has similar dynamic characteristics in both its extended and retracted configurations. The most significant differences are in the damping of the symmetrical motions in the retracted configurations and the aileron sensitivity in the extended configuration.

Further research has to be performed regarding the dynamic stability of the aircraft as development advances and certain parameters, such as the mass moment of inertia and aerodynamic are better known. But for now it seems that the Morphlight has similar dynamic behaviour and handling characteristics compared to the Cessna 172S Skyhawk.

11

Structural Analysis

For the wing to be able to carry the aerodynamic loads to the fuselage, an internal structure is required. This structure needs to leave enough space for systems integration, be strong enough to not fail during manoeuvres, and be as lightweight as possible. Therefore, a wing box is designed as it is assumed to be an ideal morphing structure, allowing extension and retraction of the span. The positions of the front and rear spar have to be determined, as well as whether a strut is needed or beneficial. For the purpose of determining the wing box parameters an optimisation program is written.

11.1. Approach to Structural Analysis

There are many programs available which can evaluate any given wing box and check for failure; CATIA[1] and ABAQUS[2] are examples of these. ABAQUS includes an optimisation function which can vary thicknesses along a spar, or make holes in the spar to make the construction lighter. However, with these programs it is difficult to vary positions of the spars and especially a strut over the span, while evaluating the drag of the total structure at the same time. Moreover, the same holds for multiple load cases for every structure. To be able to obtain the most optimum configuration, an optimisation program is written in Python[3]. First, the analytical equations are presented, using the classical approach, after which the numerical representations follow. Then, the strut incorporation is discussed, followed by a description of the failure criteria. Finally, the implementation into the program is described.

Since the wing needs to be able to extend, a telescopic beam structure is needed. To preserve torsional rigidity, a wing box shape is assumed. The wing box will consist of a front and rear spar, a top plate and a bottom plate. The half span wing box is built up from three parts: the root part, middle part and tip part. Stiffeners shall be omitted, since the middle part has to be able to slide inside the root part and over the tip part, whereas stiffeners on the middle part would render this telescoping mechanism unusable. Furthermore, the wing box is assumed to be 12 cm high, whereas the wing is 13.5 cm thick at its thickest point. Due to this limited space, it will not be possible to fit any stringers outside of the wing box, nor any on the inside due to the morphing mechanism.

11.1.1. Analytical Approach

The wing box is modelled as a simple beam, this approach is described in Aircraft Structures for Aerospace Students [35]. This approach uses classical beam theory, which is Euler-Bernoulli beam theory. When using this method, the assumptions are as follows.

- Normals to the neutral axis remain normal after deformation.
  This implicates that the bending radius of a beam under pure bending is constant.

[1] `http://www.3ds.com/products-services/catia/`
[2] `http://www.3ds.com/products-services/simulia/products/abaqus/`
[3] `https://www.python.org/`

- The shear flow is constant through the thickness.
  With this assumption, an average value for the shear flow is taken, so the maximum shear stress is actually higher.
- The mass of the wing box is assumed to act through the local centre of pressure.
  In reality there will be an offset; the resulting additional stress is small in comparison to the local bending stresses.

Using these assumptions, the beam can be modelled. The lift force and the weight of the box are the only forces acting on the beam. Therefore, the internal shear force, bending moment and torque are as in Equations (11.1) - (11.3).

$$S_z(y_{cut}) = \int_0^{y_{cut}} q(y)dy \qquad (11.1)$$

$$M_x(y_{cut}) = \int_0^{y_{cut}} y \cdot S_z(y)dy \qquad (11.3)$$

$$T(y_{cut}) = \int_{LE_{y_{cut}}}^{LE_{tip}} x \cdot S(x)dx \qquad (11.2)$$

These forces can then be converted to stresses as in Equations (11.4) - (11.8).

$$\sigma_y = \frac{I_{xx}M_z - I_{xz}M_x}{I_{xx}I_{zz} - I_{xz}^2}x + \frac{I_{zz}M_x - I_{xz}M_z}{I_{xx}I_{zz} - I_{xz}^2}z \qquad (11.4)$$

$$q_b = -\frac{I_{xx}S_x - I_{xz}S_z}{I_{xx}I_{zz} - I_{xz}^2}\int_0^s txds - \frac{I_{zz}S_z - I_{xz}S_x}{I_{xx}I_{zz} - I_{xz}^2}\int_0^s tzds \qquad (11.5)$$

$$S_x\eta_0 - S_z\xi_0 = \int_s pq_b ds + 2A_{q_{s0}} \qquad (11.6)$$

Equation (11.6) is a moment equilibrium equation around some arbitrary point '0.'

$$q_s = q_b + q_{s0} \qquad (11.7)$$

$$\tau = q_s/t \qquad (11.8)$$

11.1.2. Numerical Approach

The equations from Section 11.1.1 are converted to be applicable to a numerical analysis. In order to do so, the beam is discretised into n sections. For the sake of simplicity, the sections are distributed evenly (constant Δy). Then, the forces have to be summed over the beam in order to represent an integral. Furthermore, the following additional assumptions are needed apart from the ones mentioned in Section 11.1.1.

- The geometry of a section is assumed to be constant for Δy.
  Due to possible taper, for example, this is not true in reality. However, as the number of sections increases, the implicated error will decrease.
- Every section is a clamped beam with a tip load, moment, and torque.

A boundary condition is imposed at the tip; the shear force, moment, and torque equate to zero. Therefore, it is convenient to start summing from the tip. In the following equations, j represents the cutting location at which the forces are evaluated. The shear force, S, is computed by division of the total lift over the wing area, multiplication by the chord, and, finally, multiplication by the shape of the pressure distribution along the span, which averages unit magnitude.

$$S_j = \sum_{i=0}^{j} S_i\Delta y \qquad (11.9)$$

$$M_j = S_j\Delta y + M_{j-1} \qquad (11.10)$$

$$T_j = S_j\Delta x + T_{j-1} \qquad (11.11)$$

To convert these forces to stresses, the same equations employed in the analytical approach can be used, namely Equations (11.4) - (11.8). However, the integral in Equation (11.5) is evaluated analytically, using the Computer Algebra System Maple[4].

[4] `https://www.maplesoft.com/products/maple/`

11.1.3. Strut Incorporation

The aim of this program is to produce an optimal configuration of the wing box, including the possibility to incorporate a strut. By definition, evaluation of the strut placement dictates governing equations. These are derived in this section whilst assuming the following.

Therefore, equations for the strut need to be derived, using the following assumptions.

- The strut reaction forces are point loads.
  In reality the strut implicates stress concentrations.
- The strut will only take tensile loads.
  This assumption will save strut weight since the strut does not have to be designed for buckling, though an additional system is needed that unloads the strut for negative load cases.
- The force, due to the strut on the wing box, in the axial y direction is assumed to be evenly distributed over the available area of the section.
  As mentioned before, in reality there will be stress concentrations. However, these concentrations will fade out over the span.
- The vertical shear force, due to the strut, is assumed to create no additional torque; the force acts through the shear centre of that section.
  The stress implicated by the horizontal offset of the strut in x direction is negligible in comparison to the bending stress.
- The strut is assumed not to bend, meaning it is simply supported.
  This implicates a hinge between the strut and the vertical strut offset part.
- The strut will only be able to deflect vertically.
  The axial loads on the wing are small in comparison to the lift, as a result, the implications are small.
- The strut is be modelled as a linear spring.
  This will only hold when the strut is deforming elastically.

The wing will have a deflection at some arbitrary load. When the wing deflects upward, the strut will give a force downward. The further the wing deflects, the more opposing force the strut will give. A schematic overview of the parameters of the strut is depicted in Figure 11.1. A suitable material is chosen for the strut regarding the involved stresses and strains.

The strut is assumed to be a material that can handle the direct stresses and strains.

If the strut is modelled as a simple beam, the stiffness of the beam is evaluated as shown in Equation (11.12).

$$k = \frac{EA}{L} \tag{11.12}$$

However, the strut is limited to only deflect in the z direction. Therefore, an equivalent spring stiffness is needed. The total energy in the equivalent spring stiffness and the normal stiffness should be equal. When rewriting the energy equation for both springs, Equation (11.13), one arrives at Equation (11.14).

$$1/2 \cdot k \cdot \delta_{axial}^2 = 1/2 \cdot k_{eq} \cdot \delta_z^2 \tag{11.13}$$

$$k_{eq} = \frac{E_{strut} A_{strut}}{L_{strut}} \cdot \sin^2(\varphi) \tag{11.14}$$

With this equivalent stiffness, the energy in the strut can be calculated. Since the problem with the strut is statically indeterminate, additional methods are needed to solve for the strut force. When the box and the strut bend or elongate, they take up energy. According to Castigliano's theorem as in [35], the total internal energy, U, of a deflected structure should be minimal. Therefore, the total energy in the strut and the box should be summed and minimised. The total energy can be calculated with Equations (11.15) - (11.17).

$$U_{strut} = \frac{F^2}{2k_{eq}} \tag{11.15}$$

$$U_{box} = \int_0^{b/2} \frac{M^2}{2EI} dy \tag{11.16}$$

$$U_{total} = U_{strut} + U_{box} \tag{11.17}$$

Another aspect of the strut is the offset to the wing and the interference drag it causes. A perpendicular surface to the wing produces lower interference drag when compared to a surface under an angle. Moreover, an offset has structural benefits, since the strut relieves the box of internal moments for

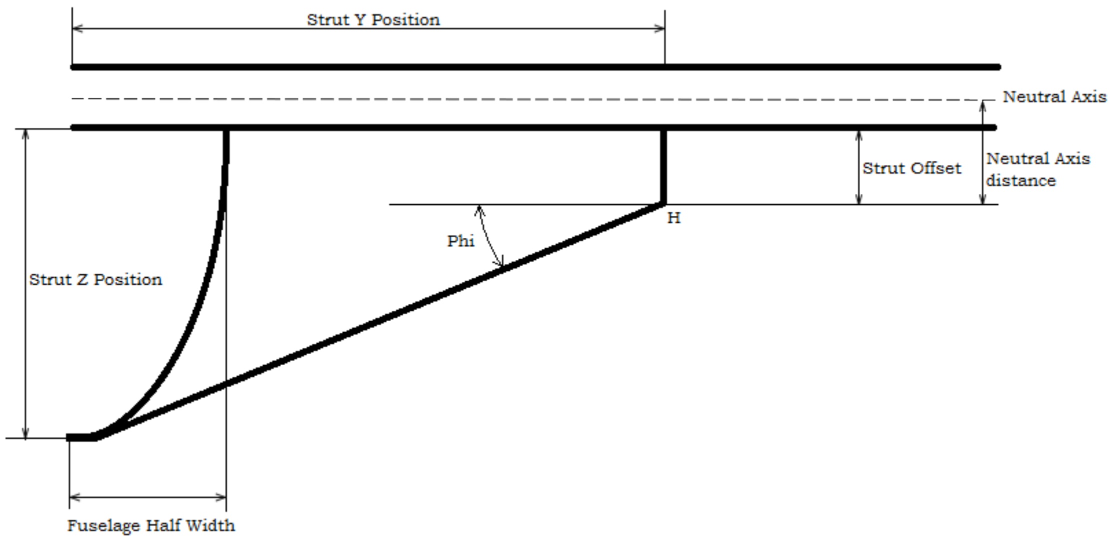

Figure 11.1: Schematic overview of strut parameters, where the fuselage is on the left and the wing tip on the right. The strut is hinged in point H

positive load cases. However, this offset will increase the total length of the strut, so a relation between the drag and the weight of the total wing structure has to be found.

Analytical equations for determination of interference drag between a strut and a wing are obtained from a thesis research [36], these are shown in (11.18) and (11.19). The reference wing area in the thesis is equal to $355.7m^2$; the coefficients have been scaled to be applicable to the Morphlight. The third equation follows from Torenbeek [20] and the last equation scales the profile drag coefficient to be applicable to the entire wing.

$$C_{L_{interference}} = -0.0026R + 0.0148 \tag{11.18}$$

$$C_{D_{interference}} = 0.0031 - \left(\frac{0.0013 \cdot R}{0.2208}\right) + 0.0011 \tag{11.19}$$

$$C_{D_{strut}} = 0.015\left(1 + \left(\frac{t}{c}\right)_{strut}\right) + \left(\frac{t}{c}\right)^2_{strut} \tag{11.20}$$

$$C_{D_{profile_{strut}}} = \frac{C_{D_{strut}} \cdot c_{strut} \cdot L_{strut}}{S_{wing}} \tag{11.21}$$

The symbol R represents the radius of the smallest circle inscribed in the strut - wing interference structure, for clarity, see Figure 11.1. A larger radius leads to less interference drag and lift. In contrast, the formula for the relieving moment is rather straightforward and is shown in Equation (11.22).

$$M_{strut} = d_{NeutralAxis} \cdot Y_{strut} \tag{11.22}$$

This moment can be passed on to the structure as a point load. When using a simple box of 2 cm high, 4 cm wide, and 2 mm thick, the strut might yield for moments higher than $100,000$ Nm. Therefore, the maximum internal moment in the strut may not exceed this value. The introduced force in the y direction will be assumed to be distributed evenly over the area at that section. In reality this is not true, as there will be a load concentration. A FEM analysis can be used to further design for this load

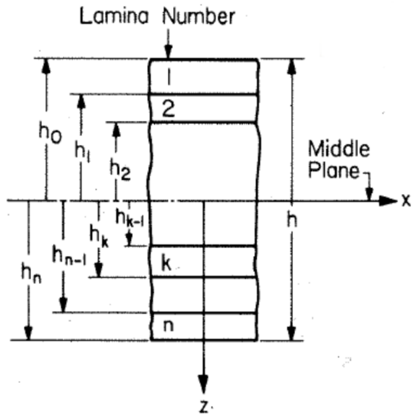

Figure 11.2: Graphical definition of h in Equation 11.29 [37]

introduction section.

11.1.4. Failure Criteria

The use of composite materials implies a different approach regarding failure criteria than applicable to isotropic materials. The difference originates from the various lamina; these build up the composite laminate and cause variations in strength characteristics per orientation. In order to properly construct the bending stiffness matrix for a specific lay-up, it is assumed that the laminate only consists of plies which have an orientation of either 0°, 90°, -45°, or 45°. Furthermore, the laminate is assumed to be symmetrical in the thickness direction of the laminate. Since the wing box is subjected to relatively large direct stresses, the 0° orientation is set to be in spanwise direction. In order to maximise the capability of carrying direct stresses, the upper ply of the composite laminate is always orientated in the 0° direction. As previously stated, stiffeners can not be placed due to space restrictions.

In order to check for buckling and ply failure, it is necessary to have knowledge about the bending stiffness matrix of the composite laminate. Each ply will have its own bending stiffness matrix, Q_θ, with respect to the 0° orientation. The bending stiffness matrix, which is applicable to the laminate as a whole is defined to be D. Equations (11.23) to (11.28) describe how each entry for the Q matrix can be obtained [37].

$$Q_{11} = Q_{11}\cos^4\theta + Q_{22}\sin^4\theta + 2\left(Q_{12} + 2Q_{66}\right)\sin^2\theta\cos^2\theta \tag{11.23}$$

$$Q_{22} = Q_{11}\sin^4\theta + Q_{22}\cos^4\theta + 2\left(Q_{12} + 2Q_{66}\right)\sin^2\theta\cos^2\theta \tag{11.24}$$

$$Q_{12} = \left(Q_{11} + Q_{22} - 4Q_{66}\right)\sin^2\theta\cos^2\theta + Q_{12}\left(\cos^4\theta + \sin^4\theta\right) \tag{11.25}$$

$$Q_{66} = \left(Q_{11} + Q_{22} - 2Q_{12} - 2Q_{66}\right)\sin^2\theta cos^2\theta + Q_{66}\left(\sin^4\theta + \cos^4\theta\right) \tag{11.26}$$

$$Q_{16} = \left(Q_{11} - Q_{12} - 2Q_{66}\right)\cos^3\theta\sin\theta - \left(Q_{22} - Q_{12} - 2Q_{66}\right)\cos\theta\sin^3\theta \tag{11.27}$$

$$Q_{26} = \left(Q_{11} - Q_{12} - 2Q_{66}\right)\cos\theta\sin^3\theta - \left(Q_{22} - Q_{12} - 2Q_{66}\right)\cos^3\theta\sin\theta \tag{11.28}$$

The D matrix can be computed as shown in Equation (11.29), where h is defined to be the distance of the laminate to the middle plane (as visually shown in Figure 11.2). Prevention of extensive calculations for different lay-ups across the wing box is achieved by scaling the laminate bending stiffness to the power of 2 with respect to the laminate thickness. As Equation (11.29) shows, addition of an extra ply contributes stiffness to the power of 3 with respect to the laminate thickness. The Young's modulus of the laminate is calculated through the rule of 10% [38]. As a final remark on the material implications, it must be stated that the program does not account for any material deficiencies.

$$D_{ij} = \frac{1}{3}\sum_{k=1}^{n}\left(Q_{ij}\right)\left(h_k^3 - h_{k-1}^3\right) \tag{11.29}$$

$$F.I. = \left(\frac{\sigma_1}{\sigma_{1Y}}\right)^2 + \left(\frac{\tau_{12}}{\tau_{12Y}}\right)^2 \tag{11.30}$$

Three modes of failure are analysed: yield of the composite laminate, shear buckling of the web, and Euler buckling of the skin. The maximum allowable stress is evaluated through the Tsai-Hill theory [39].

An element is considered to be of optimum dimensions if the Tsai-Hill failure index is just below 1. Since aerodynamic drag is omitted from the analysis, only longitudinal and shear stresses will be present in the structure; σ_2 is equal to zero. Taking this into account, the equation for the Tsai-Hill theory leads to Equation (11.30). Note that a Y subscript indicates a yield stress.

Shear buckling of the wing box elements is mainly governed by the bending stiffness of the laminate. Every element is considered to be long; implying the lowest critical buckling load. This choice is made due to a lack of stringers and will lead to a conservative design. The skin and webs are assumed to be simply supported along all four edges. The critical buckling stress of the front and rear wing box elements is calculated by using Equation (11.31). The values for D_{11} and D_{22} can be obtained through Equation (11.29).

The top and bottom elements of the wing box are assumed to be uni-axially loaded and experiencing a uniform stress distribution. Because of this, the critical buckling stress can easily be computed. Euler buckling of the top and bottom elements of the wing box is governed by Equation (11.32).

$$N_{xy}^{cr} = K_{xy}\frac{\pi^2}{b^2}\sqrt[4]{D_{11}D_{22}^3} \qquad (11.31) \qquad\qquad N_{eu}^{cr} = \frac{\pi^2 E I_c}{a^2} \qquad (11.32)$$

11.1.5. Program Implementation

The quickest, yet reliable, way to analyse different geometries of the wing box is to make a program that can evaluate all stresses in the wing box for different load cases. Therefore, inputs and outputs of the program have to be defined, as in Table 11.1.

The program varies the variable outputs, and evaluates the wing box according to the flow chart in Figure 11.3. Note in the diagram that the wing box is evaluated for different load cases, and that the strut is inactive during negative load cases. As previously stated, these load cases are defined by an aerodynamic analysis, and to be found in the flow chart as the block 'Get pressure distribution.' For safety, a dump file is created, so that after every loop, intermediate results are saved.

11.2. Optimisation and Constraints

All functions of the program are defined in order to analyse a wing box, however the purpose of the program is to come up with the lightest design possible. Therefore, the total mass of the structure must be minimised. For this purpose, the function 'minimize' in the module 'optimize' from SciPy is used. This program function attempts to minimise a given mathematical function. In order to minimise the weight, the program must be able to calculate the weight of the structure and estimate the drag. To get to an optimal structure, these need to be expressed relative to each other, since it is possible that a small addition in weight, but a large reduction of drag, leads to a better overall performance. Therefore, a sensitivity analysis is performed, as seen in Section 8.5. When taking the average of the sensitivities of weight and C_{D_0} in Table 8.4, a increase in weight of 1% leads to an average reduction in performance of 0.73%, and an increase of 1% in drag results in 0.15% reduction in performance. Therefore, the relative weight-to-drag ratio is $13.9 : 1$ (since the wing is responsible for around 35% of the C_{D_0}).

For the program to comply with this relative importance, a corrected mass is needed. General penalties, denoted as p, are introduced for this matter. For example, the lift and drag caused by the strut leads to p_{lift} and p_{drag}. These penalties need to be a multiplication factor with a slope, so that the derivative at some arbitrary point always points to the solution space. The method selected for the analysis is the 'Nelder-Mead'[5] optimisation method, due to its robustness and reliability. The penalties, apart from the previously treated lift and drag penalties, are presented below.

The program may not be allowed to build a bigger wing box than the wing itself, therefore bounds are introduced. If the program will violate these bounds, a penalty p_{bound} is introduced. These bounds can be found in Table 11.2.

As can be seen from Table 11.2, there are two output parameters missing: t_{slope} and $t_{slope_{tip}}$. Since

[5] `http://www.brnt.eu/phd/node10.html#SECTION00622200000000000000`

Table 11.1: Input and output variables for structural optimisation tool

Input	Description	Unit	Output	Description	Unit
$pos_{frontspar_{min}}$, $wb_{lengthFrac_{min}}$, $t_{frac_{top_{min}}}$, $t_{frac_{bottom_{min}}}$, $t_{frac_{front_{min}}}$, $t_{frac_{rear_{min}}}$	Lower bound for the position of the front spar, length of the wing box, and thicknesses around the wing box as percentage of the chord	[%]	$pos_{frontspar}$, $wb_{lengthFrac}$, $t_{frac_{top}}$, $t_{frac_{bottom}}$, $t_{frac_{front}}$, $t_{frac_{rear}}$	Position of the front spar, length of the wing box, and thicknesses around the wing box as percentage of the chord	[%]
$strut_{Ypos_{min}}$, $strut_{offset_{min}}$, $strut_{c_{min}}$	Lower bound for the spanwise position of the strut, vertical strut offset and strut chord	[m]	$strut_{Ypos}$, $strut_{offset}$, $strut_{c}$	Spanwise position of the strut, vertical strut offset and strut chord	[m]
$num_{ribs_{min}}$, $t_{slope_{min}}$, $t_{slope_{tip_{min}}}$	Lower bound for the number of ribs, thickness decay along from the root and from the strut to the tip	[-]	num_{ribs}, t_{slope}, $t_{slope_{tip}}$	Number of ribs, thickness decay along from the root and from the strut to the tip	[-]
$pos_{frontspar_{max}}$, $wb_{lengthFrac_{max}}$, $t_{frac_{top_{max}}}$, $t_{frac_{bottom_{max}}}$, $t_{frac_{front_{max}}}$, $t_{frac_{rear_{max}}}$	Upper bound for the position of the front spar, length of the wing box, and thicknesses around the wing box as percentage of the chord	[%]	$mass$	Mass of the wing box	[kg]
$strut_{Ypos_{max}}$, $strut_{offset_{max}}$, $strut_{c_{max}}$	Upper bound for the spanwise position of the strut, vertical strut offset and strut chord	[m]	$mass_{penalised}$	Penalised mass of the wing box	[kg]
$num_{ribs_{max}}$, $t_{slope_{max}}$, $t_{slope_{tip_{max}}}$	Upper bound for the number of ribs, thickness decay along from the root and from the strut to the tip	[-]	p_{bound}, $p_{constraint}$, p_{lift}, p_{drag}	Penalty parameters for the bounds, constraints, lift and drag	[-]
n, $num_{stations}$	Number of sections along the span and number of points around the wing box	[-]	$geometry$, $load$, $stress$	Matrix filled with geometry properties (e.g. local thickness, I_{xx}), load and stress at some point	[various]
$\vec{x}_0$	Initial guess for the output	[various]			
$wFactor_{weight}$, $wFractor_{drag}$	Weight correction factors for the weight and drag	[-]			
b, $c_{average}$, c_r, $halfwidth_{fuselage}$	Span, average and root chord, and half the diameter of the fuselage	[m]			
$sweep$	Trailing edge sweep	[rad]			
$(\frac{t}{c})_{wb}$	Height to chord ratio of the wing box	[-]			
$strut_{Z_{position}}$, c_{strut}, t_{strut}	Vertical strut mount distance on the fuselage, strut chord and strut box thickness	[m]			
$strut_{lengthFrac}$, $(\frac{t}{c})_{strut}$	Strut length and height as fraction of the chord	[-]			
N_{max}, $N_{ultimate}$, $N_{negative_{max}}$, $N_{negative_{ultimate}}$	Maximum load factors	[g]			
$pos_{lift_{N_{max}}}$, $pos_{lift_{N_{ultimate}}}$, $pos_{lift_{N_{negative_{max}}}}$, $pos_{lift_{N_{negative_{ultimate}}}}$	Position of center of pressure as fraction of the chord	[%]			
g	Gravitational acceleration, typically 9.81	$[\frac{m}{s^2}]$			
$kink$	Position of the kink as fraction of the span	[%]			
m_{max}	Maximum mass	[kg]			
E, E_{11}, E_{22}	Global, longitudinal and transverse Young's Modulus	[Pa]			
σ_b, σ_s	Compressive and shear yield stress	[Pa]			
ν_{12}, ν_{21}	Longitudinal and transverse Poisson's ratio	[-]			
G_{12}	Shear modulus	[Pa]			
ply_{order}	Stacking angle sequence	[rad]			
h_{ply}	Ply thickness	[m]			
ρ	Material density	$[\frac{kg}{m^3}]$			

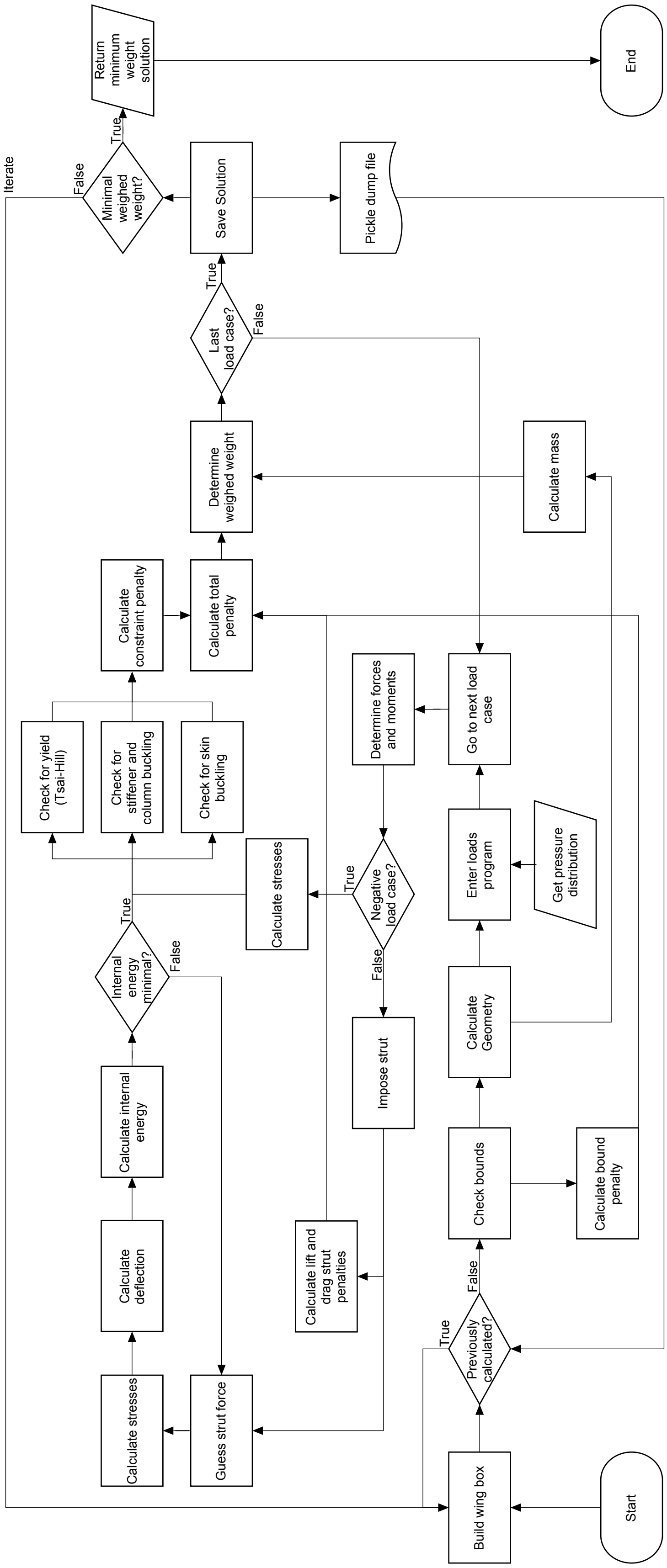

Figure 11.3: Flow chart for structural analysis program.

Table 11.2: Bounds for the optimisation tool.

Parameter	Lower bound	Upper bound	Unit
$pos_{frontSpar}$	0.1	0.4	[-]
$wb_{lengthFrac}$	0.1	0.5	[-]
$t_{frac_{top}}$	0.001	0.1	[-]
$t_{frac_{bottom}}$	0.001	0.1	[-]
$t_{frac_{front}}$	0.001	0.1	[-]
$t_{frac_{rear}}$	0.001	0.1	[-]
num_{ribs}	1	35	[-]
$strut_{Y_{pos}}$	0.5	2.5	[m]
$strut_{offset}$	0.0001	0.5	[m]
c_{strut}	0.03	0.15	[m]

Table 11.3: Tested load conditions.

Load Case	Lift position	Tsai-Hill	Buckling
3.8	0.25	True	True
5.7	0.26	True	False
-1.52	0.17	True	True
-2.28	0.17	True	False

the thickness has some minimum value, the tip thickness has to be evaluated, and is therefore included in the constraints. The thickness of the top, bottom, front and rear panel are calculated as in Equation (11.33).

$$t_{local} = t_{frac_{top/bottom/front/rear}} - t_{slope} \cdot y - t_{slope_{tip}} \cdot \left(y - strut_{Y_{pos}}\right) \tag{11.33}$$

The rightmost part of Equation (11.33) is only included in the calculation if $\left(y - strut_{Y_{pos}}\right) > 0$. The thickness also has the same slope for all panels, since otherwise the program has three extra variables to evaluate and would consume too much computational resources.

Also, the wing box is not allowed to fail in the maximum load case. For this case, constraints are introduced. These constraints lead to penalties if the box fails in a situation. These constraints are amended by geometry constraints, since they have to be evaluated at some points as they are not simply an output parameter of the program. The constraints are listed below.

- The parameters may not be negative.
- The thickness at the tip may not be less than 1 mm.
- The Tsai-Hill failure index may not be larger than 1.
- The local critical normal, shear and Euler buckling stress may not be lower than the actual stress at all points.
- The maximum rear spar location is 60% of the chord.

The wing box is tested for different load conditions, as in Table 11.3. These load factors come from the requirements in [1], whereas the pressure point (lift position) is derived from the aerodynamic analysis in Chapter 9. The Tsai-Hill failure index is checked for every situation, because yield will most likely cause the composite to break. Buckling, however, is not checked in every case, since the material is allowed to get damaged during a load case of 5.7. Therefore, the plies may be delaminated in the ultimate load case, though shall not yield.

The most critical case is taken as the output for the value for the optimisation program, and the penalised mass is returned according to Equation (11.34). All penalties are entered as dimensionless correction factors.

$$mass_{penalised} = W_{box} \cdot \frac{p_{drag} \cdot p_{bound} \cdot p_{constraint}}{p_{lift}} \tag{11.34}$$

11.3. Verification

If the program as in Section 11.1.5 is implemented, everything can be calculated. However, it can not be stated that everything is calculated correctly; the entire program has to be verified. This is done by verifying that each function correctly calculates what it should do. Verification is carried out by comparing the program's results to analytical values. If the error margin is less than 0.1%, the function is considered verified.

These functions consist of defining the geometry of the wing box, defining the forces acting on the wing box, restate those to stresses, and finally check for any failures. For 200 sections and 160 stations, the accuracy of the final answers are found to be within a 0.1% margin compared to analytical values. This margin is sufficiently small and the program is considered to be verified. For further analysis, the combination of 200 sections and 160 stations around the wing box is used.

The optimisation returned a design with a higher thickness than expected. This higher thickness renders the assumption of a constant shearflow through the wall invalid, though the shear stress is negligible in comparison with the bending stress. Therefore, this will have no further implication to the result. All other assumptions remain valid.

As mentioned in Section 11.1.2, Maple was used to evaluate equations. Maple can also be used to convert the equations to Python language, using the CodeGeneration package. This package seems to have an issue converting equations in the form of $1/(1+x)$, forwarding them as $1/1+x$. Therefore, the equations had to be checked thoroughly, especially on these divisions. To minimise the occurrence of this error, all functions were simplified so no further divisions in the functions would be present. Apart from that, Maple is not able to always solve a function. If Maple was not able to do so, Ti-Nspire CAS Teacher Software[6] is used. This program was able to correctly evaluate all functions, though is not capable of changing a variable later on in the process, whereas with Maple the server can simply be reset. Therefore, for future reference, equations from Maple should be checked with a second reliable program.

The optimisation method used is the 'Nelder-Mead' method. This seems to be a reliable and robust method, though it cannot handle bounds and constraints. Therefore all bounds and constraints have to be converted to penalties, so the program will receive high output values and knows it should not search in that area. The Nelder-Mead method, however, is only capable of finding a local minimum. By trial and error, the solution is found to be a global minimum, though for future work a global version of the Nelder-Mead method can be used. Further optimisation is possible on multiple aspects of the wing box; for example the thicknesses along the span. These can be evaluated pointwise, but will take a lot of computing time. This is not used in this project since the main goal is to determine the main wing box geometries, whereas programs such as ABAQUS can further optimise the wing box.

11.4. Validation

In order to ensure realistic output of the software, it must be tested against proven software as a means of validation. Any discrepancies between the output of the Python program and the validated data may originate from invalid assumptions or incorrect governing equations. If discrepancies are below 5%, the data is considered to be valid. A sample wing box is set up which can be put into both the Python program and ABAQUS. Table 11.4 shows the dimensions of the sample wing box. Moreover, it states the direct-, shear-, and Von Mises stresses at various key locations of the wing box. Note that Von Mises is only used as a validation method, it is discarded for failure criteria as it does not apply to composites. Conform to the sample case used as input for the Python program, the lift force is assumed to be acting on the front spar. Minimisation of discretisation errors is achieved through having a constant thickness throughout the sample wing box.

Discrepancies can be found between the numerical results of the Python program and the validation data from ABAQUS. The most striking difference between the two approaches can be found in the direct stress distribution. By inspection of the output data it becomes clear that ABAQUS adds the shear stress, denoted as S_{12} by ABAQUS, to the direct stress, denoted as S_{11} by ABAQUS. Reversal of this process leads to a bending stress in the front spar of 134.9 MPa as computed by ABAQUS. This shows a discrepancy of 2.20% with the numerical result of the Python program. The shear stress in the top of the front spar has a discrepancy of 1.84% with respect to the numerical analysis. The discrepancies are well below 5%; the Python program is regarded as validated.

[6]https://education.ti.com/en/us/products/computer_software/ti-nspire-software/ti-nspire-and-ti-nspire-cas-teacher-software/

Table 11.4: Validation results of the structural Python program compared to ABAQUS

Parameter	Python program	ABAQUS	Unit
Wing box length	7500	7500	[mm]
Wing box height	120	120	[mm]
Wing box width	300	300	[mm]
Top skin thickness	1	1	[mm]
Front skin thickness	1	1	[mm]
Bottom skin thickness	1	1	[mm]
Rear skin thickness	1	1	[mm]
Direct stress in top front	-132.0	-115.8	[MPa]
Direct stress in bottom rear	$+132.0$	$+153.8$	[MPa]
Shear stress in top front	$+16.6$	$+16.3$	[MPa]
Shear stress in bottom rear	-4.6	-4.5	[MPa]
Von Mises stress in top front	135.1	116.0	[MPa]
Von Mises stress in bottom rear	132.0	153.8	[MPa]

11.5. Preliminary Structural Optimisation Results

The entire program is defined, and the total penalised mass can be minimised. This leads to the following result, as in Table 11.5. A graphical result can be found in Figure 11.4.

Table 11.5: Optimised wing box configuration

Parameter	Output	Unit
$pos_{frontSpar}$	0.2410	[-]
$wb_{lengthFrac}$	0.1000	[-]
$t_{frac_{top}}$	1.86×10^{-2}	[-]
$t_{frac_{bottom}}$	1.55×10^{-2}	[-]
$t_{frac_{front}}$	1.20×10^{-2}	[-]
$t_{frac_{rear}}$	7.78×10^{-3}	[-]
$mass_{penalised}$	65.43	[kg]

Parameter	Output	Unit
num_{ribs}	33	[-]
$strut_{Y_{pos}}$	2.5	[m]
$strut_{offset}$	0.1623	[m]
c_{strut}	0.1005	[m]
t_{slope}	3.142×10^{-5}	[-]
$t_{slope_{tip}}$	1.676×10^{-4}	[-]
$mass$	62.29	[kg]

As can be seen, the position of the front spar is between the pressure points in the different load cases as defined in Table 11.3. By trial and error, the wing box is found not to break if the position of the front spar is between 0.23 and 0.29 of the chord. This adds a degree of freedom to the integrability of the wing box in the wing. Since there is no place for stiffeners (the wing box is 12 cm high, whereas the maximum thickness of the airfoil is 13.5 cm), the amount of ribs is high and the wing box length fraction is as small as possible (defined by the bounds).

The thicknesses are rather large, except for the rear spar. Also, since the thicknesses are larger than expected, the assumption of constant shear flow through the thickness will not hold, and the shear stresses are higher than calculated. However, the shear stresses are negligible in comparison to the bending stresses, so the result will still be valid if a safety factor is applied. The thicknesses are decaying along the span, though can decay faster, as one can see in Figure 11.4.

The strut is positioned on the inner wing box as outboard as possible. If the strut would be on the morphing part, it would introduce high axial loads and additional morphing systems would have to be designed. The offset of the strut is found to be optimal at 16 cm from the bottom of the wing to have the most optimal weight/drag ratio, whereas the chord of the strut should be 10 cm. These seem both to be acceptable values and the internal moment in the strut is low enough for the vertical part of the strut not to yield, as described in Section 11.1.3. However, at a load case of 3.8 g, the vertical deflection of the strut is 0.177 m. This equates to a strain of $\epsilon = 2.9\%$. This is a very high strain, and unlikely to be met by any material that will have enough stiffness to resist flutter. Currently, the material of the strut was assumed to be the same as the material of the wing box, which has a maximum strain of 0.8%. Therefore, a constraint of $\epsilon_{max} = 0.8\%$ has to be implemented into the program in order to incorporate for the strain of the strut. Another way is to build a spring damper system into the fuselage. This is already a necessity since the strut is inactive for negative load cases. The spring is designed to maximally deflect, and the strut will be limited to its maximum strain.

The mass of the wing box as in Table 11.5 is 62.29 kg. The mass is build up as follows, 59.52 kg for the box itself, 2.66 kg for the ribs and 0.11 kg for the strut. However, at the tip, the wing box is over designed, and weight can be saved at this point. The program is not able to decrease the thickness any further, since otherwise the box would fail near the strut. Therefore, it might be interesting to implement a quadratic decay of the thickness of the wing box along the span, or to evaluate the thicknesses individually along the span, since between the root and the strut, the stress is actually lower than just after the strut ($y > 2.5$ m). Evaluation of the thicknesses at every point individually will, of course, lead to the best result.

If the program is ran without a strut, the true mass and penalised mass are both 87.82 kg (there is no strut lift and drag penalty). The wing box has a significant better true mass of 62.29 kg (penalised mass of 65.43 kg), if a strut is incorporated.

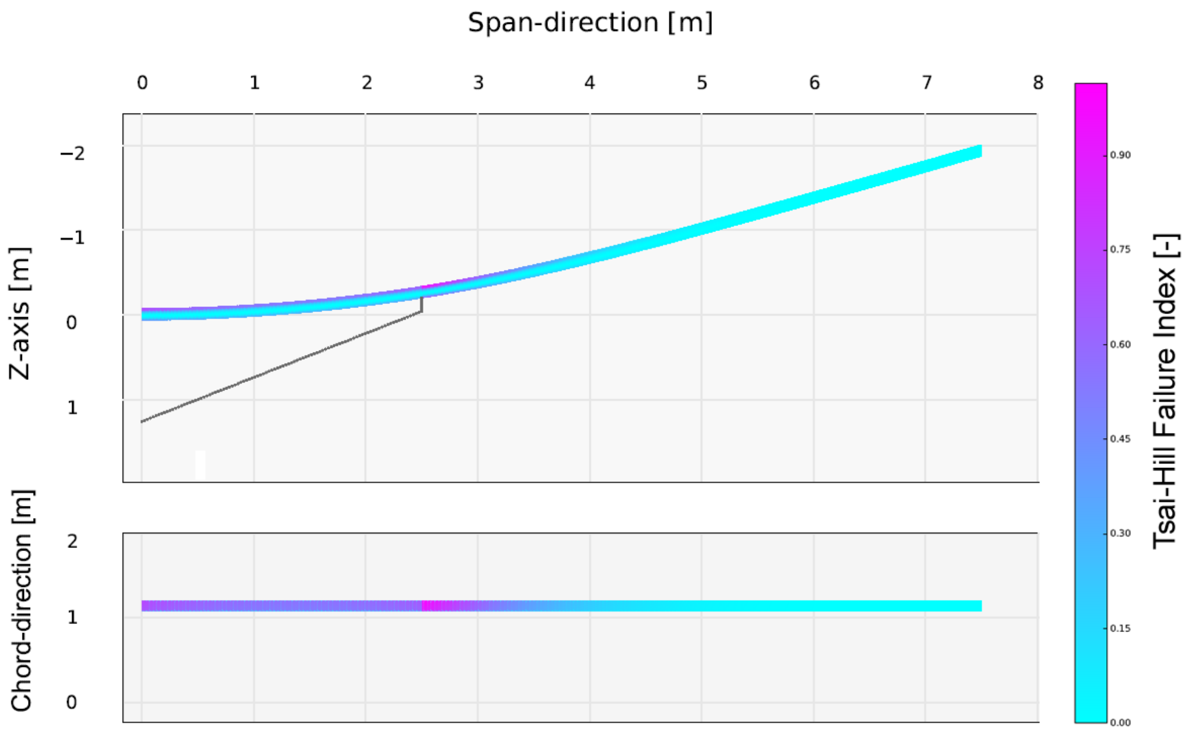

Figure 11.4: The upper part of the graph displays the front view of the wing box, including a strut, at a load case of +5.7g. The lower part of the graph displays the top view. The Tsai-Hill failure index is plotted on the structure

11.6. Load Transfer

The wing box is able to morph in accordance with the wing. The aerodynamic loads introduced to the wing box need to be transferred from one box to another. This shall be done by using a material that is capable of sustaining high normal loads and has decent sliding wear resistance. Full surface contacts between the wing boxes will lead to a more evenly distributed transfer load than ball bearings; for that particular reason UHMW-PE is chosen as surface contact material. The high strength, together with its toughness, makes this material well suited for high normal loads that are transferred during flight. The properties of UHMW-PE can be found in Section 14.4. The abrasive wear coefficient for the UHMW-PE[7] is equal to $2.94 \cdot 10^{-4}$ ${}^{mm^3}/_{Nm}$ using silica particles as abrasive material. The maximum stress

[7]http://e-collection.library.ethz.ch/eserv/eth:28580/eth-28580-02.pdf

the UHMW-PE has to endure during the morphing is equal to 33 MPa for morphing at maximum 2G. Assuming that dirt is present in between the two coatings, a 1 mm coating is able to withstand at least 166 cycles and this number increases with coating thickness. Without the dirt, the amount of cycles is increased and the coating should only be replaced depending on its condition.

The ribs in the morphing region of the wing move over the wing boxes during extension and retraction using the same coating of UHMW-PE as described in Section 13.5.

11.7. Further Optimisation

Figure 11.4 shows large overdesigned areas with a fairly low Tsai-Hill failure index. An attempt to further reduce the weight of the wing box is made through the use of ABAQUS. The final 100 mm of the span was, at the time, designed to not carry any loads. Thus, the input wing box length was set to be $7,400$ mm. A parametric CATIA model is created to have the opportunity to quickly make adjustments to the wing box' layout. The Python program showed a weakness in addressing individual thicknesses to specific spanwise stations. The CATIA model is imported for evaluation in ABAQUS; thickness sections can be assigned to each individual segment as the wing box is split up by the ribs. In order to improve the reproducibility of the ABAQUS analysis and optimisation, the general work flow is described next. It must be noted that the CATIA model is exported in millimetres. ABAQUS does not keep track of units and does not perform any conversions; this stresses the need for a correct input of units.

The wing box is imported as a set of surfaces exported by CATIA (in .igs format). The three boxes are assigned sections of which the thickness can be defined individually. Each wing box carries 11 ribs, and, thus, is divided into 10 segments. One segment consists of four surfaces. The overlapping segment of the mid and outer wing boxes are initially defined to have equal thicknesses to the neighbouring segment they are connected to. For initial optimisation purposes, the wing boxes are modelled to be made of a quasi-isotropic carbon fibre reinforced polymer.

The meshing element is chosen to be a deformable shell. Because of the rectangular nature of the wing box, it is meshed in a structural manner with quad elements. A structured manner of meshing cannot be applied to the ribs due to their irregular shape; triangular elements are applied to the ribs through a sweep method. The global seed size is set to 11, this results in an equal number of cells in the spanwise direction and 4 in chord-wise per station.

Load transfer from one wing box to the other is modelled with the use of surface-to-surface contacts. Tangential behaviour is controlled through a friction penalty and normal behaviour is defined to be a hard contact which does not allow separation. The latter statement is chosen as the wing box is only tested against positive load cases. Application of forces which are aligned with the front spar will not cause any axial loading in the chord-wise direction. The friction coefficient is entered as 0.1[8]. To justify this choice, a quick study is performed on the influence on the produced direct stresses as a result of bending. As expected, this effect is negligible, the results can be seen in Table 11.6.

Table 11.6: Sensitivity analysis on the effect of adjusting the friction coefficient for the surface-to-surface contact between the wing boxes. It can be seen that the effect is marginal on the resulting bending stresses

Friction coefficient	Tip deflection	Max. tensile stress front spar	Max. compressive stress
0.1	2,079 mm	334.1 MPa	376.3 MPa
0.2	2,072 mm	333.4 MPa	376.5 MPa
0.3	2,053 mm	333.0 MPa	376.6 MPa

The root of the wing box is modelled to be clamped; it is restrained in translation along and rotation about all three axes. No further constraints are imposed on the structure. A quick and straightforward work flow is achieved by modelling the aerodynamic lift to act on the front spar. The actual aerodynamic lift, as discovered by the aerodynamics group, acts at 26% of the chord at a load case of $5.7g$. Placing

[8] https://www.redwoodplastics.com/brochures/uhmw-engineering-data.pdf [cited 22 June 2015]

the lift force on the front spar, which is at 23% of the chord, will lead to a conservative design.

The magnitude of the lift force acting on each station's front spar is retrieved from the Python program. For this specific purpose, the wing box is divided in 1000 stations and the index corresponding to the ABAQUS station is rounded down to ensure a conservative determination of the shear force. No drag force is introduced in the structure. The strut reaction forces and moment are left out during the first part of the optimisation to be able to compare results with the strut-less wing box computed by the Python program. As a final optimisation, strut reaction forces are placed.

As initial input, the thicknesses of the various elements are chosen to correspond as closely as possible with the output of the Python program. Regarding the optimisation strategy, firstly all thicknesses are reduced to have as little margin as possible with respect to the allowable direct stresses for a load case of $5.7g$. This is a highly iterative process and has been carried out for 9 times. The final iteration concluded a decrement in weight of 0.95% over the previous iteration and is considered to be sufficiently optimised. The results can be found in Table 11.7 in Section 11.8. It must be noted that this intermediate result has not been tested against buckling of the top skin elements.

Applying a strut to the wing will not affect a wing box' geometry at stations which have a more outboard location than the strut; only the inner wing box is optimised during the final step. The applied strut reaction forces and moment are set equal to the result of the energy minimisation process performed in the Python program as described in 11.1.3.

After the second phase of thickness reduction, every top skin element is checked for buckling. This check is carried out in a separate analysis. Buckling loads are determined for plates with thicknesses ranging from 2 mm to 11 mm. The plates are modelled to be pinned to the ribs and have a symmetry constraint along the spanwise edges; this approach simulates wide column buckling. A compressive load of unit magnitude is placed at one of the pinned edges; running a buckling simulation will cause ABAQUS to increase the unit load until the first Eigenmode of the panel is reached. This load is considered to be the critical buckling load. The progression of the critical buckling load with increasing thickness can be seen in Figure 11.5.

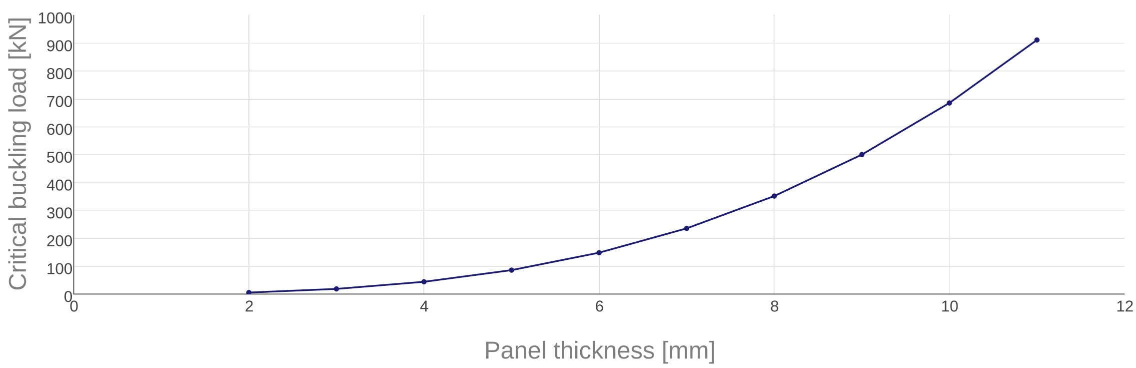

Figure 11.5: A plot displaying the trend of increasing critical buckling load with increasing thickness for a simply supported plate

The actual normal force is assumed to be related to the bending moment in the manner as described in Equation 11.35. Please note, the evaluated bending moments are derived from a load case of 3.8g.

$$S_y = \frac{M_x}{\left(\frac{t}{c}\right)_{wb} \cdot c} \tag{11.35}$$

The thicknesses of the top elements are increased until the corresponding critical buckling load exceeds the introduced normal force. The updated thickness distribution is fed back to the bending analysis which produces stress distributions across the final wing box. The results of the ABAQUS optimisation are displayed in the next section.

11.8. Final Structural Optimisation Results

Results regarding the optimised wing box are presented in this section. The thickness variation for the final optimised wing box is shown graphically in Figures 11.6 and 11.7.

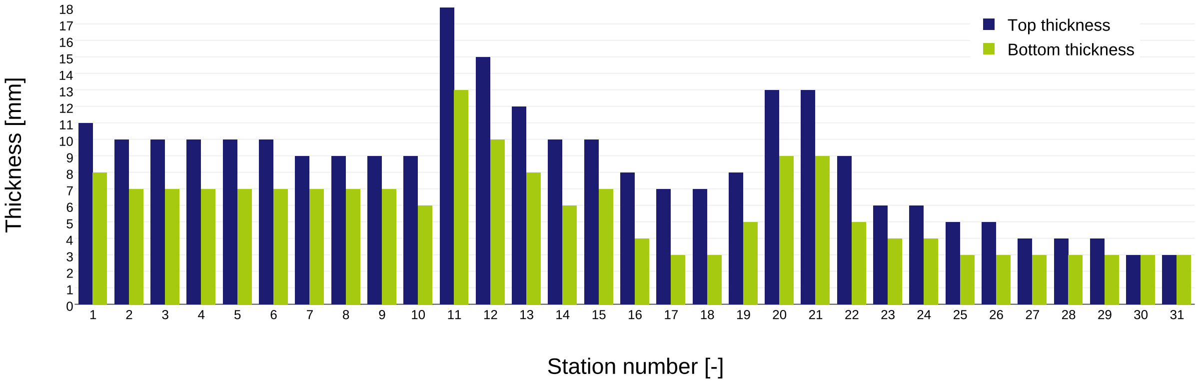

Figure 11.6: The final thickness distribution across the top and bottom elements. Note that every station has a length of 0.231m

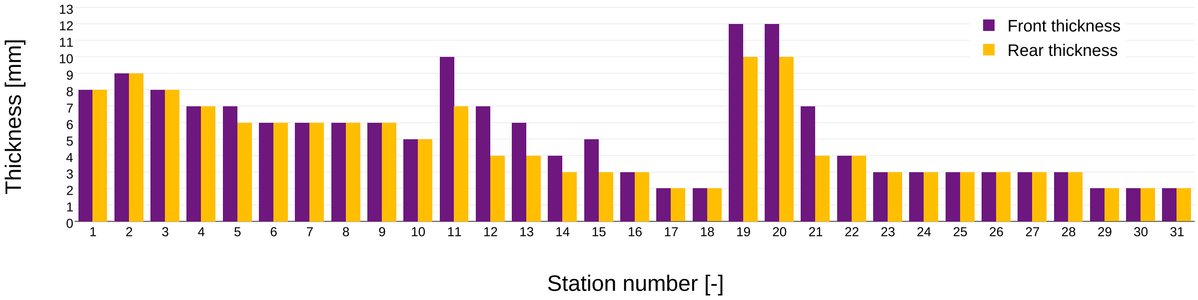

Figure 11.7: The final thickness distribution across the front and rear elements. Note that every station has a length of 0.231m

Table 11.7: The calculated weights for the wing box structure during the various design phases

Design phase	Wing box [kg]	Ribs and strut [kg]	Total [kg]
Python without strut	85.16	2.66	87.82
ABAQUS without strut	49.62	2.66	52.28
Python with strut	59.52	2.77	62.29
ABAQUS with strut	36.10	2.77	38.87

Figure 11.8 shows the direct stress distribution across the rear spar and top skin of the optimised wing boxes for the strut incorporating design. Finally, Table 11.7 shows the final results for both the Python program and the ABAQUS approach. The ABAQUS optimisation approach has further reduced the structural weight of the wing with 40.47%, in the case of no strut placement, and 37.60%, with the strut in position. Further investigation is recommended by adjusting the CATIA model to allow the actual realisation of the wing box. Currently, there is a gap of 5 mm between each wing box; this is too small to facilitate a fit of the sliding boxes.

11.9. Flutter Analysis

Flutter is an aeroelastic phenomenon in which the structural damping of the wing is cancelled by the aerodynamic damping of shedding vortices from the trailing edge. A so called flutter point is defined as the point where the net damping of the wing is zero; a further increase in aerodynamic damping will cause a self-oscillating motion with severe consequences for the structural integrity.

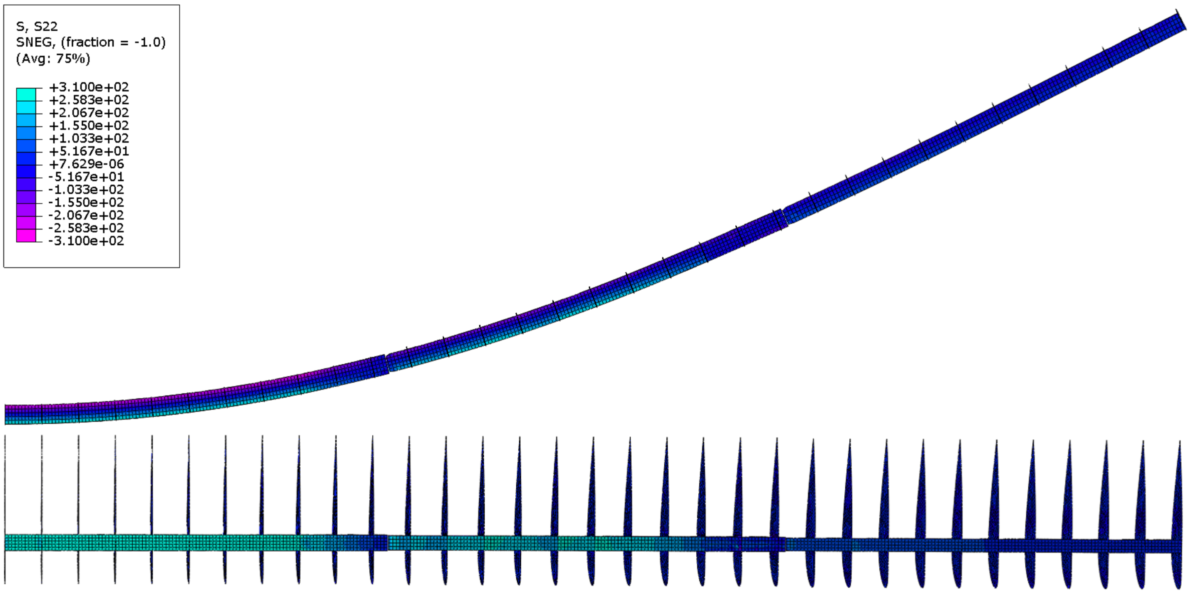

Figure 11.8: Shown in the upper part of the plot is the direct stress distribution for the rear elements of the final wing box. The top elements of the wing box are presented by the lower part of the plot. A blue color represents compressive stresses, whereas a pink color displays tensile stresses

The Eigenfrequencies and corresponding flutter speeds of the final wing box are determined through ABAQUS. The model entered in ABAQUS has been simplified to one wing box in order to eliminate unknown consequences of the contact constraints and the wing boxes not being one integral structure. As a result, individual thicknesses per station could not be entered. Instead, averages were taken for the top, front, bottom and rear thicknesses across the entire span. These equate to 7, 5, 6, and 5 mm, respectively.

Table 11.8: The Eigenfrequencies for the integral final wing box and their corresponding flutter speeds

Eigenmode	Eigenfrequency [Hz]
First	2.2
Second	2.3
Third	13.5
Fourth	14.3
Fifth	37.5

Further research on the structural behaviour, as a result of the passing air flow, must be conducted in order to draw conclusions about the sensitivity towards flutter. Due to the complex interaction between the structure and the fluid no extensive results have been obtained other than the Eigenfrequencies. An iterative process is needed which links CFD to FEM analysis. Moreover, a 2D airfoil simulation of vortex shedding will provide valuable information on critical airspeeds as the vortex shedding frequency can be acquired.

12

Aircraft Subsystems

This chapter describes several subsystems of the Morphlight. Section 12.1 starts with the engine after which the electrical system is explained in Section 12.2. The environmental control system is explained in Section 12.3. In Section 12.4 the fuel system is defined. The hydraulic system is outlined in Section 12.5. The landing gear is discussed in Section 12.6. The sizing of the flaps is described in Section 12.7 and the sizing of the speedbrakes is shown in Section 12.8.

12.1. Powerplant and Thrust Delivery Method

This section defines and justifies the chosen powerplant configuration and thrust delivery method. First, the choice of powerplant is explained in Section 12.1.1, after which the concept for the conversion of shaft power into thrust is explained in Section 12.1.2.

12.1.1. Powerplant Choice

Given the driving requirements for the aircraft as defined in Chapter 2, the powerplant selection is done with great care in order to achieve all the goals set for the new Cessna Morphlight. First of all, the current engine is evaluated after which other possible powerplants are considered and investigated in further detail. The chosen powerplant is defined at the end of this section.

The current engine used for the Cessna 172S Skyhawk is the Textron Lycoming IO-360-L2A with the characteristics as listed in Table 12.1.

Table 12.1: Current engine (IO-360-L2A) specifications

Weight	303	lbs	137	kg
Power	180	hp	134	kW
Fuel consumption in cruise	9	gal/h	34	L/h
Taxi/Take-off fuel	1.4	gal	5.3	L
Price	$ 79,603		€ 69,827	

As can be seen from Table 12.1 the current engine uses 34 L/h during cruise. This results in an endurance of about 5 hours with a legal reserve of 45 minutes. As defined in the requirements in Chapter 2 the endurance should be at least 10 hours. Therefore the current engine does not meet this requirement. A second requirement which it does not meet is the taxi and take-off fuel requirement of at most 2.5 L. This justifies the need for a different engine.

An engine is required that is most fuel efficient at the required power for cruise and still provides enough power during take-off in order to remain within the take-off distance requirements. The use of a hybrid engine design can overcome the large difference in required power during cruise and take-off. In this configuration a conventional engine is optimised for cruise condition and assisted during take-off by an electric engine. This electric engine is powered by low-weight batteries which provide enough power for two minutes at full power.

To meet all the requirements set in Chapter 2, a different engine is selected. A total of six different engines were investigated and are listed in Table 12.2.

Table 12.2: Engine options for the Cessna Morphlight

Engine manufacturer	Rotax Engines	Rotax Engines	Continental	Continental	Siemens	Siemens
Engine type	912 iS	914F	CD-135	CD-155	electric	electric
Power	73.5 kW	84.5 kW	100.7 kW	114 kW	85 kW	200 kW
Weight	75.4 kg	74.7 kg	134 kg	134 kg	14 kg	52 kg
Cruise fuel consumption 65%	16 L/h	12.5 L/h	17.5 L/h	19 L/h	50 kW	100 kW
Cost	€18,957[1]	€24,782[1]	€49,123[2]	€65,000 (est.)	€10,000 (est.)	N/A

The engine power at the cruise condition of the Cessna Morphlight equals about 85 kW. The engine selection is now performed such that the engine has its best economy regime at this power output. Using Table 12.2 as a reference, it becomes clear that with a power requirement of 85 kW at optimal specific fuel consumption only one engine is capable to perform for the required 10 hours. This is the Continental Diesel CD-155 which consumes 19 L/h of diesel or Jet A-1 during cruise while producing 97 kW of power. The maximum power output of this engine is 114 kW, which is 20 kW short of the maximum power output of the original engine. Therefore the need for a hybrid system arises. The 85 kW Siemens engine well overcomes this gap with a small weight penalty. This electric engine is supplied with power from batteries capable of providing two minutes of full electric engine power. This equals 1.6 kWh, but for contingency 1.8 kWh is used for battery sizing. The battery itself is a system of low weight lithium polymer cells weighing only 11 kg. The total hybrid engine weight comes in at just under 170 kg.

The two engines, the conventional diesel and the electric engine are coupled through a planetary gear to combine their power output to the shaft. Together they can maximally produce 199 kW (266.8 hp) for two minutes, greatly improving the take-off characteristics of the Cessna Morphlight. However, due to REQ-CON-PROP-2, the total power cannot be higher than that of the Cessna Skyhawk, at 180 hp. Therefore, all performance requirements are determined with the same power as the Skyhawk. The electric engine is then not used at its full potential. As can be seen in Chapter 19, all performance requirements are met using 180 hp. If the same take-off power of 134 kW (180 hp) is maintained, the pilot can benefit from the extra power for 9 minutes, providing him/her with a better climb profile. During cruise and most of all the descent, the battery is charged, ready for the next flight.

The engine of the Morphlight provides a significant improvement over the engine of the Skyhawk. First of all, it is much more efficient in terms of fuel consumption. At any power setting, the diesel engine uses less fuel than the engine of the Skyhawk even at its most efficient setting. In addition, the new engine meets the take-off fuel consumption requirement, whereas the reference engine does not. This makes the Morphlight more sustainable. Also, because the diesel engine can run on diesel fuel or Jet A-1 instead of leaded avgas, it produces fewer harmful emissions. Finally, Jet A-1 is available at most airports, whereas the availability of avgas is in decline[3].

12.1.2. Thrust Delivery Method

The second aspect of the powerplant as a system is the conversion of the shaft power delivered from the engine into thrust. As the engine provides shaft power and not a direct thrust like a jet engine does, the need for a propeller is present.

Two main propeller types are available. These are a fixed pitch propeller, which is used for the current Cessna 172S Skyhawk and a variable pitch propeller. The need for the most efficient power conversion

[1] http://www.leadingedge-airfoils.com/services.htm [cited 20 May 2015]

[2] http://www.avweb.com/blogs/insider/Continental-Diesels-Crunching-the-Numbers-220202-1.html [cited 20 May 2015]

[3] http://www.nbaa.org/ops/environment/avgas/ [cited 19 June 2015]

suggests the use of a variable pitch propeller. This is because a fixed pitch propeller is most efficient for only a small range of airspeed. The blade angle of a variable pitch propeller can be adjusted in flight, resulting in a wider region of efficient propeller use.

With the variable pitch propeller, the propulsive efficiency can be increased. Especially during take-off, this can have a pronounced effect, because a fixed pitch propeller is typically designed for cruise, and is relatively inefficient at take-off speeds. By using a variable pitch propeller, it is assumed the propulsive efficiency is slightly improved for high speeds. For take-off speeds, the propulsive efficiency is assumed to improve by a larger margin, because the initial condition is less efficient.

12.2. Electrical System

The electrical energy for the aircraft is supplied by a 12-Volt, direct current, negative ground electrical system. A battery, also supplying 12 Volts, provides power for starting. This battery is also used in case of an alternator failure. The electrical engine, used as an alternator, is the main source of power during flight [40]. The alternator of the Cessna Morphlight has to deliver more power than the current alternator, since the morphing concepts are electrically actuated.

Due to the complexity of the flight control systems in the morphing sections and the inherent extra weight they would contribute, the flight control system for the ailerons is redesigned to a fly-by-wire control type. This reduces weight over the mechanical system and is less complex to comply with the span morphing. Note that the rudder and elevator will remain mechanically actuated to ensure the safety and reliability of the aircraft.

The aircraft lighting system consists of landing and taxi lights, navigation lights, anti-collision strobe lights, ground recognition beacon lights, instrument flood lights, map light, control wheel map lights, compass and radio dial lights and interior lights [40].

An electrical heater is installed in the pitot tube, which prevents ice formations on the pitot tube [40].

A block diagram of the Morphlight's electrical system is given in Figure 12.1. Here the electrical engine functions as the alternator.

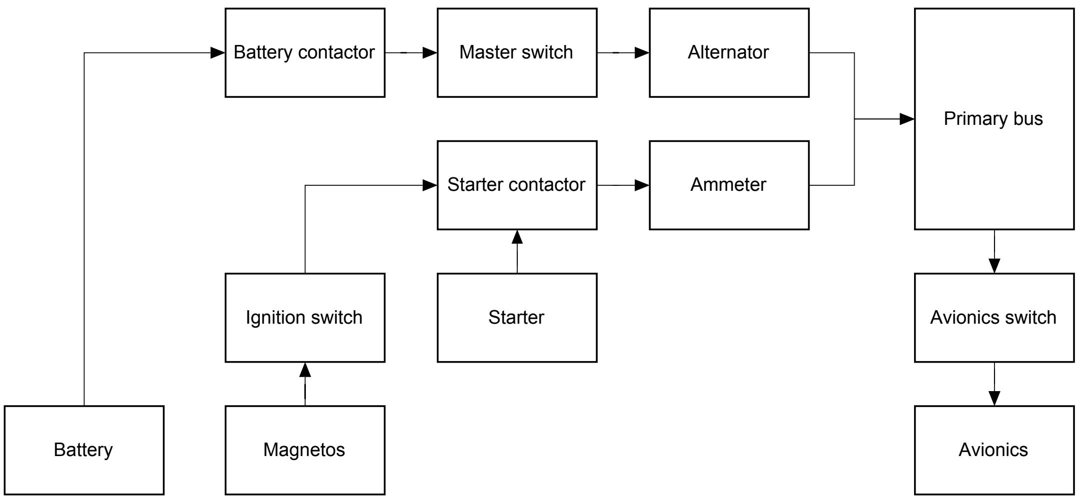

Figure 12.1: Block diagram of the Morphlight's electrical system.

12.3. Environmental Control System

The environmental control system of the Cessna Skyhawk consists of a windshield defroster, a fan, a heating system, soundproofing and a carbon monoxide detection system [41]. These systems are considered to be sufficient for the Cessna Morphlight as well.

12.4. Fuel System

The fuel system consists of the following parts [41]:

- Electric auxiliary fuel pump
- Engine driven fuel pump
- Integral fuel tanks
- Fuel selector valve
- Fuel shutoff
- Fuel strainer
- Fuel tank quick drain
- Fuel sampler cup
- Fuel vapor return system

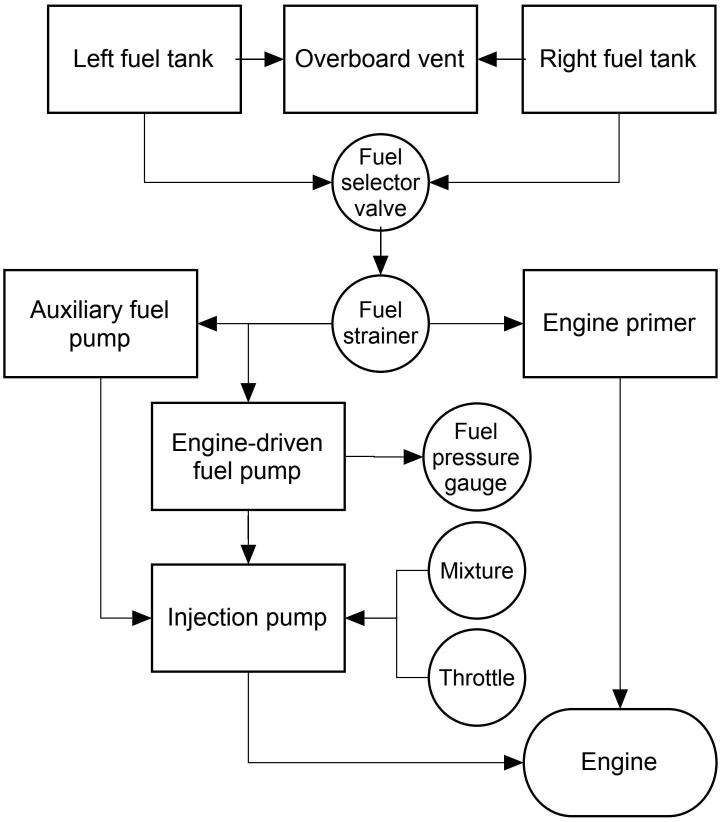

Figure 12.2: Block diagram of the Morphlight's fuel system.

The fuel is led from the tanks to the injection pump through a selector valve and a fuel strainer. The strainer is equipped with a quick-drain valve which provides a means of draining trapped water and sediment from the fuel system [40]. The overboard vents can direct excessive pressures outside the fuel tank. A block diagram of the Morphlight's fuel system can be found in Figure 12.2. Since the fuel tanks may be placed further from the engine in the Cessna Morphlight, some parts need to be elongated. Since the wing also has a smaller chord than the original wing, there is less space for the fuel tanks. This means that the fuel tank have a different shape than the current fuel tank, as described in Section 13.7. Apart from that, the fuel system will remain the same.

12.5. Hydraulic System

The hydraulic system of the Skyhawk is straightforward, since the hydraulic brake system is the only part where hydraulics are used. The brake master cylinders, which are located just forward of the rudder pedals, are actuated using hydraulic fluid. This is a direct link, not requiring any pumps [40].

For the Morphlight, the retractable landing gear is also hydraulically actuated. An electrical pump pressurises this system. A hand driven backup pump is included to extend the landing gear in case of an electric (pump) failure. This backup pump cannot be used to retract the gear.

A block diagram of the Morphlight's hydraulic system is given in Figure 12.3. Only the hydraulic components of the landing gear are shown. The hydraulic brake system is not included because it is a direct system. It does not have a pump so it is also not related to the landing gear circuit.

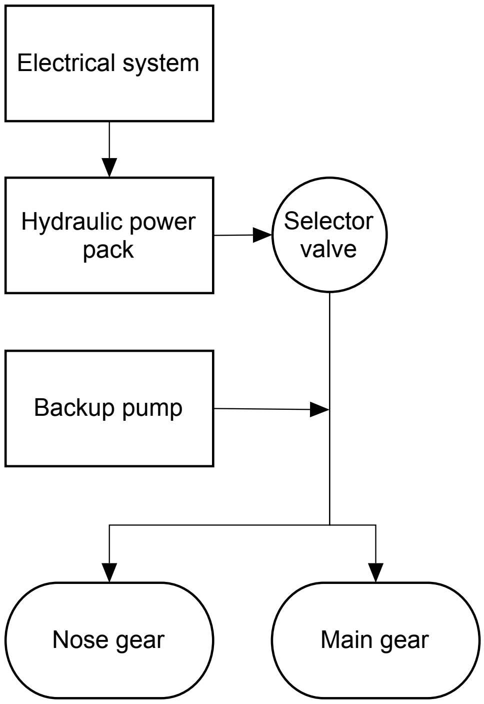

Figure 12.3: Block diagram of the Morphlight's hydraulic system.

12.6. Landing Gear

The original Skyhawk has a fixed landing gear, comprised of a steerable nose wheel on a shock strut, and a main gear with a wheel at the end of a strut on either side of the fuselage. Shock absorption on the main gear is handled by a spring in the strut. In flight, the combination of wheels and struts of the landing gear accounts for circa 8.5% of parasitic drag. Since the landing gear is only used during take-off and landing, it is a useless drag contributor for the largest portion of a flight. By retracting the gear or optimising the aerodynamic shape of the components, drag can be significantly reduced. This chapter assesses various methods to achieve such a drag reduction and concludes with a design for the selected method.

12.6.1. Gear Type Selection

The biggest advantage of retracting the landing gear in flight is to reduce drag and consequently increase performance. The Cessna 182 Skylane comes in two versions, one with a fixed gear and one with retractable gear (RG). Both have similar engine power and other characteristics, allowing for a quantitative comparison. The RG model has a climb speed of up to 1,140 fpm, whereas the fixed gear Skylane reaches only 924 fpm (a 23% increase)[4]. The cruise speed of the retractable version is also considerably higher at 156 kt, compared to the 140 kt of the fixed gear (a 11% increase)[4]. Another advantage is that the need for wheel fairings is removed. This will save some weight and additionally increase drag when the gear is extended, which is favourable for the landing performance.

There are also disadvantages associated to retractable gear systems. For flight training, fixed gear

[4] `http://www.planeandpilotmag.com/pilot-talk/x-country-log/why-retract.html` [cited 5 June 2015]

aircraft are usually preferred, as they provide an easier starting point for students. Since the Morphlight has morphing systems, the Morphlight will be less suitable for flight schools. Flight schools are thus less of a target market than initially thought. However, the increase in performance will also attract a new target audience. A retractable system increases maintenance tasks, like checking the hydraulics for leaks, greasing pivots and testing the retraction mechanism. The only thing that really needs to be checked on a fixed gear is the tire pressure. For the C172RG, a landing gear system check should be performed every 25 hours. A final disadvantage of a retractable system is the added weight. According to the Cessna method, a retractable landing gear adds circa 1.4% of the maximum take-off weight to the total aircraft weight [13].

There already is a RG variant of the Cessna 172 (see Figure 12.4). Its main gear swings backwards, storing the wheels in two cavities in the tail section, below the aft baggage compartment. The nose gear retracts forward into a section of the fuselage that is otherwise closed off by gear doors. Since the Morphlight is derived from the same airframe, the 172RG approach is taken as an initial design.

Figure 12.4: Cessna 172RG Cutlass RG II retracting its gear[5].

On the C172RG, the retraction and extension is performed by hydraulic actuators that are powered by an electrical system. As a backup, the C172RG has a hand pump to manually actuate the hydraulic system. This can only be used to extend the gear.

An alternative method to reduce parasitic drag is to add fairings to the wheels and shape the struts in a more aerodynamic shape, as if they were miniature airfoils. Using an airfoil section for a strut decreases its parasitic drag by an order of 10, while fairings half the drag from the wheels [42].

12.6.2. Landing Gear Performance Assessment

The contribution of the landing gear to the parasitic drag of the aircraft can be split into two parts: the wheels and the struts. A simple estimate for them is given by Equations (12.1) and (12.2) respectively [42]. The parameters S_{wheel} and S_{strut} are the frontal areas per wheel and strut, whereas S denotes the wing reference area, which is 16.2 m^2 in case of the Cessna 172 [43]. Through technical drawings, the dimensions of the Cessna 172S are determined.

$$C_{D_{0_{wheel}}} = \sum_{i=1}^{n} C_{D_{wheel}} \frac{S_{wheel_i}}{S} \qquad (12.1)$$

$$C_{D_{0_{strut}}} = \sum_{i=1}^{n} C_{D_{0s_i}} \frac{S_{strut_i}}{S} \qquad (12.2)$$

$C_{D_{wheel}} = 0.15$ for a wheel with fairing, and 0.30 for a wheel without. This means that a wheel with a fairing has only 50% of the drag of a bare wheel. A strut with an airfoil shape has $C_{D_{strut}} = 0.1$, while a normal circular cylinder has $C_{D_{strut}} = 1$.

[5] `http://www.airliners.net/photo/Cessna-172RG-Cutlass/2129379/L/` [cited 5 June 2015]

Table 12.3: Drag contributions of the landing gear of a Cessna 172S. The percentages are relative to the $C_{D_0} = 0.028$ of the complete aircraft.

Component	C_{D_0}	
Wheels (no fairings)	0.00327	11.7%
Wheels (with fairings)	0.00164	5.9%
Struts (simple cylinder)	0.00685	24.5%
Struts (airfoil shape)	0.00069	2.5%

As can be seen, the (unoptimised) landing gear is responsible for a significant amount of parasitic drag. It must be noted that parasitic drag is only a part of the total drag, so the actual drag reduction is less. When optimised by adding wheel fairings and changing the struts to an airfoil shape, the landing gear is responsible for 8.4% of the parasitic drag. When the gear is retracted, the contribution to C_{D_0} is approximately zero. It is not completely zero, because the main gear is not stored behind doors, so there is a small amount of turbulence created by interruptions in the fuselage skin, but this is neglected in these preliminary calculations.

In order to see the difference in performance for a fixed and retractable landing gear, one must look at the resulting lift over drag ratio. The required lift coefficient can be found through Equation (12.3), the total drag can be calculated as shown in Equation (12.4). The results of these calculations are presented in Table 12.4 for the C172S and C172RG.

$$C_L = \frac{W}{0.5\rho V^2 S} \qquad (12.3)$$

$$C_D = C_{D0} + \frac{C_L^2}{\pi A e} \qquad (12.4)$$

Table 12.4: Lift and drag characteristics of the Cessna 172S and 172RG. For the computation, standard air density at 2600 m and a speed of 250 km/h were used.

		C172S	C172RG
MTOW	[kg]	1157	1202
Aspect ratio	[-]	7.52	7.52
Wing area	[m^2]	16.2	16.2
Oswald factor	[-]	0.75	0.75
C_L	[-]	0.663	0.689
C_D	[-]	0.053	0.052
C_L/C_D	[-]	12.555	13.131

The RG variant has a 5% better lift over drag ratio. For the Morphlight, the 1.4% weight penalty corresponds to 17.5 kg. Combining the reduced drag and increased weight in the performance program, the fuel consumption on a 2000 km mission reduces by 2.3%.

With the sensitivity from Section 8.5, the relative importance of a reduction in weight versus a reduction in drag can be determined. From the analysis, it is found the a reduction in weight is 4.85 times as important as a reduction in drag. The 1.4 % increase in weight, as estimated by the Cessna method, can be justified if the decrease in parasitic drag is $1.4 \cdot 4.85 = 6.8\%$. The RG has a C_{D_0} that is 8.4% lower, so the benefit of the drag reduction outweighs the increase in weight.

12.6.3. Landing Gear Cost

Since a retractable landing gear involves more mechanisms and hydraulics than a fixed gear this will introduce some additional costs. However this was already accounted for in the cost estimation performed before. For this estimation the DAPCA IV method was used which assumes a retractable landing gear and includes this in the manufacturing and materials cost. To find the actual landing gear cost, it was found in [44] that when using a fixed gear $7,500 should be subtracted from the total cost. Therefore this is the value assumed to be accounted for in manufacturing the aircraft.

On first hand this seems like a rather large investment. However, when looking at the second hand market and comparing aircraft with retractable to fixed gear it can be observed that the retractable option is worth on average $20,000 more than the fixed option. This analysis has been done on the Cessna 177 Cardinal aircraft which is similar to the Skyhawk and comes in two configurations with only one difference: fixed or retractable gear. A linear regression was made with aircraft originating from 1967 to 1977 versus the retail price ranging from $40,000 to $90,000 as can be seen in Figure 12.5. From this it can be concluded that from an economical point of view buying an aircraft with retractable gear is the better option.

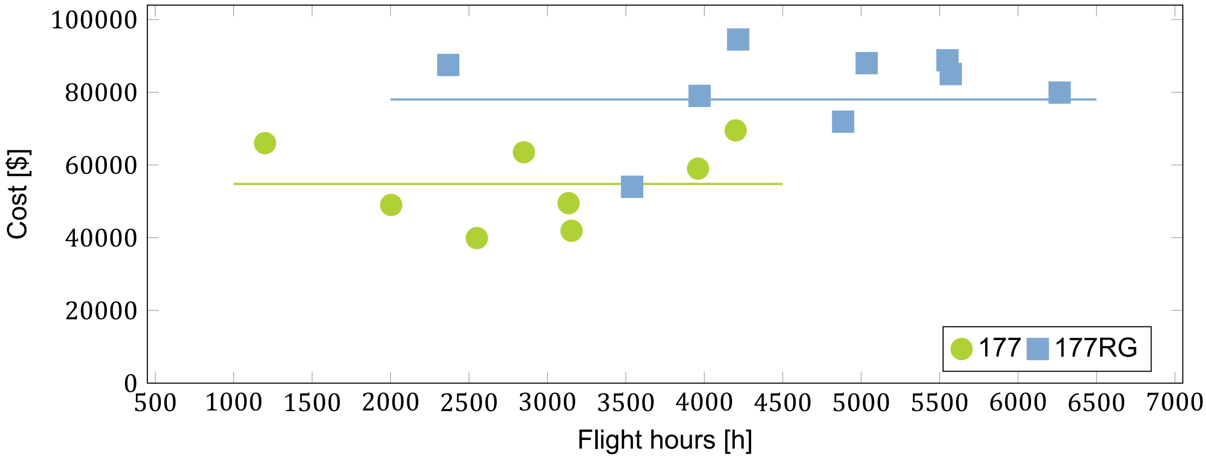

Figure 12.5: Comparison of the cost of used Cessna 177 models with fixed and retractable landing gears

Another disadvantage regarding the cost is that a retractable landing gear results in higher insurance costs. This is due to the fact that the system is relatively vulnerable to pilot error, which is a significant contributor to the total amount of accidents. According to analysed statistics in [45], 10 percent of all accidents were due to problems with the gear mechanism.

12.6.4. Conclusion and Landing Gear Type Selection

Considering that the performance requirements are very demanding and the weight and cost budgets allow for contingency, it can be concluded that the benefits regarding the performance outweigh the cost and weight penalties. All in all it can be concluded that is is advantageous to incorporate a retractable landing gear system. Therefore the fixed landing gear is replaced by a retractable gear which is similar in its layout and design as that of the Cessna 172RG.

12.7. Flap Sizing

This section describes the sizing of the high lift devices. The high lift devices are the way in which the Morphlight changes its chord and camber. This is done using Fowler flaps, as described in Chapter 7.

Fowler flaps are an excellent solution for the Morphlight, because they provide a means to increase both the chord and the camber of the wing. The additional benefit of the Fowler flaps is that the chord is extended before the camber increases, which makes it also suitable for take-off, where a large wing area is desired, but not the high drag associated to a high lift coefficient. Then, when the camber is fully increased, the drag of the flap can be very high, which is desirable for landing. In fact, the zero lift drag of the airfoil with a flap can increase by as much as 10 times when they are close to the maximum lift [46].

Sizing the Fowler flaps was done with the procedure outlined in [46]. Only the direct contribution of the flaps to the maximum lift coefficient was considered. The other effects of the flaps are minor and ignoring these makes the estimation conservative. The increase in lift coefficient due to the flaps is determined by Equation (12.5). As can be seen, the increase in maximum lift coefficient is determined by the sectional increment in lift ($\Delta C_{l_{max}}$) of the flapped area of the wing (S_{w_f}). The lift increase of the airfoil section is shown by Equation (12.6). The primary source of the increase of the lift is the deflection angle δ_f. Hereby the camber of the airfoil is increased. The increase in chord is included in the term $\frac{c'}{c}$. The airfoil properties are included through C_{l_α}. The parameters α_δ and K_Λ are the airfoil lift effectiveness and a planform correction factor, which are approximately 0.4 and 0.92, respectively [46].

$$\Delta C_{L_{max}} = \Delta C_{l_{max}} \frac{S_{w_f}}{S} K_\Lambda \qquad (12.5)$$

$$\Delta C_{l_{max}} = C_{l_\alpha} \alpha_\delta \frac{c'}{c} \delta_f \qquad (12.6)$$

It is important to consider the increase in wing area only once in the calculation of lift. Since the wing area with extended chord was taken in the sizing for take-off and landing, the increase in $C_{L_{max}}$ should not take into account the additional lift due to the chord extension. The effects of the flaps on the maximum lift coefficient were determined with the actual chord extension, but the result is shown without the chord extension term $\frac{c'}{c}$.

The Fowler flaps can be deflected by 45 degrees, which is typical for this type of flap system [34]. The area of the wing affected by the flaps is about 50% (see Figure 13.2). The maximum possible extension of the flaps is about 35% of the chord. This is limited by the location of the wing box (which also limits the length the flap itself), the actuator, and the mechanism. A global increase in the maximum lift coefficient of 1 was estimated to meet the landing requirement and 0.2 for the take-off requirement. With the flaps extending by 35% of the chord and deflecting by 45 degrees, the increase in the maximum lift coefficient is about 0.98, which is sufficient to meet the landing requirement. The result is shown in Table 12.5. The flaps are also able to provide sufficient lift in take-off configuration, with a flap deflection of around 7 degrees.

Table 12.5: Contribution of Fowler flaps to maximum lift coefficient in landing and take-off configurations. Effect of wing area increase not shown for increase in maximum lift coefficient.

Configuration	**Extension [%c]**	**Deflection [deg]**	$\Delta C_{L_{max}}$ **[-]**
Landing	35%	45	0.98
Take-off	35%	7	0.20

12.8. Speedbrake Sizing

In order to meet the landing requirement, a high level of drag is desired to make the approach glide path steeper. From the performance analysis from Chapter 8, an additional equivalent flat plate drag surface ($C_D \cdot S$) of 0.5 is required. However, this drag is not desired at take-off since it would increase the take-off distance. Therefore the option of speedbrakes is favourable since they can be deployed when necessary and thus will not compromise the take-off performance.

There are several ways to increase drag on demand. The NASA Space Shuttle used a spreading rudder concept, in which the rudder surface is split in a left and right surface, which both rotate outwards to act as speedbrakes. However, this solution adds a significant amount of complexity to the tail and would be detrimental to the reliability of the rudder as a critical control surface. It was therefore considered an infeasible option.

Another used option to apply a speedbrake is on top of the main wing. For the Morphlight this is impracticable as well, since it is made of the zero Poisson skin. The roof of the cabin however is made of a composite and thus allows for the application of a flap. This location also ensures the least interference with the control surfaces. On approach the aircraft flies with a pitch up attitude, meaning that most of the wake behind the plate would not affect the rudder. Flat plates extending from the lower side of the fuselage were ruled out as their wake would interfere with the horizontal tail surfaces. Ground clearance on landing and the prevention of tail strikes would also be more difficult in that case. A final advantage of placing the flap on top of the cabin is that it is close to the centre of gravity, and thus not affecting stability and control much. Having a single system instead of one on either side of the fuselage reduces complexity and the consequences of a system failure (asymmetric drag).

Considering the aerodynamic forces and moment generated by the speedbrake, it is advantageous as well to position the brake on top of the fuselage. The generated drag force will generate a pitch up moment which can balance the pitch down moment from the deployed flaps. In this way the horizontal stabiliser will have to produce less pitch down moment to keep the aircraft in equilibrium. This effectively results in less lift required from the tail. This is beneficial since this improves the controllability of the aircraft.

The actuator does add a small amount of complexity and maintenance requirements, but due to its simplicity and non safety critical application, this is considered a minor inconvenience.

To meet the requirement of the additional drag, first it is determined how the drag coefficient depends on the angle of attack of the plate. From an analysis of a flat plate at different angles of attack it was found that the drag coefficient is approximately 0.75 at an angle of 40 degrees and increases to 1.0 at 60 degrees [47]. Furthermore, from this analysis it can be seen that the aspect ratio also has an effect on the aerodynamic coefficients. Although this effect is observed to be small, the largest C_D values can be found with an aspect ratio of 1 (a square plate). During operation the speedbrake is designed to be able to rotate to 60 degrees. However, ensuring some margin and taking into account that the effective angle of attack of the brake can decrease due to a positive pitch angle, the drag coefficient of the speedbrake is taken as 0.75. This implies that the speedbrake should have an area of 0.67 m^2. This way, when the speedbrake is deployed at a deflection angle of 40 degrees it will generate sufficient drag. The plate rotates around a hinge at the front side and is actuated by two actuators at the back.

13

Detailed Aircraft Layout

In this chapter the detailed layout of the Cessna Morphlight is described. It is mainly focused on the wing design, but the fuselage and empennage are mentioned as well. Some sections are not described in detail because the design has already been given in an earlier chapter.

13.1. Fuselage

The fuselage has a slightly changed shape compared to the Cessna 172 Skyhawk to improve the aerodynamic flow around the aircraft. To store the retractable landing gear used on the Cessna Morphlight two storage bays for the wheels and struts are located in the tail section below the aft baggage compartment and one is located under the engine. This forward landing gear bay is closed during flight.

13.2. Landing Gear

The landing gear design is described in Section 12.6. The design is the same as for the Cessna 172RG Cutlass, however, because the MTOW of the Cessna Morphlight is approximately 50 kg higher it requires a minor redesign to cope with the higher forces.

13.3. Wing Shape

The wing shape is determined by the wing planform and the airfoil. The planform is determined in this chapter and the airfoil selection is described in Section 9.2.

13.3.1. Wing Planform

For the wing planform multiple solutions have been considered. Four configurations have been analysed on investment and production cost, induced drag, fuel storage and structural characteristics. The four planforms are shown in their retracted position in Figure 13.1. It should be noted that for planforms 2, 3 and 4 a taper ratio of 0.5 is chosen for good visualisation, but for the wing of the Cessna Morphlight a higher taper ratio is used.

Planform 1 and 4 are the cheapest to produce and investment costs are the lowest. This is because the entire morphing section of the wing has the same chord. Also production is faster and assembly is simpler. The aerodynamic performance of planform 2 is the best of the four options because constant taper is used. All other options result in more induced drag, but by testing models in XFLR5 the difference in total drag between the best and worse case is found to be 1.6% at a lift coefficient of 0.55 and a cruise speed of 250 km/h. Induced drag can be minimised by using raked wing tips. Fuel storage at the root is best possible for planforms 2 and 4. This is because the root chord is the highest. The structural characteristics of planforms 2 and 4 are the best for the same reason. A comparison between

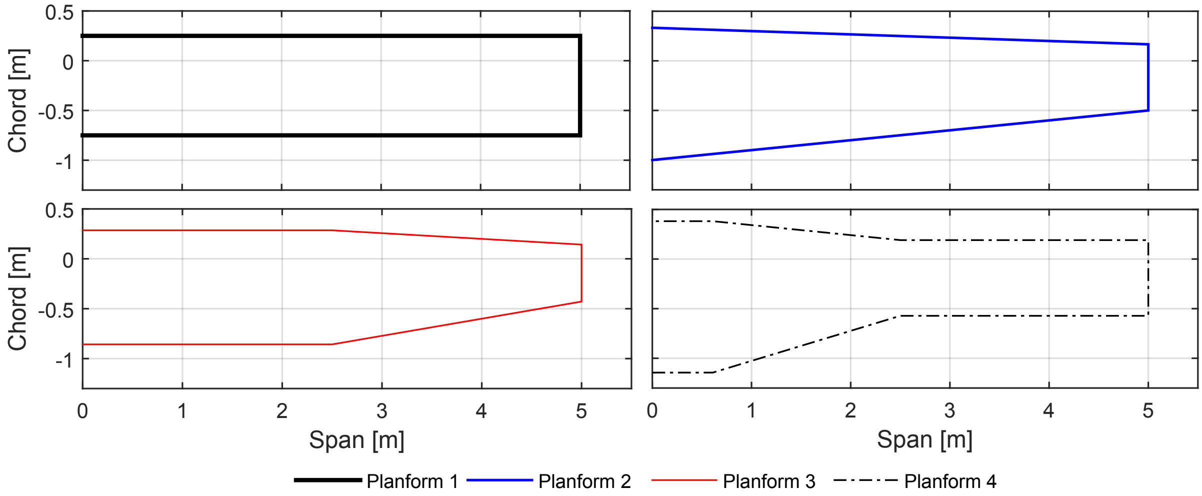

Figure 13.1: Four possible planform layouts. The layouts are shown with a taper ratio of 0.5 for the retracted configuration, while the wing of the Cessna Morphlight has a higher taper ratio. The quarter-chord line is chosen to be on the line for which $y = 0$. The fuselage ends at 0.61 m span and morphing starts at 2.5 m span.

the planforms is shown in Table 13.1.

Table 13.1: Comparison between possible planforms.

	Cost	**Induced drag**	**Fuel storage**	**Structural performance**
Planform 1	+	-	-	-
Planform 2	-	+	+	+
Planform 3	-	o	o	o
Planform 4	+	o	+	+

Planform 4 is used for the Cessna Morphlight, because its relatively low costs, high fuel storage capacity and good structural performance. The induced drag of the wing is minimised by using smoother edges than shown in Figure 13.1 and a small raked wing tip is used. Because the chord is desired to be as large as possible for system integration and the mean aerodynamic chord (MAC) is required to be 1.00 m as determined in Chapter 8, which is already relatively low, a taper ratio of 0.8 is used. Using the aileron dimensions given in Section 10.2.1 and by placing the flaps on the remaining area at the trailing edge the final wing planform is shown in Figure 13.2.

13.3.2. Wing Airfoil

The airfoil selection is described in Section 9.2. The airfoil of the wing of the Cessna 172 Skyhawk is NACA 2412. For the Cessna Morphlight the NACA 35013.5 is selected, with a design lift coefficient of 0.5 and maximum camber located at 26% of the chord.

13.4. Wing Skin

For the non-morphing skin a regular structure is used. For the morphing skin, however, a zero Poisson structure is used which is described in Appendix A. This zero Poisson skin takes up approximately 1.0 cm on each side and thus reduces the space available for the internal structure. The dimensions of the honeycomb structure is not optimised in this report. As can be seen in [48] this requires research on its own. To determine the best configuration of the structure accurately, results from CFD analysis should be implemented in a FEM model of the skin. By determining a maximum out-of-plane skin deflection, as well as a maximum out-of-plane honeycomb deflection, dimensions can be optimised.

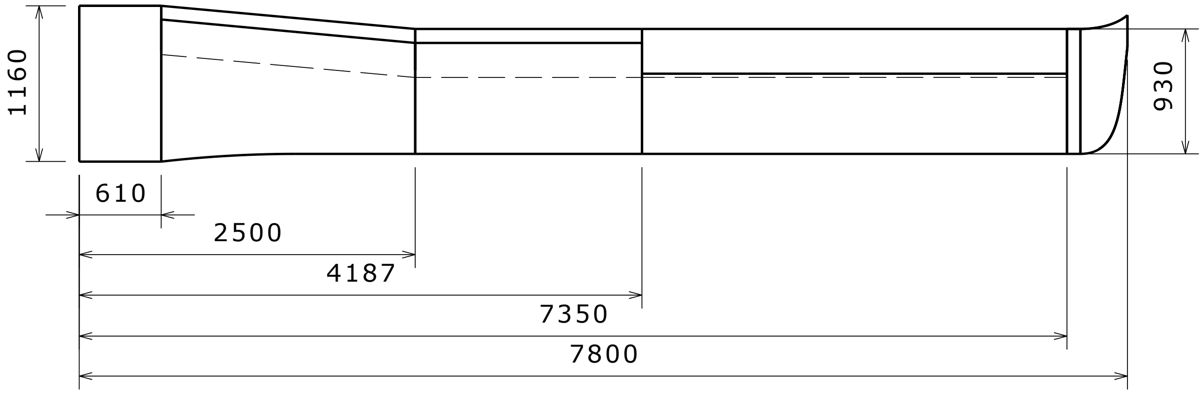

Figure 13.2: The final planform layout for the Cessna Morphlight shown in the extended configuration. The dashed lines indicate the most forward edges of the flaps and aileron.

13.5. Internal Wing Structure

Inside the wing a number of components can be recognised. These are the wing boxes, ribs, the span extension mechanism and the fuel tanks.

13.5.1. Wing Boxes

The wing box sizing is described in Chapter 11 and the final dimensions are given. As described a total of five wing boxes are used: one fixed central box extending into both wings and two sliding boxes on each side. The outer boxes are placed inside the one closer to the root and are separated by a thin layer of UHMW-PE (ultra-high-molecular-weight polyethylene) as described in more detail in Section 14.4. This material is used to reduce friction and wear in the wing boxes. This system is shown in Figure 13.3.

The front of the central wing box is located at 25% of the chord and has a width of 10 cm and a height of 12 cm.

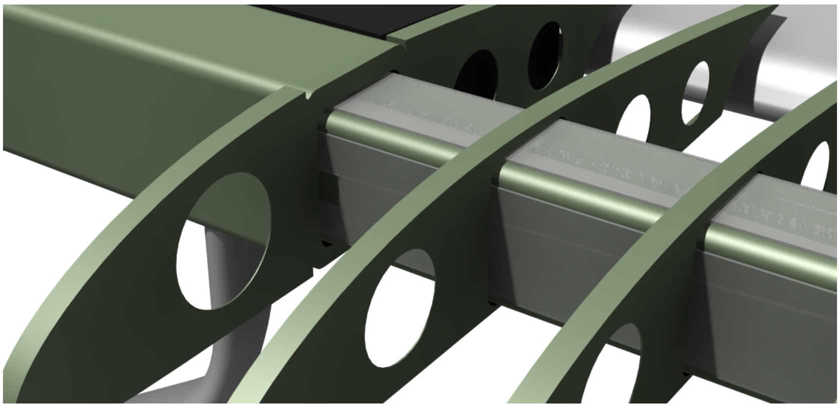

Figure 13.3: A thin layer of UHMW-PE is used to allow the boxes and ribs to slide over each other.

13.5.2. Ribs

Two types of ribs can be recognised. Some ribs are rigidly connected to the wing boxes and some are sliding over the boxes using the aforementioned UHMW-PE material. The moving ribs are connected rigidly to the morphing honeycomb structure. The ribs to which flap actuators and tracks, as well as ailerons, are connected, are rigidly attached to the boxes. The ribs are connected to the normal skin in the non-morphing section and to the rib-shaped structures of the honeycomb structure morphing region of the wing as described in Section 16.3 and shown in Figure 13.4. As described in Chapter 11 ribs have a spacing of 22 cm in the configuration with maximum span.

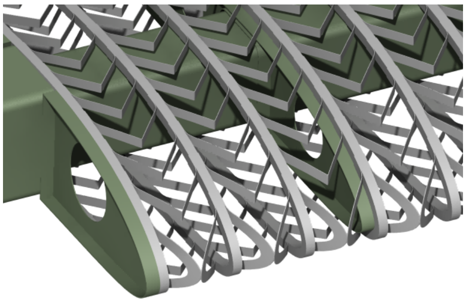

Figure 13.4: Connection between the ribs and the honeycomb structure in extended configuration.

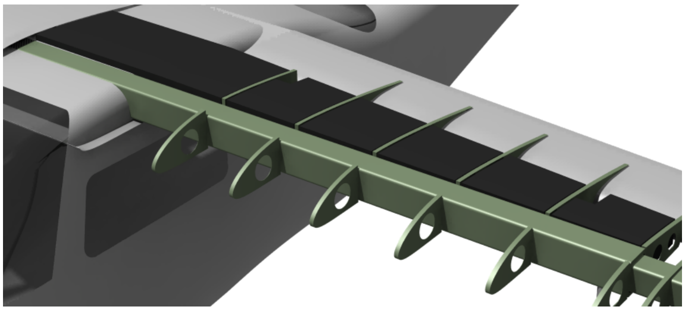

Figure 13.5: Fuel tanks are placed between the ribs in the non-morphing section of the wing.

13.5.3. Span Extension Mechanism

For the span extension mechanism a number of options have been considered. The first option is a linear screw actuator as used frequently for flaps on large aircraft. The advantage of this mechanism is reliability and the use in the aforementioned application. The disadvantages, however, are that the actuator is in compression while extending the wing, which would require a stronger, thus heavier, mechanism to withstand buckling. Also the system takes up a lot of space. The second option is a cable system that is located on the tip of the first and the second wing box with the cable connected to the root of the second and third wing box respectively. Because a cable is used which is in tension the weight is relatively low. This does however only work when a small slot is created in which the cable is placed. This is not ideal for the structural properties of the wing boxes. Also stress concentrations are located at undesired locations. The third and selected mechanism is a rack and pinion system placed at the front side of the wing boxes. A rack is attached on the second and third box respectively and a small electric motor with a pinion is placed at the tip of the first and second box respectively. The pinion is attached to the rack through a small slot in the box on the outside. This system is relatively lightweight and reliable. A small motor is sufficient since the forces acting on the rack and pinion system are relatively low as found by using a preliminary force analysis using the method described in [48]. The maximum forces acting on a single motor are approximately 150 to 250 N.

13.6. Strut

A lift strut is used to reduce stresses in the wings and allow for a more lightweight design. As described in Chapter 11 the strut is located at 2.5 m from the plane of symmetry of the aircraft, thus at the the tip of the non-morphing section of the wing. The strut uses a NACA 0030 airfoil, to reduce aerodynamic drag, whereas the Cessna 172 Skyhawk uses an ellipse for its strut cross-section. The strut has its curved shape, as visualised in Figure 13.7, to avoid buckling in the strut skin and to minimise drag. The chord is 10 cm.

13.7. Fuel Tanks

Due to the relatively small chord compared to the Cessna 172 Skyhawk and the wing box located in the middle of the wing, placing fuel tanks is difficult. For this reason eleven separate tanks are required, compared to two used in the Cessna 172 Skyhawk. One fuel tank is located in the wing above the cockpit and five more fuel tanks are located in the non-morphing section of each wing, in between the ribs. The fuel tanks are visualised in Figure 13.5. The cut-outs in two of the fuel tanks are due to the flap tracks located there.

13.8. Flaps

To increase chord length and camber sufficiently a Fowler flap mechanism is used, described in Section 12.7. Three mechanisms have been considered for this flap mechanism as shown in Figure 13.6. The first option is a very simple actuator system placed on the bottom side of the wing, used on the

McDonell Douglas DC-9. The advantage of this mechanism is the low amount of maintenance required and the simplicity during production. The disadvantages, however, are the large amount of drag they generate, regardless of the use of flap track fairings. It is also not able to perform chord and camber morphing separately. The second option is a four bar mechanism used in many large aircraft, for example the Boeing 787 Dreamliner and the Airbus A320. This mechanism is capable of carrying high loads, but this is not required for the Cessna Morphlight. The system is complex, which is undesired from a production and maintenance point of view, and the weight is relatively high. Also placing the system in the limited space available would pose a serious issue. The third and selected mechanism is based on the flap track used on the Melmoth 2[1], a homebuilt 4-seat single-propeller aircraft. Flap tracks are placed on the top side of the wing and first allow chord morphing after which the flap is rotated. The mechanism is relatively lightweight and simple and maintenance can easily be performed. The design has be flight proven on the aforementioned aircraft.

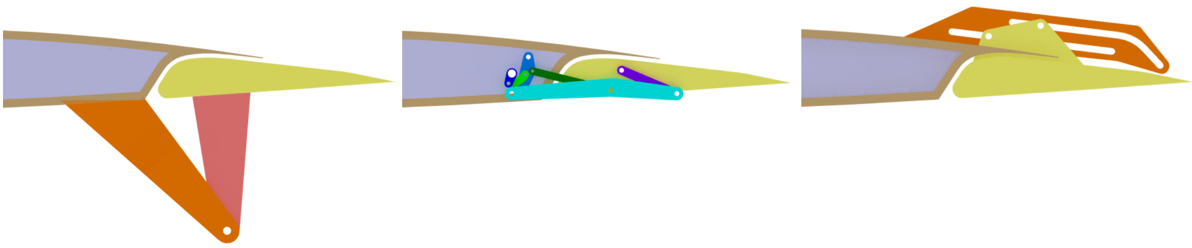

(a) Hinge mechanism (b) Four bar mechanism (c) Slider mechanism

Figure 13.6: Three options for the flap mechanism.

As described in Section 12.7 the flaps cover the span of the wing from the root at 0.69 m from the plane of symmetry to 3.335 m in the retracted position. When the span is extended the flaps cover the span up to 4.27 m from the plane of symmetry. The Fowler flaps are moved aft with an average of 35% of the chord and deflected 45° downwards.

13.9. Ailerons

A differential aileron mechanism is used for the Cessna Morphlight. This mechanism is used on many aircraft to counteract adverse yawing moments. The aileron is attached close to the top skin and the actuator is connected on the bottom side.

As described in Section 10.2.1 the ailerons cover the span of the wing starting where the flaps end and ending 10 cm from the wing tip. This means that the ailerons covers the wing span from 3.335 m to 4.900 m measured from the plane of symmetry and 4.270 m to 7.400 m for the retracted and extended positions, respectively. The ailerons cover 35% of the chord at the trailing edge of the wings and can deflect 20° upwards and 20° downwards.

13.10. Empennage

The empennage is not designed in detail in this report, but a preliminary design is created.

13.10.1. Horizontal and Vertical Stabiliser

The horizontal and vertical stabiliser are designed using a multi-spar system as can be seen in the AW169 horizontal tail plane[2]. This principle uses the post-buckling principle, meaning that buckling of the skin is allowed at 70% of the limit load. For the AW169 this means that the structure is 15% lighter than that it would be for a fully rigid structure[3].

[1] `http://www.melmoth2.com/texts/Pictures.htm` [cited 17 June 2015]

[2] `http://www.ptonline.com/articles/thermoplastic-composites-save-weight-in-rotorcraft-aerostructure` [cited 15 June 2015]

[3] Arnt Offringa, Director of R&D, Fokker Aerostructures. Personal Interview. 8 June 2015.

Both the horizontal and vertical stabiliser use the same airfoil as the Cessna 172 Skyhawk. The root of the horizontal stabiliser has a NACA 0012 airfoil and the tips have a NACA 0009 airfoil. The vertical stabiliser has the NACA 0009 at the root and the NACA 0006 at the tip. The airfoil gradually changes between the root and tip. As described in Section 10.1 the horizontal stabiliser has a wing span of 3.45 m, a root chord of 1.40 m and a tip chord of 0.785 m. The half-chord line has no sweep. The vertical stabiliser has an area of 2.31 m² compared to 1.68 m² for the Cessna Skyhawk. A dorsal fin is used to improve the stability of the aircraft.

13.10.2. Elevators and Rudder

The elevators and rudder are designed using the multi-rib principle as already done in the Gulfstream G650 and the Dassault Falcon 5X. For this principle many ribs are used and a very thin skin. This can save weight up to 10% and costs up to 20%, compared to regular honeycomb sandwich design [49].

As described in Section 10.1 the elevators have a chord of 0.50 m at the root of the horizontal stabiliser and a chord of 0.20 m at the tip, resulting in an area of 0.54 m² for each elevator. The elevators can deflect 28° upwards and 23° downwards. The rudder is sized along with the vertical stabiliser and thus has an area of 0.96 m². The rudder has a deflection of 16° in both directions.

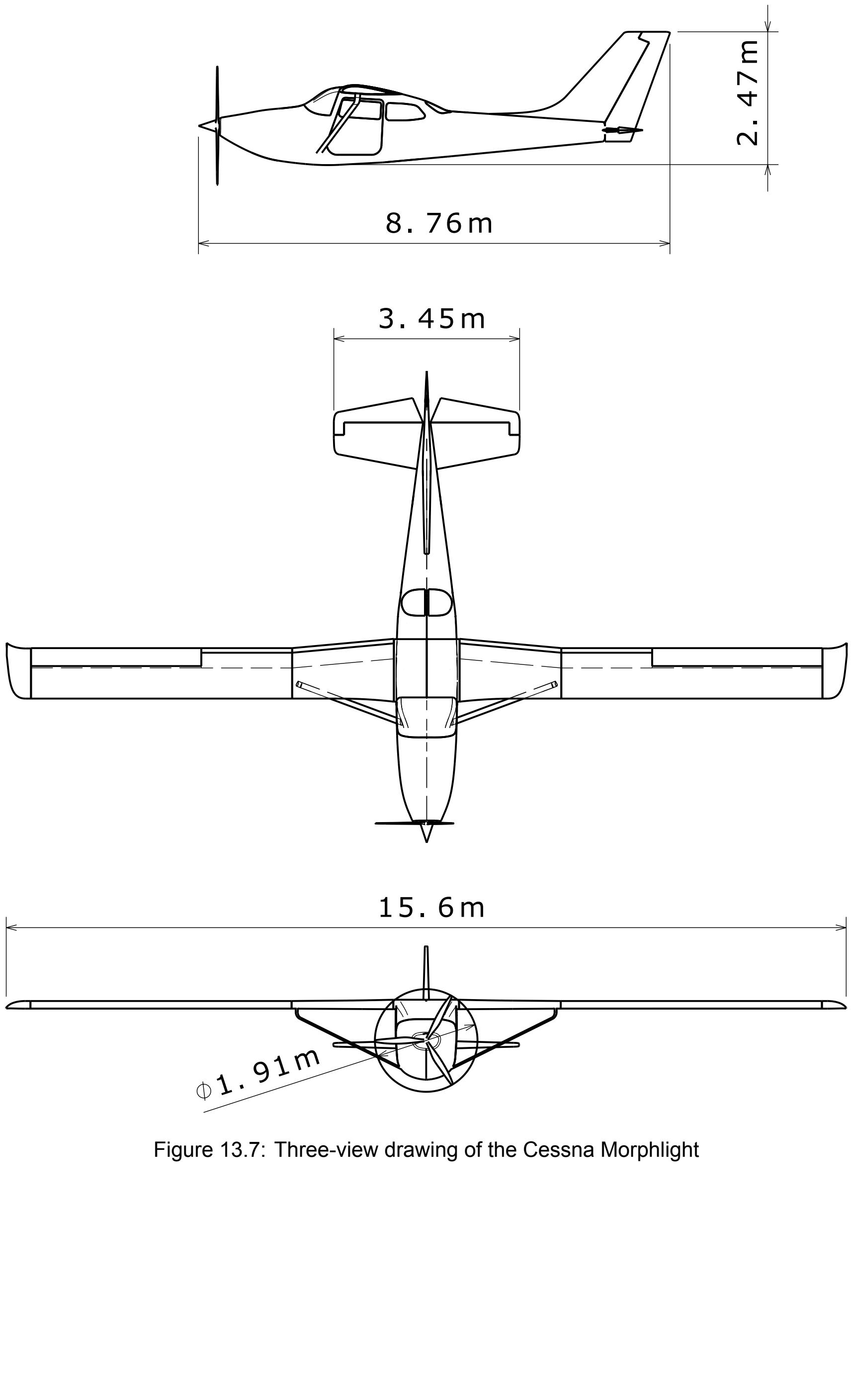

Figure 13.7: Three-view drawing of the Cessna Morphlight

14

Material Selection

In this chapter the material selection for the Cessna Morphlight is explained. Because the implementation of morphing systems adds weight to the aircraft and the operational empty weight should remain the same, weight is removed from other components. A very effective method for doing so is by replacing most of the 2024-T3 aluminium alloy used on the Cessna 172 Skyhawk by a more lightweight alternative. At the same time a limited cost increase is allowed for the change in materials.

A current trend in aircraft design is the use of carbon fibre reinforced polymers (CFRPs) in wing, empennage and fuselage sections. This trend is visible in homebuilt general aviation aircraft, for example the DAC (Dutch Aeroplane Company) RangeR, but also in large commercial airliners, for example the Boeing 787 Dreamliner and the Airbus A350 XWB. Glass laminate aluminium reinforced epoxy (GLARE) is used in fuselage sections and on the empennage of the Airbus A380 and reduces the weight of the aircraft significantly[1]. GLARE also has very good fatigue and damage resistance characteristics. This material, however, is not very applicable to small aircraft such as the Cessna Morphlight, due to the relatively large thickness required for the material and the relatively low freedom of design. Also the potential weight savings achieved by this material are not as high as for CFRPs.

In Table 14.1 the most relevant mechanical properties are shown for the aluminium alloy used on the Cessna 172 Skyhawk and for a Poly-Phenylene-Sulfide (PPS) carbon fibre unidirectional composite. This composite, produced by Celanese using fibres by TenCate Advanced Composites, is a good representative of thermoplastic CFRPs used in aerospace applications. It should be noted that in this table properties are shown for 0° and 90° fibre orientation, while for most components the fibres are oriented such that the material shows quasi-isotropic characteristics.

Table 14.1: Mechanical properties of 2024-T3 aluminium alloy and Fortron® PPS Carbon Fiber Unidirectional Composite Thermo-Lite® 1466P. Properties of the aluminium alloy are shown for a thin flat sheet. Properties of the PPS carbon fibre composite are shown for 0° and 90° fibre orientation.

	2024-T3 Aluminium[2]	**PPS CF UD** [50]	
Density	2.78	1.61	g/cm³
Ultimate tensile strength	435	0°: 2,045 90°: 50	MPa
Yield strength	290	-	MPa
Tensile modulus	73.1	0°: 127 90°: 8.8	GPa
Strength to weight ratio	156.5	0°: 1270 90°: 31.1	(N · m)/g

[1] `http://www.airbus.com/aircraftfamilies/passengeraircraft/a380family/innovation/` [cited 10 June 2015]

[2] `http://www.matweb.com/` [cited 10 June 2015]

CFRPs can be split in thermoplastic and thermoset CFRPs, which display similar strength characteristics, but differ significantly in formability, recyclability, impact resistance and glass transition temperature (Tg). Thermoset CFRPs are still the most dominant of the two in aerospace applications, but due to new production methods developed by among others Fokker Aerostructures and Fiberforge, thermoplastic CFRPs are becoming more popular. While this type does not have as much design freedom as thermoset CFRPs, structures can be up to approximately 20% cheaper depending on the resin used, as mentioned by Arnt Offringa, Director of R&D at Fokker Aerostructures in a personal interview conducted on 8 June 2015. In addition, impact and crack growth behaviour is better, it is recyclable in contrary to thermoset CFRPs, it can be welded and production time is shorter.

Another advantage of thermoplastic CFRPs is that structures can be reshaped at temperatures around 300°C using pressure. This is beneficial for the production process, because parts do not need to be formed into the final shape in one step. A disadvantage that comes with this is that the Tg of thermoplastic CFRPs are relatively low and special care should be taken in high temperature environments. The Tg of thermoplastic CFRPs are in the range of 80°C for PPS to 160°C for Poly-Ether-Ketone-Ketone (PEKK), while thermoset CFRPs are able to withstand temperatures up to approximately 900°C.

For the aforementioned reasons thermoplastic CFRPs are preferred where the shape of the structure and the ambient temperature allows so. Among thermoplastic CFRPs used in aerospace applications, four matrix materials can be recognised [51]. The first to be used was Poly-Ether-Ether-Ketone (PEEK), after which came Poly-Ether-Imide (PEI), PPS and PEKK. In Table 14.2 mechanical properties of the matrices are compared. For use in the Cessna Morphlight PPS and PEKK are the most interesting, because PEEK is very expensive while it has approximately the same characteristics as PEKK and PEI scores poorly on chemical resistance. Between PPS and PEKK, PPS is cheaper and has a lower processing temperature, but PEKK has better mechanical properties, for example it is tougher, it has a higher Tg and it has better bonding characteristics. For example, PEKK can be bonded to titanium very well.

Table 14.2: Comparison between thermoplastic matrices for aerospace applications [51].

	Mechanical properties	Cost	Processing temp	Tg	Chemical resistance	Bonding
PEEK	++	-	o	+	+	-
PEI	+	+	+	+	-	+
PPS	+	+	+	o	+	-
PEKK	++	o	o	+	+	+

Besides thermoplastic CFRPs other materials are used for some components. This is described per structural component in the following sections.

14.1. Fuselage

The fuselage is divided into five sections as described in detail in Section 16.1 and per section an appropriate material is selected. Currently the fuselage skin is made of the 2024-T3 aluminium alloy and can be replaced by more lightweight materials as described in the introduction of this chapter. In the nose section where the engine is located a thermoset CFRP is preferred over a thermoplastic CFRP due to the high ambient temperature and the double curvature of the skin. A number of single propeller general aviation aircraft use glass fibre reinforced polymers (GFRPs) for the fuselage skin, but this is not preferred due to the relatively high density of the material. GFRP has a density of 2.0 g/cm³ [49], whereas CFRP has a density of 1.61 g/cm³. For the cockpit a thermoset CFRP is preferred as well due to the complex shape of the structure. For the tail section carbon fibres are used with the thermoplastic resin PPS. Even though PEKK is preferred over PPS for its excellent mechanical properties, PPS is used to keep costs low.

14.2. Landing Gear

The main landing gear of the Cessna 172 Skyhawk is produced out of 6150M spring-steel alloy, cantilevered with attaching parts of 7075-T73 aluminium alloy forgings. The nose gear components are 4130 steel alloy with 7075-T73 aluminium alloy forgings [52]. To reduce weight of the landing gear of the Cessna Morphlight the use of a grade 5 titanium alloy is investigated. Other general aviation aircraft use titanium alloys for the landing gear, of which the Pipistrel Panthera is an example. Its landing gear weights only 17 kg, compared to 50 kg for similar aircraft[3], which is a saving of 66%. Other advantages of titanium are, among others, its good corrosion resistance and its good fatigue characteristics. Disadvantage, however, are its difficulty to process the material and its very high cost. Because the weight budget in Section 18.1 states weight saving is not necessary for the landing gear and the costs of alternatives are very high, a steel retractable landing gear is used.

14.3. Wing Skin

The wing skin can be divided into two categories, non-morphing and morphing skin. The first is a regular wing skin and the second consists of an internal honeycomb structure and an elastic matrix composite (ECM) on the outside.

14.3.1. Non-Morphing Skin

For the non-morphing thermoplastic CFRP is used because of the advantages described in the introduction of this chapter. The possibility to do so is proven by the design of, among others, the AgustaWestland AW169 tailplane, the Gulfstream G650 and Dassault Falcon 5X rudder and elevator. The matrix used is PPS, because of its low price compared to PEKK.

14.3.2. Morphing Skin

For the morphing skin the same approach is taken as researchers at the University of Maryland as described in Appendix A.

Honeycomb Structure

The honeycomb structure has been tested using an acrylic-based photopolymer [53] and titanium [48]. Because the first is only sufficient for a small scale wind tunnel test and the second is too expensive for the budget of the Cessna Morphlight an alternative material is selected. Aluminium was considered, but due to the high production costs this option is discarded. After contact with Boikon, specialist in thermoplastic composites machinery, and a personal interview with Arnt Offringa[4], it is decided to separate the honeycomb structure into two parts for the production process. The production process is described in more detail in Section 16.2.2. Both parts of the honeycomb structure are produced out of thermoplastic CFRPs, with the airfoil-shaped part using short fibres and the V-shaped components using long fibres.

Elastic Matrix Composite

The EMC is built up from a 70 Shore A hardness polyurethane elastomer, sandwiching a layer of uni-directional carbon fibre, as described in [48]. The reason for not changing the skin used by the researchers at the University of Maryland for the application on the Cessna Morphlight is because of the complexity of the skin analysis. The design of the material can not be analysed with basic FEM tools. An interesting option would be to replace the polyurethane elastomer by a self-healing material. An example of this is a blend of poly(ethylene-co-methacrylic acid) with acid groups partially neutralised with sodium ions (EMNa) and oxidised natural rubber (ENR) as described in [54]. A self-healing material could possibly increase the impact resistance of the EMC.

[3] `http://www.hangarflying.eu/nl/content/een-kat-om-zonder-handschoenen-aan-te-pakken` [cited 18 June 2015]

[4] Arnt Offringa, Director of R&D, Fokker Aerostructures. Personal Interview. 8 June 2015.

14.4. Internal Wing Structure

The wing boxes, stiffeners and ribs are all produced out of thermoplastic CFRPs, though different production methods are used for each of these as described in more detail in Section 16.3. The use of these CFRPs for this application has been proven in, among others, the AgustaWestland AW169, Gulfstream G650, Dassault Falcon 5X and the Airbus A380. Similar to the fuselage internal structure, the wing internal structure uses PPS as matrix for the thermoplastic CFRP.

To reduce friction and wear in the sliding wing boxes, UHMW-PE (ultra-high-molecular-weight polyethylene) is used to coat the sliding surfaces. The low weight and high strength properties are ideal for application in the Cessna Morphlight. By using this coating the friction coefficient between the CFRP boxes is reduced to between 0.05 and 0.2[5] depending on the load and type of UHMW-PE used. The yield stress of the UHMW-PE is 22 MPa. The abrasion tests performed indicate that it is equally wear resistant as carbon steel while being much lighter.

14.5. Flaps and Ailerons

The ailerons are completely span morphing, whereas the flaps in the section closest to the root maintain their size and after the kink are span morphing. The part of the flaps that stays the same size is composed of a thermoplastic CFRP using PPS as matrix. The morphing flaps and ailerons use the same materials as the morphing skin as described in Section 14.3.2. For the flap tracks the 7075-T6 aluminium alloy is used because of its high mechanical properties and good stress corrosion cracking resistance. CFRPs are not desired in this application.

14.6. Empennage

Similar to the fuselage and non-morphing part of the wing, the horizontal and vertical stabiliser, elevators and rudder are completely composed of thermoplastic CFRP with a PPS matrix.

14.7. Sustainability

To meet the requirement of at least 80% of recyclable parts used for the morphing sections (REQ-CON-SUST-2), only reusable materials are used for the morphing wing section. In fact, the only part of the new aircraft not easily recyclable is the cockpit section of the fuselage. Therefore the recyclability of the morphing sections is close to 100%. However, due to production, there also have to be connections between the morphing components. For example, the skin and the honeycomb are attached by means of adhesives. These do not have good recylability. Also the actuators for extending and retracting the wing will not be completely recyclable. Still, because the morphing components themselves make up most of the morphing systems, it can confidently be determined that the recyclability of the morphing systems will be greater than 80%.

[5]`https://www.redwoodplastics.com/brochures/uhmw-engineering-data.pdf` [cited 22 June 2015]

15
Risk and RAMS

Section 15.1 describes the risk assessment of the systems present in the Cessna Morphlight. Section 15.2 evaluates the Reliability, Availability, Maintainability and Safety (RAMS).

15.1. Risk

Section 15.1.1 gives an overview of the technical risks of the systems of the Cessna Morphlight. These risks are shown graphically in a risk map in Section 15.1.2.

15.1.1. Technical Risk of Design Options

This section describes the technical risk associated to the design options of the Morphlight.

1. **Hybrid engine**
   A hybrid engine has more parts than a normal engine, which causes a higher risk. An engine failure means that the mission needs to be aborted. The aircraft is able to land without an engine, thus the consequence is critical. Hybrid engines have been used in existing aircraft, which means that the probability of the combination in the Morphlight can be extrapolated from existing flight design.
2. **Retractable landing gear**
   Moving parts such as a retractable landing gear have a higher risk than the fixed gear. The associated risk is marginal due to the possibility to extend the gear manually and a failure to retract will only influence the mission. If the gear mechanism would get stuck, the aircraft would still be able to land without its landing gear extended, albeit with subsequent damage. Since the stall speed is very low, the probability of landing safely in such an event is relatively high.
3. **High lift devices**
   Without the proper operation of the high lift devices, the aircraft can continue to fly, but will not be able to fulfil its mission. Therefore the consequence of a failure of the HLDs is classified as marginal. HLDs are however used extensively on current aircraft, which makes it a proven flight design.
4. **Telescopic wing box extension**
   The wing box is extended using an actuator. The actuator design is fail-safe, which means that if multiple components fail the wings will simply stop in the current position. If this occurs, the aircraft can still fly, land, and manoeuvre with the wings in any position. Thus an actuator failure has marginal consequence. A small scale model of an aircraft with a wing box extension has been tested in a wind tunnel [55], which makes it a working laboratory model.
5. **Skin**
   The zero Poisson skin and the honeycomb structure have not been used before. The skin has been tested in a wind tunnel [53], which makes it a working laboratory model. The consequence of a failure in the skin is critical, since the aircraft has to land as soon as possible. The material of the skin will not fail completely if there is a small crack in the skin, since the material is connected to the honeycomb structure at several locations.

6. **Electrical system**
   When the engine does not provide electrical energy, the fly-by-wire system fails. The ailerons are actuated using fly-by-wire, so the manoeuvrability is decreased in case of a failure. However, the rudder and elevator are not electrically actuated, which means the aircraft still can manoeuvre. Furthermore, the navigation panel, the lights and morphing systems use electric power. The pitot heater is also electric. A failure here will cause faulty airspeed and pressure readings. Combining all consequences of an electric system failure, the aircraft has to land as soon as possible.
7. **Fuel system**
   A fuel system failure has large consequences, since the engine will not provided with fuel anymore. Therefore, the aircraft has to land as soon as possible.
8. **Environmental control system**
   A failure of the environmental control system has no consequences during flight. The aircraft can continue to fly without problems. When landed, the system should be repaired, since the carbon monoxide detection system warns the pilots when there is not enough oxygen in the aircraft.
9. **Hydraulic system**
   The hydraulic system only consists of the brakes and the landing gear. A failure in the hydraulic system may cause the landing gear not to retract, but the landing gear can still extend, since it has a manual backup. The hydraulic brakes do not use any hydraulic pumps, only hydraulic fluid, thus the chance of failure is small. The consequence of a failure is that braking becomes impossible, thus the landing distance is increased enormously. Combining these effects, the consequence of a hydraulic system failure is critical.

15.1.2. Technical Risk Map

Figure 15.1 provides an overview of the technical risks with associated probability and consequences. It can be seen that the zero Poisson skin (option 5) has the highest level of risk. This is to be expected, since morphing concepts are still relatively experimental in their nature. Not many aircraft have been produced using multiple morphing concepts at the same time. However, the increase in performance enabled by morphing is such that the additional risk is considered acceptable. When further research on the zero Poisson skin and honeycomb is performed, the feasibility of this concept can be determined with greater accuracy, also reducing the associated risk.

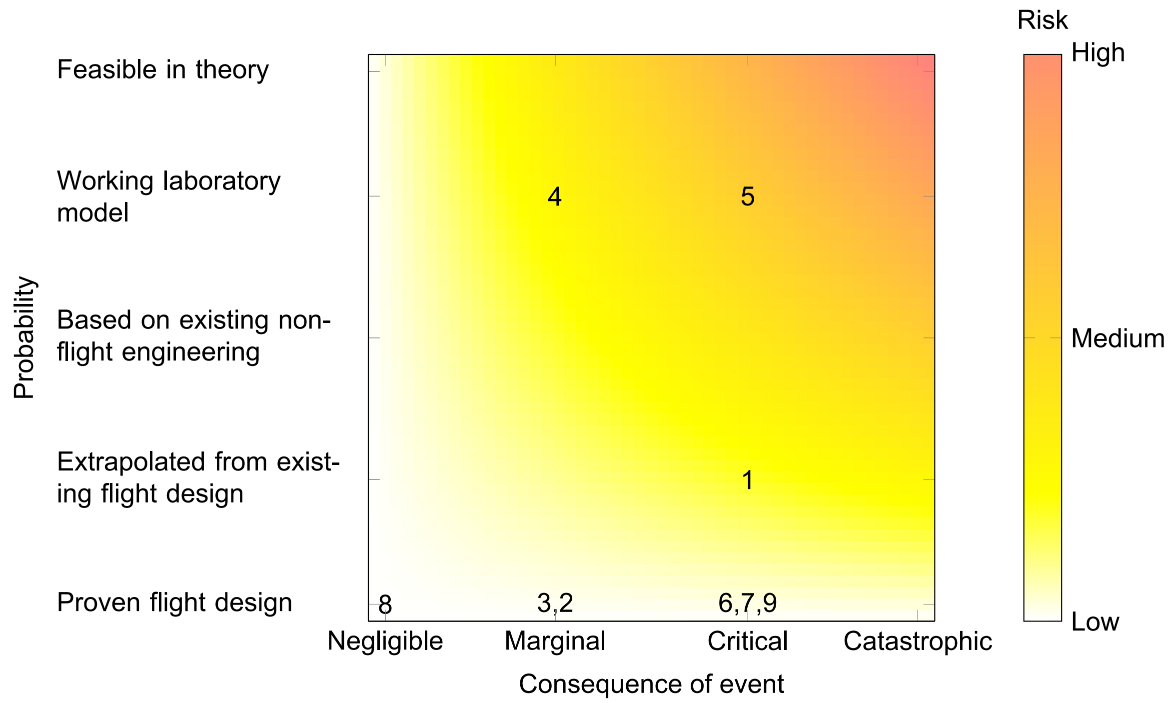

Figure 15.1: Technical risk map. Numbers refer to the list below. The consequences are defined in Table 15.1.

Table 15.1: Definitions of event consequences for risk assessment

Consequence	Definition
Negligible	Inconvenient, but can continue flying. Mission is still within reach
Marginal	Not able to fulfil mission, but can continue flying
Critical	Has to land as soon as possible
Catastrophic	Unable to continue flying

15.2. Reliability, Availability, Maintainability and Safety

In this section the Morphlight design is evaluated upon the Reliability, Availability, Maintainability and Safety (RAMS) criteria. Compared to the Skyhawk, the Morphlight features several new technologies. Therefore, to ensure the new aircraft has the same RAMS characteristics as the original aircraft these new subsystems should be analysed. From Chapter 13 it can be seen that the most significant difference lies in the fact that the the largest part of the wing will be made of a honeycomb core with a zero Poisson material as skin. Furthermore the aircraft body and some parts of the wing consist of composite materials. The engine is assisted by an electric motor. Finally chord morphing is realised by using a Fowler flap at the trailing edge.

15.2.1. Reliability and Availability

Availability is defined as the percentage, typically measured in days per year, when the aircraft is ready to fly. Time spent in the workshop either for scheduled maintenance or for an unexpected event that requires special attention, decreases the aircraft's availability. The availability of an aircraft is very much dependent on the reliability. Outside scheduled maintenance all other maintenance or replacements causing a decrease in availability can be related to the reliability of the aircraft.

Reliability is a measure for the ability of the aircraft probability of failure. An industry standard for reliability is 98%, with airframe parts like the wing and fuselage being closer to 100%, as they are crucial for safety [56].

The reliability strongly correlates to the amount of different subsystems on board and how susceptible they are to failure. Since the aircraft features many new technologies they will have to be evaluated upon their reliability. First of all the Fowler flaps are very common in aircraft and therefore are considered to be relatively insensitive to failure. Furthermore since the original aircraft also uses flaps, the reliability will not be affected. Concerning the honeycomb structure and zero Poisson skin, the reliability can only be assumed since this has not yet been demonstrated in a flying model. However, the use of a honeycomb core has been experimentally tested and proved to be suitable for aircraft applications [53]. Considering fatigue characteristics the structure is appropriate as well. To maximise the reliability the honeycomb should be designed to cover the entire lifetime of the aircraft.

To asses the number of cycles that the structural parts of the aircraft need to be designed for, the number of cycles of current aircraft can be investigated (Table 15.2). The average number of landings is higher than the average flight time. Therefore, the average duration of a flight is less than 60 minutes. This can be partly explained by the fact that training flights may perform multiple landings in a row to practice. Based on these historic statistics and including an uncertainty margin, the number of flights per aircraft per year is estimated at 200. Over the lifetime of the aircraft of 40 years, this yields a total of 8,000 cycles. The morphing parts of the aircraft are extended on takeoff, retracted during climb, extended for the landing and retracted again to store the aircraft. These two cycles per flight add up to 16,000 cycles over the lifetime of the Morphlight.

As the maintenance intervals are kept the same, as stipulated by the requirements, the availability only depends on the length of the maintenance services and unforeseen repairs. The ease of maintenance is proportional to the number of access holes. More holes generally corresponds to faster maintenance and thus an increased availability. The location of the maintenance holes however should be chosen appropriately. This is further discussed in Section 15.2.2.

The application of relatively novel materials and techniques requires special skills of the maintenance

Table 15.2: Average annual flight cycles and flight time per fixed wing single engine aircraft.

	Australia [57]	**USA** [4]			
	2012	2000	2010	2012	2013
Number of landings	179	198	143	124	130
Flight time [h]	113	126	87	89	86

personnel. During a transition period, until those novelties become more common, the availability of personnel may be limited. This can have an adverse effect on the availability of the aircraft, since the aircraft may need to be ferried to a remote airport with special facilities and the number of people available to do the work may result in queues.

15.2.2. Maintainability

For maintenance, some parts in the wing need to be accessible. Electrical wiring and control cables require checking and may require replacement. For the control system, pulleys need to be greased every now and then and checked for proper routing, condition and security. Furthermore the fuel system should be checked every 1000 hours. Therefore also this section needs to be accessible.

In conventional aircraft where no morphing is applied the access holes are covered by detachable plates in the skin. This way they can be removed easily during maintenance without requiring additional structural reinforcements. Since the Morphlight's skin is mostly made of zero Poisson material it is not favourable to detach a part of a plate. Therefore to still account for accessibility, at the end of the second wing box there is a small section on which non-morphing composite skin is placed. This plate can be removed after which a small part of the internal structure can be reached. The honeycomb structure can be split in two parts by removing bolts at this location. This allows the skin and honeycomb structure to be slid aside after which the motor for span morphing can be accessed. For thorough maintenance the entire morphing section can be removed by unbolting the honeycomb structure from the non-morphing section. The location of this maintenance access panel is shown in Figure 15.2.

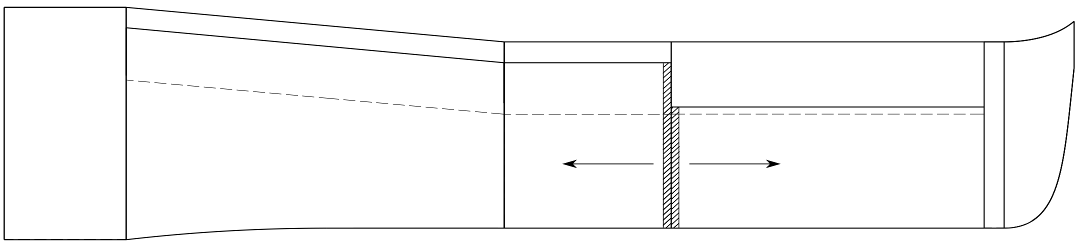

Figure 15.2: Maintenance access area in the morphing part of the wing

Another advantage of dividing the morphing sections of the wing by a non morphing section is that in case of damage less skin has to be replaced. This makes it more convenient and will reduce the cost of replacement.

Moreover, there are several items on the wing that do not morph, thus not requiring a stretchable skin at their location. On the section closest to the root there is a hole to fill the fuel tanks. Further towards the tip of the wing, the strut is attached to the lower side of the wing and a landing light is placed in the leading edge. The wing tips house a navigation light and an anti-collision strobe light. At these sections it is therefore advantageous for maintainability purposes to not have a zero Poisson skin but use a non morphing material instead. Therefore it is aimed for to place these items on the non morphing strokes.

It is desirable to place the access holes at the same span locations as those items, to minimise the number of needed composite sections. Cables can be inspected by putting small bore cameras through these holes, reducing the number of holes required.

The use of composites for the main structure of the fuselage will not bring many additional maintenance issues. By splitting the fuselage section up into three main sections: nose, cockpit and tail, these sections remain accessible. Furthermore the root section of the wing is made out of composite as well to be able to access the fuel tanks. A disadvantage of using composites however is that it is harder to detect damages. Since composites do not dent but delaminate, the surface remains smooth when damaged. Damage is therefore easier to miss during a regular inspection. Non Destructive Test (NDT) methods are required to detect damage. Once damage is detected, it may be harder to fix than conventional materials like aluminium. Nevertheless, there are techniques available that allow bolted repairs, similar to those commonly found on metal aircraft, while also requiring similar tools and skills[1].

Concerning the maintenance expenses however composites prove to have lower cost than comparable aircraft made out of aluminium. As an example, Boeing claims their 787's airframe maintenance cost to be 30% below that of comparable aircraft[1]. This is because composites bring a lower risk on corrosion and fatigue than metals, resulting in reduced scheduled maintenance cost.

Expected Maintenance Tasks

According to [40] the expected maintenance tasks and intervals related to the engine, tail and wings are as follows. The horizontal and vertical stabilisers are checked every 100 hours. Therefore, it can be assumed the morphing systems should also be checked in the same interval.

- Daily
  - Cleaning of fuel vent
  - Cleaning of pitot tubes
  - Oil check
- Every 25 hours
  - Check hydraulic landing gear system pressure
- Every 100 hours
  - Morphing systems – Check condition, security, operation, actuators.
  - Zero Poisson's structure – Check for damage of skin.
  - Horizontal and vertical stabiliser internals.
  - Elevator Trim System – Check cables, push-pull rods, bellcranks, pulleys, turnbuckles, fairleads, rub strips, etc. for proper routing, condition, and security.
- Every 200 hours
  - Ailerons and Cables – Check cables for tension, routing, fraying, corrosion, and turnbuckle safety.
  - Inspect pulleys, cables, sprockets, bearings, chains, bungees, and turnbuckles for condition and security.
  - Wing Structure – Inspect spars, ribs, skins, and stringers for cracks, wrinkles, loose rivets, corrosion, or other damage.
  - Flaps and Cables – Check cables for proper tension. routing, fraying, corrosion, and turnbuckle safety.
  - Trim Controls and Indicators – Check pulleys, cables, sprockets, bearings, chains, bungees, and turnbuckles for condition and security.
  - General Airplane and System Wiring – Inspect for proper routing, chafing, broken or loose terminals, general condition, broken or inadequate clamps, and sharp bends in wiring.
- Every 1000 hours
  - Fuel Tanks or Integral Fuel Bays – Drain fuel and check tank interior and outlet screens.

15.2.3. Safety

Safety is defined as the number of accidents due to functional failures of the aircraft. By far the largest share (85%) of the accidents involving a C172 can be attributed to pilot error[2], mostly due to pilots feeling overconfident. For the C172, less than 7% of the accidents can be attributed to the aircraft[2]. The occurrence of such accidents should at least stay the same for the Morphlight, but preferably be decreased by improving the design of the aircraft. The same holds for the sensitivity of the system to

[1] http://www.boeing.com/commercial/aeromagazine/articles/2014_q4/pdf/AERO_2014q4.pdf [cited 2 June 2015]

[2] http://www.aopa.org/News-and-Video/All-News/1995/December/1/Cessna-172-Safety-Review [cited 7 May 2015]

pilot errors.

The current Skyhawk engine is responsible for 38% of the mechanical accidents[2]. Improving the engine will significantly improve the safety of the complete aircraft. However, with the new engine which combines conventional power with electrical power the propulsion system will be even more prone to failures. This reduces the reliability. On the other hand, since the systems to be integrated will be several decades newer from a technology point of view, the reliability will be assumed to be of higher level. Another positive aspect of the combination of the two engines is that in case of a failure of the conventional system, the electric system can still provide some level of power. This may not be sufficient to keep flying, but it can extend the glide ratio, providing valuable time for the pilot to find a spot to land.

In terms of redundancy, the Morphlight has two flaps instead of one. When one of the flaps fails, the landing/take-off speed and length will be larger, but smaller than in the case of a total flap failure. Another redundancy option is to asymmetrically extend (one of) the flaps as a backup for aileron control. Differential span extensions serve as another backup option. This does require coupling between the directional controls and the flaps. With fly-by-wire (FBW), this can be relatively simple. As mentioned in Section 12.2, the ailerons will make use of FBW. This has the added advantage that the forces and deflection exerted by the pilot can be similar regardless the level of morphing. If the electrical aileron control fails, still the rudder can be used as a means of roll control.

The elevator and rudder controls do not make use of fly-by-wire. Since the tail does not morph, cable controls can be maintained. Cable controls provide a direct link between the cockpit and the control surfaces, and provide the highest level of safety. There is no redundancy in the cables in the Skyhawk. However, since these are checked every 100 hours (Section 15.2.2), using cables is a safe solution.

The movement of the wing boxes for the span extension is done by electrical motors. There is one motor for every wing box, meaning there is no redundancy. However, there is a safety pin that keeps the wing boxes and honeycombs from moving at all times. This pin first has to be unlocked by the electrical system before the motors can extend or retract the span. This ensures there cannot be any unintended movement of the wing, either during flight or when stored on the ground. See also Section 15.1.1.

Safety of the retractable landing gear is ensured by the backup pump, with which the gear can be lowered by hand in case of a hydraulic pump failure (Section 12.5). Still, should the landing gear mechanism get stuck, it will not be possible to lower it. As the pressure in the hydraulic landing gear circuit is checked every 25 hours, the probability of a failure not being detected in time is very small.

The use of composites in the aircraft comes with a potential safety issue. Composites generally do not conduct electricity very well, leading to local burns in the case of lightning strikes. Laminating a wire mesh in the composite can circumvent this problem, while making it only slightly heavier.

III

Post Design

In Part II the aircraft is completely designed. The next step is to move on to the production of the aircraft. For this a plan is developed in Chapter 16. The planning for this stage of the project is described in Chapter 17. Finally, the design is analysed in terms of weight, cost, and investment value in Chapter 18.

16

Manufacturing, Assembly and Integration Plan

In this chapter the manufacturing, assembly and integration plan for the Cessna Morphlight is documented. The description is limited to the structures and components different than that of the Cessna 172 Skyhawk. Many parts have changed significantly compared to those in the original aircraft and thus a detailed explanation is provided.

16.1. Fuselage

As mentioned in Section 14.1 the fuselage is divided in five sections. This is done for multiple reasons. From a production point of view it is easier to produce multiple small parts than an entire fuselage at once. It also enables the option to use different materials for different sections, which is desired in this case. The division of the fuselage sections is shown in Figure 16.1. In this figure also the doors are visualised.

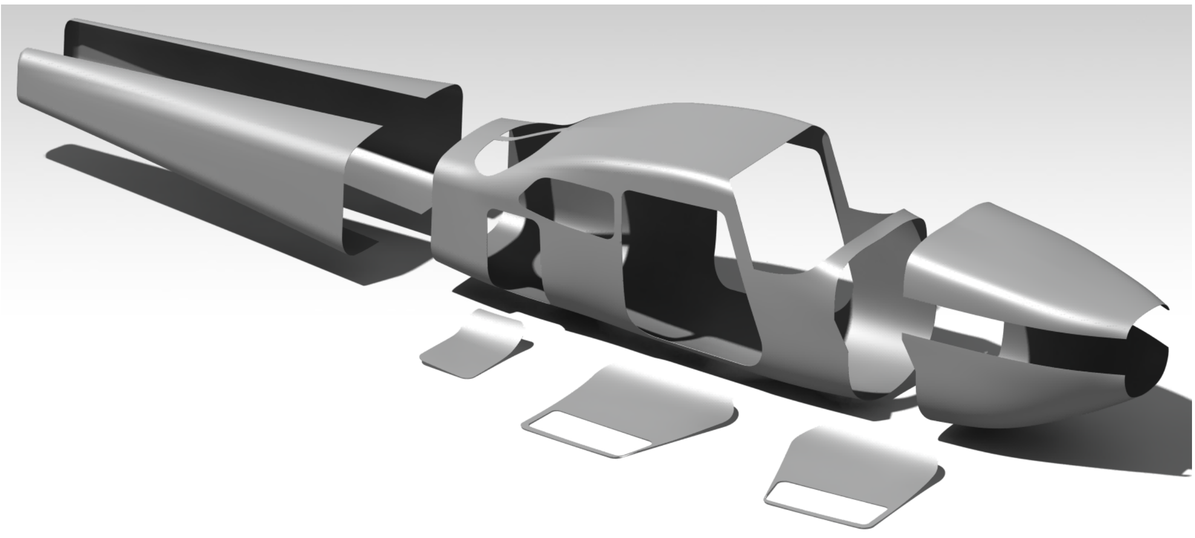

Figure 16.1: Division of the fuselage in the production process.

The nose skin is split into two parts, a top and a bottom section, which is also the case for the Cessna 172 Skyhawk. Dividing the nose allows good accessibility of the engine. The two sections are produced using a thermoset CFRP. The curvature of the skin perfectly allows for the use of prepreg in a female mould. The bottom skin overlaps the top skin with 2 cm and in the overlapping region countersunk bolts are used to fasten the sections.

Due to the complex shape of the cockpit section it will be produced using thermoset CFRP prepreg. The nose parts are connected to the cockpit using countersunk bolts. Small brackets are extending from the cockpit on the inside of the nose section to which the bolts are connected. This is very similar to the design in the Cessna 172 Skyhawk.

The tail skin is divided into two parts, a right and a left half. The halves, as well as the door, are produced using thermoforming using a thermoplastic CFRP with PPS resin. The process of thermoforming consists of three steps. PPS pellets are converted into films with a thickness of 50 to 200 μm, after which carbon fibre fabric is bonded with the PPS films. At this point a laminate is created. The next step is to press the laminate into a mould at a temperature of 285°C [50]. The laminates are bought directly at a supplier and are not produced in-house. The halves are produced such that one of the halves overlaps the other and the parts can be permanently connected using resistance welding. For resistance welding a metal grid strip is placed between the parts to be bonded and pressure is applied on the two parts. By placing electricity on the metal grid the CFRP parts melt together. This is a low-cost methods to join continuous CFRP parts [49].

The two passenger doors and cargo door are produced by thermoforming pre-consolidated thermoplastic CFRP sheets with a PPS resin. The shape of the doors are perfectly suitable for this manufacturing process.

The stiffeners in the fuselage are formed using semi-prepreg thermoplastic CFRP with PEKK resin. The stiffeners are assembled using the butt-joint principle patented by Fokker Aerostructures [49]. A laminate is cut into flat pre-forms which are used for the horizontal and vertical part of the stiffener. The flat forms are fixed together using injection-molded short fibre carbon-reinforced PEKK granulate[1]. PEKK is used because this resin is used for the tests at Fokker Aerostructures. The butt joint is approximately ten times stronger than previous welded joints and the weight reduction is 8-10%[2]. The stiffeners are co-consolidated with the fuselage sections, meaning the stiffeners will be cured in the autoclave together with the skin structure. Skipping the step of stamping and trimming the stiffener parts reduces costs.

Access panels are placed on important places on the fuselage for maintenance. The panels are connected using countersunk stainless steel bolts.

16.2. Wing Skin

The wing skin can be divided into two categories, non-morphing and morphing skin. The first is a regular wing skin and the second consists of an internal honeycomb structure and an elastic matrix composite (EMC) on the outside.

16.2.1. Non-Morphing Skin

The non-morphing wing skin is formed with thermoplastic CFRP with PPS resin. Pre-consolidated sheets are thermoformed into the final shape, as explained in Section 16.1. The non-morphing skin is divided in two parts, a top and a bottom plate. This allows for removing the panels for maintenance of the inside of the wing. An access panel is placed near the motor used for extending the wing box for easy maintenance.

16.2.2. Morphing Skin

The material choices for the morphing skin are described in Section 14.3.2. In this section the production and assembly plan are given.

[1] `http://www.compositesworld.com/articles/reinforced-thermoplastics-in-aircraft-primary-structure` [cited 15 June 2015]

[2] `http://www.compositesworld.com/articles/thermoplastic-composites-primary-structure` [cited 15 June 2015]

Honeycomb Structure

As described the honeycomb structure is divided into two components, airfoil shaped rib structures and V-shaped spring parts. The rib structures are produced by injection moulding of short fibre thermoplastic CFRP. Because the wing planform is chosen to be rectangular in the morphing region, only three moulds are needed, for the wing, Fowler flap and aileron. This saves significantly on investment costs, because a single mould costs approximately €20,000[3]. The V-shaped structures are produced in high numbers and all parts are the same. A company specialised in such parts is XPERION components, part of the AVANCO group[4]. Long fibres are used for the composite. A pre-consolidated sheet is thermoformed into the required shape after which it is cut into parts of the correct size.

The rib parts are produced with small bumps on the locations where the V-shaped components will be attached. The V-shaped parts are clamped on the rib-shaped component and bonded together using ultrasonic welding. The small bumps melt and the resin of the parts blend together. This process can be done at high speed using a dedicated robot. After connecting the components the V-shaped parts require trimming so the honeycomb structure follows the airfoil shape correctly.

Elastic Matrix Composite

The EMC is produced using the method as described in [48]. The skin is manufactured in a lay-up, making the skin thicker which each layer. First the polyurethane elastomer is stretched until it is of the correct thickness, after which unidirectional carbon fibres are placed on top of the first layer. Liquid elastomer is then spread out over the fibres and is then cured. After the second layer is cured a third layer is added, which is done by spreading out liquid elastomer until the desired thickness of the skin is reached. Similar to the second layer, the third layer has to be cured for several hours. When the lay-up is complete, excess material is removed and the skin is checked for flaws. The cross-section of the skin should be of the same thickness everywhere, no air bubbles should be present and there should be no visible flaws.

When the skin is finished it is glued on the honeycomb structure using while the honeycomb structure is in retracted (relaxed) state. After correspondence with a sales engineer at Henkel[5], specialised in adhesives, it has become clear that for this application a variety of glues can be used. The exact type has to be determined in further design, since it is dependant on many parameters. Glue is only applied on the rib-shaped components so no rotational forces are applied on the skin. Because the morphing planform is rectangular, the skin sheets used also have a rectangular shape. The end points of the skin are located at the trailing edge on the top side of the airfoil. For the Fowler flaps and the aileron the trailing edge is used as well. At these locations the air flow is likely to produce the least peeling force on the EMC.

Because it is important to be able to access the internal structure of the morphing section, because, among other reasons, the motor used for span extending needs to be investigated, the skin can be slid to the side at a number of locations. This is done using bolting connection between some of the rib shaped structures.

16.3. Internal Wing Structure

Inside the wing three structural components can be recognised: wing boxes, stiffeners and ribs. Because the stiffeners are attached to the wing boxes they are included in the section on wing boxes.

16.3.1. Wing boxes

The boxes are produced using thermoplastic CFRP prepreg using PPS resin. PPS is used instead of PEKK, because this same resin is used for the AgustaWestland AW169 horizontal tailplane torsion

[3]Arnt Offringa, Director of R&D, Fokker Aerostructures. Personal Interview. 8 June 2015.

[4]`http://www.avanco.de/products/tubes-profiles-and-laminates/composite-profiles-thermoplastic.html` [cited 15 June 2015]

[5]`http://www.henkel.nl/index.htm`

box. For the AW169 a "stepped, box-like forming tool is used which accommodates skin ply drop-offs"[6], which is perfectly applicable for the production of the Cessna Morphlight wing boxes. This is because the wing box closest to the fuselage has skin ply drop-offs on the outside and the wing box closest to the tip has skin ply drop-offs on the inside. Using this method the boxes are produced out of a single part, which provides for the best possible structural characteristics.

As described in Section 14.4 UHMW-PE (ultra-high-molecular-weight polyethylene) is used so the wing boxes can slide over each other with low friction and wear as a result. This material is applied as a coating on the boxes.

16.3.2. Ribs

The ribs are produced by cutting, for example water jet cutting, and press forming a pre-consolidated sheet of thermoplastic CFRP. This process is very similar to the procedure for press forming of sheet metal. The sheet is first cut into a desired shape after which it is heated, pressed into the final shape and cooled again. After this non-destructive testing is performed and the rib is trimmed if necessary. Press forming of the ribs saves 50% of the cost compared to traditional hand lay-up [49]. In the non-morphing region the ribs are connected to the skin by using counter-sunk bolts. Welding is a good option as well, but this is not possible because it is desired to be able to remove the skin for maintenance reasons. The ribs are are connected to the morphing honeycomb structure using resistance welding.

16.4. Flaps and Ailerons

The non-morphing flaps are produced by thermofolding a pre-consolidated sheet of thermoplastic CFRP. This procedure is very similar to thermoforming, however, only the line at which the material is bent is heated. The sheet is folded from the front side around the ribs inside the flap and is connected using resistance welding. The same procedure is used for the leading edge of the Airbus A380 main wing.

The morphing flaps and ailerons are produced in the same way as the morphing wing. The flap fairing is produced by CNC lathing of a 7075-T6 aluminium sheet and is connected to the ribs and honeycomb structure of the flap using bolts.

16.5. Empennage

The horizontal and vertical stabiliser, elevators and rudder are not investigated in depth structurally in this report. The horizontal and vertical stabiliser are produced using a multi-spar system, as described in Section 13.10. An omega-shaped structure is placed inside the torsion box after which the components are co-consolidated. The ribs are welded to the torsion box after which a thermofolded leading edge is welded to the ribs. No trailing edge is added, as done fore the AgustaWestland AW169, because at this location the elevators and rudder are located.

The elevators and rudder are built using a multi-rib system, as explained in Section 13.10. A thermoplastic CFRP skin is thermofolded around the ribs and the components are resistance welded together.

[6] `http://www.ptonline.com/articles/thermoplastic-composites-save-weight-in-rotorcraft-aerostructure` [cited 15 June 2015]

17

Operations and Logistics

This chapter documents the operational phase and the research, development, and production phase of the Cessna Morphlight. The various aspects of the operational support are shown in Section 17.1. The activities of the research, development, and production stages are shown in Section 17.2.

17.1. Operational Support

A flow chart of the operational support is presented in Figure 17.1. The various items are explained below. The operations and maintenance are supported by the lower levels in the flow chart.

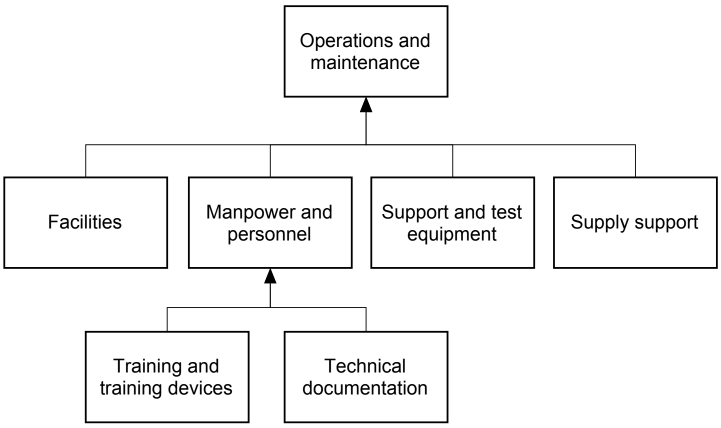

Figure 17.1: Flow chart illustrating the support for operations.

Facilities

Due to the increased wing span, a larger hangar will be needed to store the aircraft when the wing is extended. During maintenance, it may be necessary to fully extend the wing. For normal storage, the wing will most likely be retracted to save space and reduce the risk of damage.

Operations and maintenance

The operations of the Cessna Morphlight are similar to the operations of the Cessna Skyhawk, but due to the morphing concepts, the operation can be longer or be changed during flight. The maintenance planning of the Cessna Morphlight is mainly the same as the planning of the Cessna Skyhawk. The morphing concepts have to be checked more often than a normal wing, since it has moving parts. However, the frequency does not exceed once every 50 hours, not exceeding the original maintenance interval, since the maintenance frequency cannot be increased.

Manpower and personnel

The personnel executing the maintenance need to have enough knowledge about the morphing concepts of the Cessna Morphlight. Since the Cessna Morphlight is based on the Cessna

Skyhawk, it is easiest to provide retraining for mechanics of the Cessna Skyhawk.

Supply support

Spare parts for a Cessna Skyhawk are easily obtainable, since this aircraft is used a lot by private pilots. Therefore, it is important to make sure that the spare parts for morphing concepts are also available when needed. A low number of different parts will help improve the availability.

Support and test equipment

The use of novel materials may introduce the need for special tooling that is not (yet) part of the default kit of a mechanic. With the recent developments and more common use of composite materials, the mechanic will need to have the tools in order to work on more recent aircraft.

Technical documentation

The operating manual is mostly similar to the current one, except for the morphing system descriptions. The maintenance manual might require some extra chapters on the novel materials and techniques used, as most mechanics will not have encountered them during their training. The parts list will be updated with the new parts added for the morphing system.

Training and training devices

Since the morphing concepts are new to most mechanics and pilots, retraining is needed. Pilots are trained either in a special simulator, which can simulate morphing concepts, or during a training flight with a flight instructor teaching the pilot how to operate the morphing aircraft.

17.2. Post-DSE Planning

The project design and development logic in Figure 17.2 shows the activities to be executed in the post-DSE phase. The activities can be categorised in research and development, testing, production and marketing. Several activities can be executed in parallel. For example, the research of morphing concepts and the market analysis can be performed at the same time.

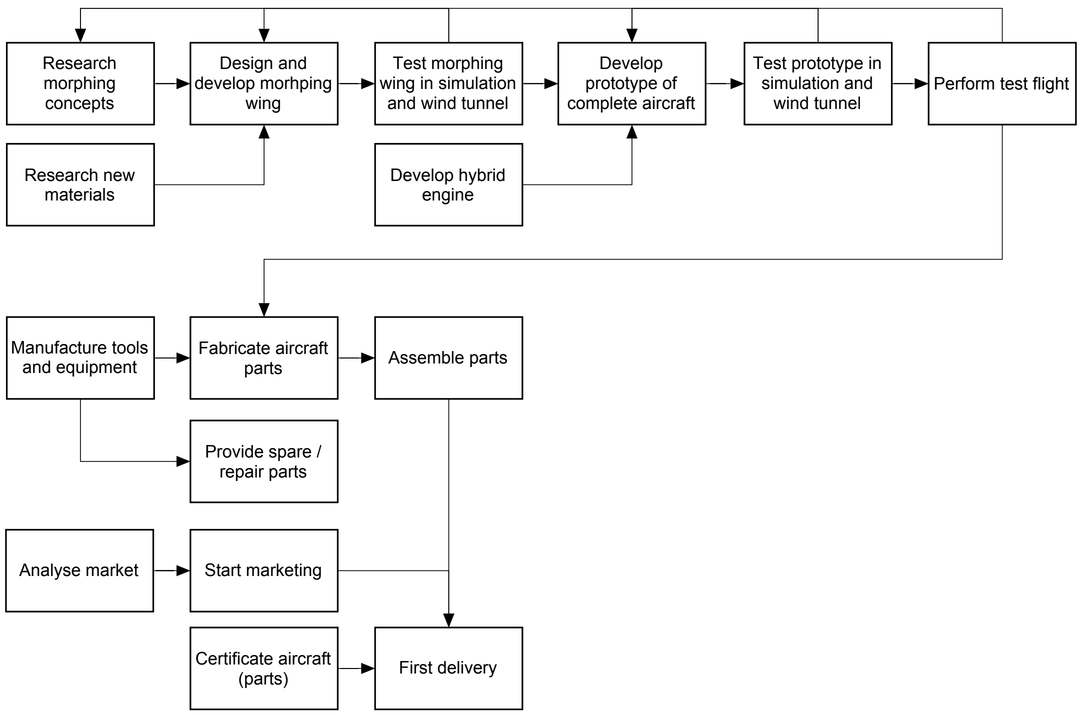

Figure 17.2: Project design and development logic

Figure 17.3 shows the Gantt chart of the activities to be executed after the DSE. The activities are planned over a period of five years, since this is usually the time needed to develop a new aircraft [58]. At the “Go-ahead”-point, which is normally reached after two years, it is decided to actually start developing the aircraft and start certification [58]. Research, development and testing are interrelated processes, which means that they are executed in the same time frame. Since it is beneficial to receive orders before the first delivery, marketing starts early in the design process.

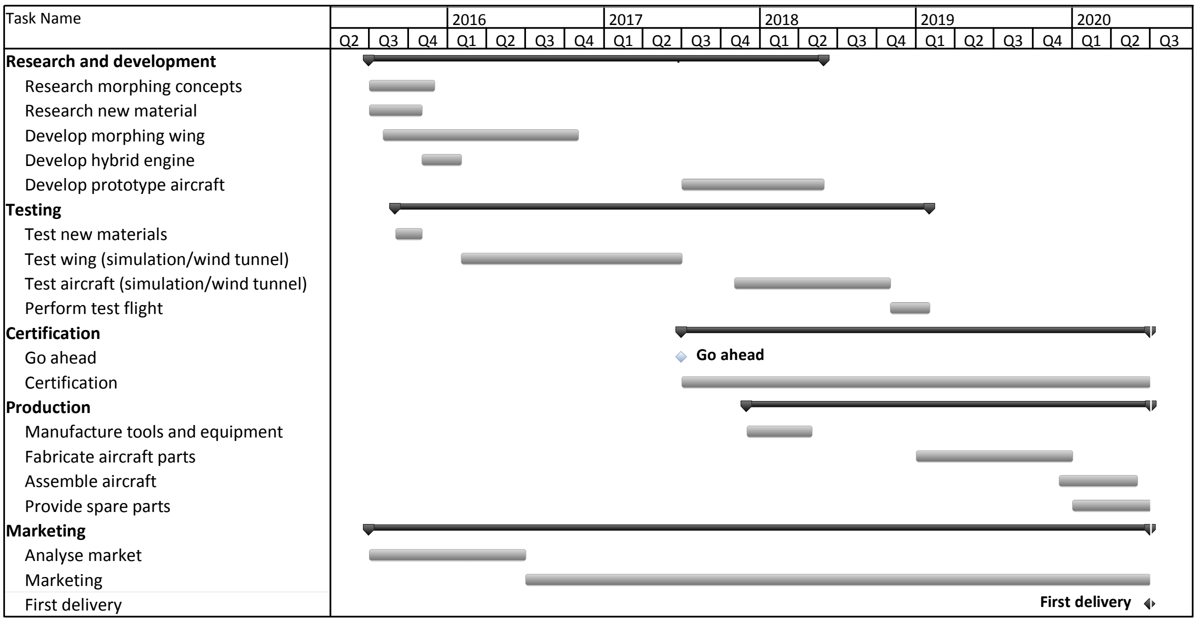

Figure 17.3: Post DSE Gantt chart

18

Weight, Cost and Return on Investment

From the complete detailed design, a good estimate for the final costs and weights can be derived. These are discussed in this chapter. Section 18.1 starts with the breakdown of the weights of the various components. The costs of these components is discussed in Section 18.2. With the finalised costs, the return on investment is determined in Section 18.4.

18.1. Weight Budget

The empty weight of the Morphlight can be divided into a structural group and a subsystems group. Since the Morphlight is designed with the Cessna Skyhawk as a reference aircraft the weight decomposition is based on this aircraft as well. To start with the subsystems, it can be assumed that most of them stay the same as those of the Skyhawk. Therefore the information manual is used to find these weights [21]. Data for the structural components consisting of the fuselage, wing, tail and landing gear could not be found for the Skyhawk, however for the 172B this data was available [20, p. 279]. The 172B is a predecessor of the Skyhawk and has a lower empty weight. A large share of this weight increase can be attributed to an update to FAR Part 23 in 1968, to increase occupant safety. The Cessna 172B was conceived in 1960, whereas the 172S was introduced in 1998. Aircraft designed under to new regulations have a significantly higher empty weight, ranging from 3% to 12% on retractable gear single engine piston aircraft [59]. To estimate the structural weight of the components of the Skyhawk the remaining empty weight of the 172S is distributed over the structural groups (fuselage, landing gear, tail and wing) with the same distribution as the 172B.

A large part of the aircraft's empty weight consists of operational equipment and subsystems. The weight of these components was determined from the Skyhawk Information Manual [21]. It is assumed that the weight of most of these components will remain the same. However since an electrical engine, consisting of a battery and alternator, is incorporated, these two components are disregarded from the electrical system.

The new engine consists of a conventional piston engine assisted by an electrical support engine and battery, of which the corresponding weights are 134, 14 and 11 kg respectively.

Furthermore, from an interview at Fokker Aerostructures it was estimated that a 30% reduction in weight can be realised when using thermoplastic composites instead of aluminium [1]. This can be justified by looking at the specific material densities of the composite versus aluminium as can be seen in Table 18.1. This reduction factor can be applied to the fuselage and the tail section since these will both be constructed from composites. The weight of the main wing consists of the wing box, strut, flaps, honeycomb and zero Poisson skin. The weight of the wing box follows directly from the optimisation program from Chapter 11 which adds up to 77.7 kg in total. Since the honeycomb is made from carbon fibre, the density of the honeycomb core is 1,610 kg/m^3. Multiplied by the total required volume as

[1] Arnt Offringa, Director of R&D, Fokker Aerostructures. Personal Interview. 8 June 2015.

derived from from the CATIA model, the total honeycomb weight is found to be 46 kg. This includes the honeycomb integrated in the flaps. Finally, the weight of the zero Poisson skin is estimated from the wetted surface area of the zero Poisson covered wing section multiplied by the specific density of the epoxy as in Table 18.1. The combined result is 12.7 kg.

Table 18.1: Density of materials used in the Morphlight

Material	**Density [kg/m^3]**
Aluminium	2,712
Carbon fibre	1,610
Epoxy	1,200
Honeycomb	1,610

The weight of the morphing systems consists of the actuators and motors for the morphing concepts. These include electric motors combined with a rack-and pinion system, serving the extension of the span and actuators for the extension of the flaps. These components are estimated to account for 25 kg in total.

By making the landing gear mechanism retractable, additional weight has to be considered. According to the Cessna method using a retractable landing gear, adds a factor of 1.4% of the MTOW to the original fixed gear weight [13]. With a maximum take-off weight of 1,272 kg this results in an extra 18 kg which is assumed to be reasonable. The landing gear on the Cessna 172RG is hydraulically actuated, so this weight is a part of the additional 18 kg. This weight is included in Table 18.2 under the landing gear.

Finally by analysing the component weights of the Skyhawk it can be observed that the weight of the furnishings is significant. Considering the requirement of 750 kg empty weight it was therefore investigated whether this weight, consisting mainly of the front and back seats, could be reduced. The seats of the Cessna 182Q were found to be much lighter at 23 lbs each [60], which brings the total empty weight under the required 750 kg. An overview of the aircraft with all component weight can be seen in Table 18.2, where the wing weight is a sum of wing box, strut, flaps, honeycomb and skin.

Table 18.2: Weight budgets for the Cessna 172S and Morphlight in [kg].

Component	**172S**	**Morphlight**
Wing	131	136
Fuselage	158	110
Engine	145	159
Engine items	21	21
Landing gear	68	85
Tail	34	26
Propeller	18	19
Air conditioning	28	28
Avionics	29	29
Electrical system	21	17
Flight controls	21	21
Fuel system	10	10
Furnishings	59	25
Hydraulic system	1	1
Morphing systems	0	25
Empty weight	744	712

18.2. Cost Budget

The cost of the Cessna Morphlight is estimated based on the DAPCA IV cost model [58]. However, this model makes use of data from the US Department of Defense and is less suited for predicting the cost for general aviation (GA) aircraft. In fact, the costs of a GA aircraft program are overestimated using this model. A modification to the DAPCA model was developed in [61] to better estimate the cost of a GA aircraft. The corrections were done such that the cost of a Cessna 172 was predicted accurately. Since the Cessna Morphlight is based on the 172, this model is used for estimating its cost.

The DAPCA model presents equations to estimate the engineering, manufacturing, material, tooling, quality control, and flight test costs. Furthermore the total cost of the aircraft contains purchased equipment such as avionics and the engine. First the equipment costs were determined and by making an inventory of all avionics and other subsystems on board and determining the approximate cost of each component. Furthermore, the landing gear structure has to be manufactured, so these costs are included in the manufacturing and material costs. Finally the interior cost was estimated by averaging offers from eBay[2] since it was not found in other references.

The cost estimates from the model are based on 1986 price and wage levels. The estimates for the required man hours are multiplied by the 'wrap rates' of 1986. This includes salaries, benefits, overhead, and administrative costs. The hourly rates in 1986 dollars are given in [34]. The final result is first converted to 2015 dollars[3] and then to euros.

The production cost depends on the number of aircraft produced. The market analysis in Chapter 4 concluded that selling about 100 to 200 aircraft per year is a reasonable estimate. The production of the latest Cessna 172 models lasted for approximately 20 years. The production span is driven by the market position, among other parameters. Given that the Cessna 172 has been a very successful aircraft over many decades, the Morphlight is also expected to be successful in its life, also because of its large increase in performance. Besides, many customers will be familiar with Cessna and the 172 model on which the Morphlight is based. The production span of 20 years is therefore also assumed for the Morphlight. At 200 aircraft sold per year, a total of 4000 aircraft will be produced.

The DAPCA model contains material and difficulty factors to account for the use of complex materials. These were set to the highest levels of the range provided in [58] because of the novel materials used for morphing and other parts of the aircraft. The difficulty factor accounts for the "very aggressive use of advanced technology" [58, p. 27]. The material correction accounts for the use of carbon composites.

The morphing concepts are expected to add a considerable amount to the production cost. The morphing concepts are relatively new and will require research before they can be implemented on the aircraft. They also use expensive materials or expensive mechanisms, which will add to the cost. For these reasons, an additional cost margin is added on top of the complete production cost of the aircraft. The main morphing components that are different from conventional aircraft and that need to be produced are the zero Poisson skin and the honeycomb structure. Because the span morphing part of the wing is straight, the same parts can be produced multiple times, and few moulds are needed (Chapter 16). This saves on manufacturing costs, as these parts can be produced on a large scale. If the zero Poisson skins are produced on a large scale, the production costs will be acceptable. The margin for morphing is therefore taken as 25%.

There will be no increase in cost by making use of thermoplastic composites. That is because the manufacturing cost of thermoplastic components is lower than aluminium components, whereas the material cost is slightly higher[4]. This could also be expected when observing the trend of using more and more composite materials in the aerospace industry nowadays. Thermosets however, which are used for the cabin, are slightly more expensive. Their decrease in weight justifies the extra cost.

The addition of a retractable landing gear adds about $7,500 to the manufacturing cost [44, 61]. However, this margin is already accounted for in the DAPCA IV model. The extra cost is justified by the higher value of retractable landing gear aircraft on the second hand market. The difference in value is approximately $20,000. Therefore, buying an aircraft with retractable gear is attractive to potential

[2] `http://www.ebay.com/` [cited 13 May 2015]
[3] `http://www.usinflationcalculator.com/` [cited 13 May 2015]
[4] Arnt Offringa, Director of R&D, Fokker Aerostructures. Personal Interview. 8 June 2015.

customers.

The intended profit margin is set at 10%. The production costs are spread over the number of aircraft sold. With more aircraft sold, the production costs per aircraft will be less, so the total cost, and therefore sale price, is reduced. At 150 aircraft sold per year for 20 years, the cost price of €375,000 would just be reached if the profit margin would be reduced to 6.5%. Therefore, it can be assumed a profit can made with the Morphlight program. The estimated cost per aircraft, with a total production run of 4,000 at 200 aircraft per year for 20 years, is shown in Table 18.3.

Table 18.3: Morphlight cost estimation based on modified DAPCA IV cost model [61] at 4,000 aircraft sold.

Cost category	**Component**	textbfCost [€]	
Purchased equipment	A/C unit	22,401	[62]
	Avionics	52,258	[62]
	Electronics	1,035	[5]
	Engine + upgrades	76,165	
	Fuel Systems	4,498	[5]
	Hydraulics	509	[5]
	Interior	6,898	
	Propeller	7,168	[6]
	Subtotal	171,177	
Production cost	Engineering	3,361	
	Flight testing	633	
	Manufacturing	76,700	
	Materials	31,627	
	Quality control	11,026	
	Tooling	4,615	
	Subtotal	127,960	
	Morphing concepts (+25%)	31,990	
Manufacturer profit		33,113	
Total		**364,240**	

18.3. Cost Breakdown Structure

The cost breakdown structure reflects the total investment cost of the research, development and production phase. Figure 18.1 shows the cost breakdown structure for the Cessna Morphlight.

The research and development consists of marketing and research and development of new technologies. First, the market analysis is performed, since it will keep the costs down if it is known exactly what the customer wants.

The cost for producing the test aircraft are included in the € 5,000,000 needed for testing. The flight test is the most expensive test.

The cost are based on a total amount of 4000 produced aircraft. Therefore, the production cost and the purchased equipment are the largest part of the total investment cost. The purchased equipment includes the engine, the avionics and other standard equipment.

[5] `http://www.capmembers.com/media/cms/Labor_and_Parts_Pricing_Guide_ACEDA6DCEAADA.xls` [cited 22 May 2015]

[6] `http://www.avweb.com/news/maint/185020-1.html` [cited 21 May 2015]

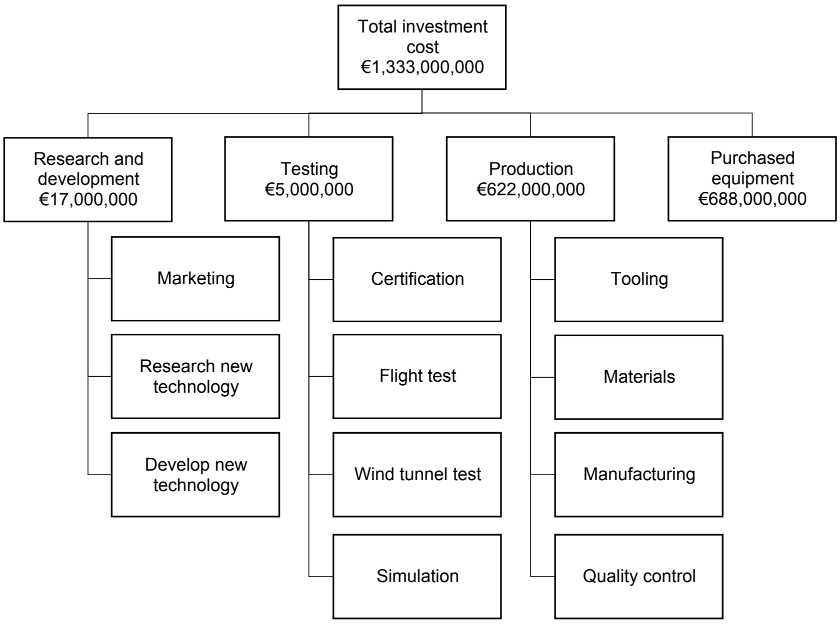

Figure 18.1: Cost breakdown structure of the research, development and production phase

18.4. Return on Investment

The return on investment (ROI) is a measure of the profitability of an investment. It serves as a metric for investors to determine whether it would be wise to invest in this company or product. The return on investment is given by Equation (18.1).

$$\text{ROI} = \frac{\text{Gain from Investment} - \text{Cost of Investment}}{\text{Cost of Investment}} \tag{18.1}$$

The ROI depends on the gain from the investment (profit) and the costs. Because they depend on the number of aircraft built and sold, the ROI varies over time. The engineering and development costs are an investment that have to be made before the first aircraft is built and sold. This period is typically about 5 years [58]. This means that there will be a negative return on investment during the initial phases of the program.

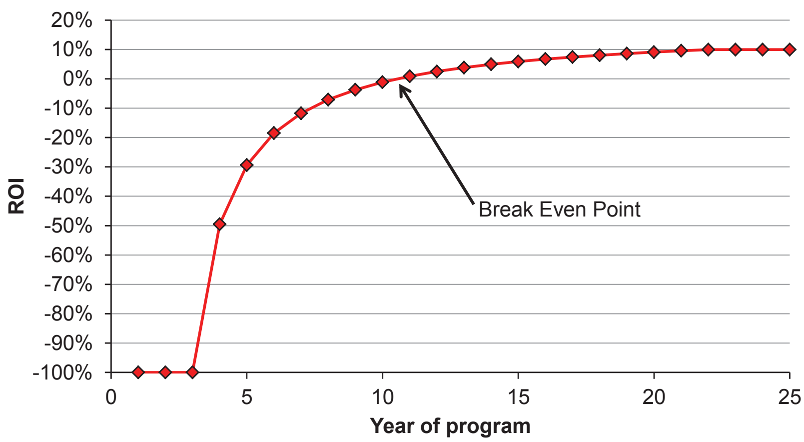

Figure 18.2: Return on investment for the Cessna Morphlight during the program

The return on investment is shown in Figure 18.2. During the first years of the program, no aircraft will be sold, so there will be no profit. This makes the ROI -100%. It can also be seen that the break-even point is at about ten years after the start of the program. At the end of the program, a ROI of 10% is achieved, which is the profit margin set in the cost estimation in Section 18.2. The investment costs include the development costs and the production costs for each aircraft. At the end of the program, 4,000 aircraft will have been produced and sold. These 4,000 aircraft at their estimated design and production cost lead to a total investment of circa €1.3 billion.

IV

Compliance and Conclusion

This part describes the compliance of the aircraft design with the requirements that were developed in Part I. It concludes the report and gives recommendations for future work.

19

Requirement Compliance Matrix

✓ Requirement exceeded • Requirement fulfilled ✗ Requirement unfulfilled

ID	Description	Final Value	
Mission requirement			
REQ-MISS-1	This project shall improve a Cessna 172S Skyhawk using existing morphing concepts found in literature, within a budget of €375,000 per aircraft, by 10 students in 11 weeks' time	-	•
Functional requirements			
Performance requirements			
REQ-FUNC-PERF-1	The aircraft shall have a landing ground roll distance of at most 120 m at standard sea level conditions in the international standard atmosphere	116 m	✓
REQ-FUNC-PERF-2	The aircraft shall have a take-off ground roll distance of at most 200 m at standard sea level conditions in the international standard atmosphere	193 m	✓
REQ-FUNC-PERF-3	The aircraft shall have a maximum range of at least 2,000 km	2,780 km	✓
REQ-FUNC-PERF-4	The aircraft shall provide an endurance time of at least 10 hours at loiter conditions	21 h	✓
REQ-FUNC-PERF-5	The aircraft shall have a cruise speed of at least 250 km/h (Amended by REQ-FUNC-MRKT-1 to 277 km/h)	250	•
REQ-FUNC-PERF-6	The aircraft shall have a cruise altitude of 2,600 m	2,600 m	•
REQ-FUNC-PERF-7	The aircraft shall have a loiter altitude of at least 2,000 m	2,000 m	•
REQ-FUNC-PERF-8	The aircraft shall have a total landing distance of at most 300 m at standard sea level conditions in the international standard atmosphere	284	✓
REQ-FUNC-PERF-9	The aircraft shall have a total take-off distance of at most 400 m at standard sea level conditions in the international standard atmosphere	336 m	✓
REQ-FUNC-PERF-10	The aircraft shall have a range no less than the reference aircraft at cruise conditions	1,790 km	✓
REQ-FUNC-PERF-11	The cruise speed shall be defined by the speed at 75% engine power	-	•
REQ-FUNC-PERF-12	The maximum range specified by REQ-FUNC-PERF-3 shall be obtained when transporting the payload described in REQ-CON-OPER-1	-	•

Market requirements			
REQ-FUNC-MRKT-1	The aircraft shall have a cruise speed of at least 277 km/h	250 km/h	✗
Safety requirements			
REQ-FUNC-SFTY-1	The aircraft shall have the same safety as the reference aircraft	-	•
Reliability requirements			
REQ-FUNC-REL-1	The aircraft shall have the same reliability as the reference aircraft	-	•
REQ-FUNC-REL-2	The morphing systems on the aircraft shall not increase the maintenance frequency	-	•

Constraints

Sustainability requirements			
REQ-CON-SUST-1	The aircraft shall consume at most 2.5 L of fuel during engine start up, taxi, and take-off	1.93 L	✓
REQ-CON-SUST-2	80% of the aircraft's morphing parts shall be recyclable	>80%	✓
REQ-CON-SUST-3	The aircraft shall have a maximum fuel capacity of at most 200 L	200 L	•
Weight requirements			
REQ-CON-WGT-1	The aircraft shall have an empty weight of at most 750 kg	712 kg	•
REQ-CON-WGT-2	The aircraft shall have a maximum take-off weight of at least 1,250 kg	1,272 kg	✓
Operational requirements			
REQ-CON-OPER-1	The aircraft shall be able to transport four persons (77 kg each [1]), including pilot(s), including luggage (54 kg), totalling 362 kg	362 kg	•
REQ-CON-OPER-2	The aircraft shall provide accommodation for two pilots	-	•
Propulsion requirements			
REQ-CON-PROP-1	The aircraft shall have one internal combustion engine	-	•
REQ-CON-PROP-2	The maximum propulsive power provided by the aircraft shall be at most equal to that of the reference aircraft	180 hp	•
REQ-CON-PROP-3	The aircraft shall be driven by a propeller	-	•
Regulatory requirements			
REQ-CON-REG-1	The aircraft shall comply with the EASA CS-23 certification specifications for normal, utility, aerobatic, and commuter category aeroplanes [1]	-	•
REQ-CON-REG-2	The aircraft shall carry reserve fuel, consisting of contingency fuel that is not less than 5% of the planned trip fuel and final reserve fuel to fly for an additional period of 45 minutes after performing the primary mission [2]	-	•
REQ-CON-REG-3	The aircraft shall have a minimum flight altitude of the sum of the maximum terrain or obstacle elevation, whichever is higher; plus 305 m [3]	-	•
Geometrical requirements			
REQ-CON-GEO-1	Morphing concepts shall only be applied to the wing, the tail, the landing gear and the engine of the aircraft	-	•
REQ-CON-GEO-2	The aircraft shall have the same fuselage dimensions as the reference aircraft	-	•
REQ-CON-GEO-3	The aircraft shall have a high wing mounted on top of the fuselage	-	•
Economical requirements			
REQ-CON-ECO-1	The cost of a single standard configuration aircraft shall be at most €375,000	€364,240	✓
Resource requirements			
REQ-CON-RSC-1	The project shall be completed within 11 weeks	-	•
REQ-CON-RSC-2	The project shall be completed by 10 students	-	•

20
Conclusion

This report presented a detailed design for the Cessna Morphlight, a variant of the Cessna 172S Skyhawk with improved performance by means of morphing systems.

Compared to the Skyhawk, the Morphlight has more stringent requirements. The aircraft shall be able to operate from shorter runways, while flying further, faster and with a higher take-off weight. Lastly, the Morphlight shall also be more sustainable than current aircraft, with a lower fuel consumption and a large share of recyclable materials.

The design of the Morphlight presented in this report meets all requirements and even outperforms on most of them. The Morphlight has a take-off distance of 336 m, a landing distance of 284 m, a cruise speed of 250 m, a range of 2780 km and an endurance of 21 hours. A morphing civil single engine propeller aircraft thus proved to be feasible. The final design parameters are described below.

The wing has a slightly tapered planform, with root fairings for a smooth transition between the wing and fuselage. The wing span can vary between 10 m and 15 m, while the average chord varies from 1 m to 1.175 m. The small wing area is used for high speed cruise, while the largest wing area is utilised on landing and take-off. With maximum span and minimum chord, the slender wing fulfils the maximum range requirement.

For span morphing, each half of wing consists of two wing boxes that can slide into each other. A central wing box on top of the fuselage connects the two wing halves. A zero Poisson skin enables the wing to extend in one direction, while not creating stress in the perpendicular direction. The first 2.5 m closest to the root of the wing does not morph and is covered with a thermoplastic skin material. This section also houses the fuel tanks and Fowler flaps.

The wing box parameters are firstly optimised by the Python program, and secondly using ABAQUS. This leads to a final wing box mass of 38.87 kg per half span including ribs and strut.

A strut with an airfoil shaped cross section is attached on either side of the fuselage and the end of the wing boxes closest to the root. The struts relieve the wing box of shear and bending stresses. Furthermore they are attached perpendicular to the wing surface with some curvature, to reduce interference drag.

The ailerons are located at 35% chord extending from 3.34 m to 4.90 m for the retracted position and from 4.27 m to 7.40 m in the extended position.

The engine is upgraded to a newer model. The chosen Continental Diesel CD-155 is short on power to meet the take-off requirements though, so a hybrid configuration is used. An electric engine supports the diesel engine during take-off.

To reduce drag, and provide sufficient space for the new engine, the nose has been smoothened and stretched. A retractable landing gear is implemented to further reduce drag during cruise. The design is identical to that of the Cessna 172RG. This adds some weight and complexity however, but can be justified by the decrease in drag. During approach and landing, drag is too low though, making it impossible to reach the landing requirement. This problem is resolved by integrating a speedbrake, positioned on top of the cabin. This speedbrake will be deflected on approach and during landing roll to increase drag and meet the requirement.

To ensure stability and control the horizontal and vertical tail surfaces were sized. The horizontal tail was required to be 3.52 m^2 where the vertical tail area is slightly increased to 2.31 m^2. Furthermore also the control surfaces were redesigned. The elevator and rudder size is kept the same as of the Skyhawk, however for the ailerons a larger chord fraction of 35% is used.

The Skyhawk is mostly made of aluminium, which is too heavy when morphing systems are added. Therefore, Carbon fibre reinforced polymers (CFRP) are used on most of the structure. The landing gear is made of steel, while the flap tracks are produced in aluminium.

20.1. Recommendations

For further development of the Morphlight, the following recommendations can be made.

The aerodynamic analysis of the raked wing tips was performed without taking the changing wing area into account. Therefore, the increase in performance coming from solely the wing tips could not be determined accurately. For a further analysis, two configurations with the same wing area should be looked at.

Another subject that was not investigated to the fullest extent is the horizontal tail size. There is currently a substantial margin between the most forward centre of gravity and the controllability limit. By shifting the main wing slightly more aft, the cg will move to the front on the MAC which will result in a smaller required tail size which in turn would lead to a weight and drag reduction.

The performance and structural optimisations should run in parallel. This will probably lead to an decreased wing box weight, as for the presented design, the box was optimised based on performance requirements from a single optimisation run. The production cost of ribs of the morphing section needs to be further investigated, since a tapered morphing section will increase aerodynamic performance, as well as leave more space for morphing systems in the wing.

Finally, as the Morphlight has a relatively low cruise speed, the effects of morphing are rather limited. Flying faster, by using a more powerful engine, would make morphing more beneficial. From a market perspective, a higher cruise speed would also make the aircraft more competitive.

Bibliography

[1] European Aviation Safety Agency. Certification Specifications for Normal, Utility, Aerobatic and Commuter Category Aeroplanes CS-23, 2012.

[2] European Aviation Safety Agency. Annexes to the draft Commission Regulation on 'Air Operations - OPS'.

[3] European Aviation Safety Agency. Acceptable Means of Compliance (AMC) and Guidance Material (GM) to Part-CAT, 2012.

[4] General Aviation Manufacturers Association. 2014 General Aviation Statistical Databook & 2015 Industry Outlook, 2015.

[5] Aircraft Owners and Pilots Association. Best Practices Guide for Maintaining Aging General Aviation Airplanes, 2003.

[6] United States Government Accountability Office. Impact of Fuel Price Increases on the Aviation Industry, September 2014.

[7] Federal Aviation Administration. FAA Issues Request for Unleaded Replacements for General Aviation Gasoline, 2013.

[8] Kovarikt, K.V. A Good Idea Stretched Too Far: Amending the General Aviation Revitalization Act to Mitigate Unintended Inequities. *Seattle University of Law Review*, 31, 2008.

[9] General Aviation Manufacturers Association. 2010 General Aviation Statistical Databook & Industry Outlook, 2011.

[10] United States Environmental Protection Agency. Lead Emissions from the Use of Leaded Aviation Gasoline in the United States. (EPA420-R-08-020), October 2008.

[11] Ruijgrok, G.J.J. *Elements of Airplane Performance*. VSSD, Delft, 2nd edition, 2009.

[12] Jha, A.K. and Kudva, J.N. Morphing Aircraft Concepts, Classifications, and Challenges. *Smart Structures and Materials 2004: Industrial and commercial applications of smart structures technologies*, 5388:213–224, July 2004.

[13] Roskam, J. *Airplane Design Part V: Component Weight Estimation*. Roskam Aviation and Engineering Corporation, Ottawa, Kansas, USA, 1985.

[14] Skillen, M.D. and Crossley, W.A. Modeling and Optimization for Morphing Wing Concept Generation. March 2007.

[15] European Aviation Safety Agency. Part SPO, 2015.

[16] Carson, B.H. Fuel Efficiency of Small Aircraft. In *AIAA Aircraft Systems Meeting*, number AIAA-80-1847, Anaheim, California, USA, 1980. American Institute of Aeronautics and Astronautics.

[17] Ojha, S.K. *Flight Performance of Aircraft*. American Institute of Aeronautics and Astronautics, Inc., Washington, DC, 1995.

[18] Washington, H.P. and Gibbons, J.T. Analytical Study of Takeoff and Landing Performance for a Jet STOL Transport Configuration with Full-span Externally Blown, Triple-slotted Flaps. Technical note, National Aeronautics and Space Administration, Washington, D.C., October 1973.

[19] Roskam, J. *Airplane Design Part IV: Layout Design of Landing Gear and Systems*. Roskam Aviation and Engineering Corporation, Ottawa, Kansas, USA, 1986.

[20] Torenbeek, E. *Synthesis of Subsonic Airplane Design*. Kluwer Academic Publishers, 1982.

[21] Cessna Aircraft Company. Skyhawk SP Information Manual, 2006.

[22] Federal Aviation Administration. Noise Levels for U.S. Certificated and Foreign Aircraft, 1997.

[23] Underwood, S.C. Performance and Emission Characteristics of an Aircraft Turbo Diesel Engine using JET-A Fuel. Master's thesis, University of Kansas, 2008.

[24] Mulder, J.A., Staveren, W.H.J.J. van , Vaart, J.C. van der , Weerdt, E. de , Visser, C.C. de , in 't Veld, A.C. , and Mooij, E. . AE3212-I Aerospace Flight Dynamics and Simulation - Lecture Notes, 2013.

[25] La Rocca, G. Requirement Analysis and Design principles for A/C stability & control (Part 2), 2015.

[26] Sadraey, M. *Aircraft Design: A Systems Engineering Approach*. Wiley Publications, 2012.

[27] Gudmundsson, S. *General Aviation Aircraft Design*. Butterworth-Heinemann, 2013.

[28] La Rocca, G. Requirement Analysis and Design principles for A/C stability & control (addendum), 2015.

[29] Federal Aviation Administration. FAR Part 23.

[30] Roskam, J. *Airplane Flight Dynamics and automatic flight controls Part 1*. Design Analysis and Research Corporation, Lawrence, Kansas, USA, 1995.

[31] Bromfield, M.A. Criteria for Acceptable Stick Force Gradients of a Light Airplane. Technical report, Brunel University, 2012.

[32] Roesch, P. and Harlan, R.B. A Passive Gust Alleviation System for a Light Aircraft. Technical report, National Aeronautics and Space Administration, 1975.

[33] La Rocca, G. Requirement Analysis and Design principles for A/C stability & control (Part 1), 2015.

[34] Raymer, D.P. *Aircraft Design: A Conceptual Approach*. American Institute of Physics, 5th edition, 2012.

[35] Megson, T.H.G. *Aircraft Structures for Engineering Students*. Butterworth-Heinemann, Oxford, 2007.

[36] Tetrault, P.-A. Numerical Prediction of the Interference Drag of a Streamlined Strut Intersecting a Surface in Transonic Flow. Technical report, Virginia Polytechnic Institute and State University, Blacksburg, Virginia, January 2000.

[37] Alaluf, D. Analysis of Laminated Composites. Active Structures Laboratory.

[38] Hart-Smith, L.J. The Ten-Percent Rule for Preliminary Sizing of Fibrous Composite Structures. *Weight Engineering*, 52:29–45, 1992.

[39] Tsai, S.W. and Wu, E.M. A General Theory of Strength for Anisotropic Materials. *Journal of Composite Materials*, 1971.

[40] Cessna Aircraft Company. *Service Manual Model 172 Series*. 1985.

[41] Cessna Aircraft Company. Skyhawk Model 172S - Specification and Description, 2012.

[42] Sadraey, M. *Aircraft Performance: Analysis*. VDM Publishing, 2009.

[43] Jane's All the World's Aircraft. Cessna 172 Skyhawk, 2014.

[44] Gudmundsson, S. *General Aviation Aircraft Design: Applied Methods and Procedures*. Butterworth-Heinemann, Oxford, UK, 2014.

[45] Prevention of Retractable Landing Gear Failures. Technical Report AC 20-34D, Federal Aviation Administration, 1980.

[46] Roskam, J. *Airplane Design Part VI: Preliminary Calculation of Aerodynamic, Thrust, and Power Characteristics*. Roskam Aviation and Engineering Corporation, Ottawa, Kansas, USA, 1987.

[47] Unsteadiness in Flow over a Flat Plate at Angle-of-Attack at Low Reynolds Numbers.

[48] Vocke, R.D. III, Kothera, C.S., and Wereley, N.M. Development of a Span-Extending Blade Tip System for a Reconfigurable Helicopter Rotor. 2012.

[49] Offringa, A. Thermoplastic Composites Technology Tutorial, 2014. Fokker Aerostructures.

[50] Celanese. Fortron PPS for Thermoplastic Composites, 2013.

[51] Fokker Aerostructures. New Evolution, Progress in Thermoplastic Composites, 2015.

[52] Cessna Aircraft Company. *Single Engine Models 172, 182, T182, 206 AND T206 1996 and on*. 2005.

[53] Vocke, R.D. III, Kothera, C.S., Woods, B.K.S., and Wereley,N.M. Development and Testing of a Span-Extending Morphing Wing. *Journal of Intelligent Material Systems and Structures*, 22, June 2011.

[54] Grande, A.M., Coppi, S., Di Landro, L., Sala, G., Giacomuzzo, C., Francesconi, A., and Rahman, M.A. An Experimental Study of the Self-Healing Behavior of Ionomeric Systems under Ballistic Impact Tests. *SPIE*, March 2012.

[55] Gevers Aircraft, Inc. *Genesis: Span Expansion*. Brownsburg, Indiana, USA, 1997.

[56] Pettit, D. and Turnbull, A. General Aviation Aircraft Reliability Study. Technical report, National Aeronautics and Space Administration, 2001.

[57] Australian Department of Infrastructure and Regional Development. General Aviation Activity 2012.

[58] Roskam, J. *Airplane Design Part VIII: Airplane Cost Estimation: Design, Development, Manufacturing and Operating*. Roskam Aviation and Engineering Corporation, Ottawa, Kansas, USA, 1990.

[59] Analysis of Empty Weight of General Aviation Piston Engine Aircraft. In *AIAA Aerospace Sciences Meeting including the New Horizons Forum and Aerospace Exposition*, January 2011.

[60] Cessna Aircraft Company. Cessna 182Q Pilot Operating Handbook, 1978.

[61] Eastlake, C.N. and Blackwell, H.W. Cost Estimating Software for General Aviation Aircraft Design. 1999.

[62] Cessna Aircraft Company. Operational Equipment Selection Guide, 2013.

A

Introduction to Zero Poisson's Ratio Skin

Conventional skin materials have positive Poisson's ratios, meaning they contract in one direction, when extended in the orthogonal direction. The main characteristic of a zero Poisson's skin is that a change in length in one direction does not effect other directions [53].

The skin developed in [53] consists of a one-dimensional morphing skin, using an elastic matrix composite, and zero Poisson substructure, using a honeycomb structure.

An elastic matrix composite (EMC) skin is used for morphing applications since elastomeric materials have a large strain capability. Elastomers alone will not provide enough resistance to aerodynamic pressure loading. The area between ribs is unsupported and a reinforcement in the skin is needed to maintain a viable airfoil surface. Besides the lack of resistance, elastomers also have high Poisson's ratios, which causes the skin surface in chordwise direction to shrink when the span extends. Fibre reinforcement in chordwise direction will mitigate this effect. Carbon fibres also deliver a higher stiffness and higher strength, while keeping the weight low. Figure A.1 shows the layers of the skin.

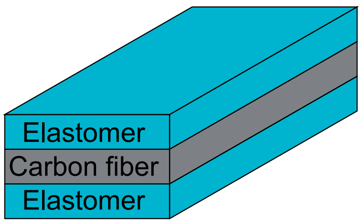

Figure A.1: Elastomeric-matrix-composite skin [53]

A honeycomb structure is needed to support the skin for out-of-plane loads. A traditional honeycomb structure has a positive Poisson's ratio. Some materials can have a negative Poisson's ratio (auxetic), which means that the material will also extend in chordwise direction, if the span is increased. This can sometimes be interesting, but extending the span while contracting the chord will not be possible in this case. Therefore, a zero Poisson ratio honeycomb structure is developed using a combination of a standard and a auxetic honeycomb structure. This can be seen in Figure A.2.

The honeycomb structure is the ideal support of the EMC skin, since it can double its area, while maintaining a high out-of-plane stiffness. Figure A.3 shows the final core design. The design has space for continuous sliding spars and a wingbox structure.

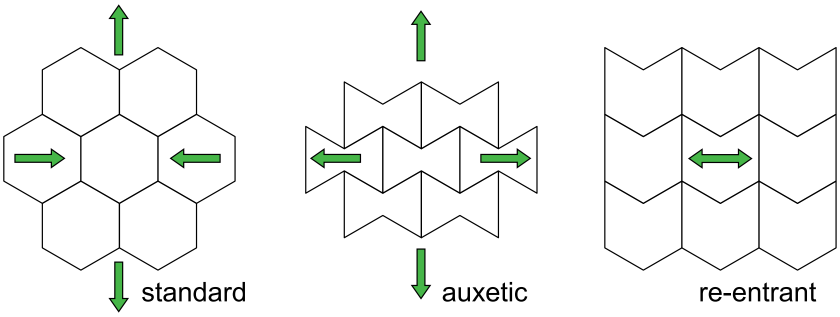

Figure A.2: Development of zero Poisson's ratio morphing core [53]

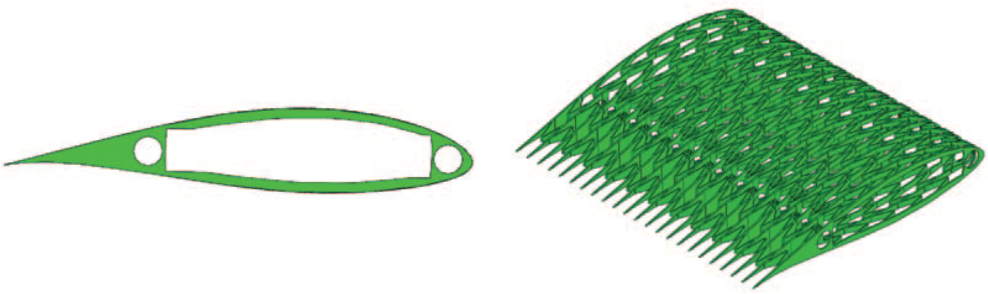

(a) Side view

(b) Isometric view

Figure A.3: Zero Poisson core design [53]